UNIVERSITÀ DEGLI STUDI DI MILANO

SCUOLA DI DOTTORATO IN
FISICA, ASTROFISICA E FISICA APPLICATA

DIPARTIMENTO DI FISICA

CORSO DI DOTTORATO DI RICERCA IN
FISICA, ASTROFISICA E FISICA APPLICATA
CICLO XXIII

SET-UP OF INNOVATIVE EXPERIMENTAL METHODOLOGIES FOR THE ATMOSPHERIC AEROSOL CHARACTERISATION AND SOURCE APPORTIONMENT

Settore Scientifico Disciplinare: FIS/07

Tesi di Dottorato di:
Vera Bernardoni

Supervisore: Dott.ssa Roberta Vecchi
Coordinatore: Prof. Marco Bersanelli

A.A. 2009-2010

A Lucia, mia figlia,

piccolo angelo volato subito via…

Index

Abstract

The PhD work presented in this thesis focuses on the set-up of innovative experimental methodologies for the atmospheric aerosol characterisation and apportionment.

Many issues are still open in aerosol science. Among them, the identification and quantification of PM sources and the separation between natural and anthropogenic contributions were explored in this work.

To improve the state-of-the-art knowledge on aerosols, it has to be considered that the higher is the time- and size-resolution, the more detailed can be the information obtained; moreover, the identification of suitable source tracers plays a key role for the identification and quantification of aerosol sources.

In this PhD thesis, three main experimental and modelling improvements were carried out:

1) set-up of an ED-XRF (Energy Dispersive X-Ray Fluorescence) spectrometer for the analysis of size-segregated samples. During the work, an experimental methodology for this kind of analysis was developed, and the obtained results were validated by an inter-comparison with PIXE technique (Particle Induced X-Ray Emission), usually used for size-segregated samples analysis. The developed ED-XRF set-up allows to obtain size-segregated elemental characterisation using a more widespread, cheap, and easy-to-use technique than PIXE. Moreover, it was used to validate a model developed in joint collaboration with the group of the University of Genoa for elemental size distribution determination (see next paragraph);
2) application of the PMF (Positive Matrix Factorization) receptor model to a 4-hour resolved dataset already available. In this work, PMF resolved seven main sources affecting the Milan urban area (re-suspended dust, construction work, secondary compounds, combustion, traffic, industry). Moreover, the combination of the source temporal trends with size-resolved number concentration gave the size-segregated source apportionment, following an approach developed in the past during a collaboration of the research groups of the Universities of Genoa, Milan, and Florence [Mazzei et al., 2007].

Moreover, in this PhD thesis - in joint collaboration with the group of the University of Genoa – the apportionment methodology approach was further developed to obtain the elemental size distribution without using multistage impactors. As previously mentioned, the ED-XRF analysis on cascade impactor samples analysis set-up in this work allowed the validation of this new methodology for size-segregated distribution estimation;

3) design, set-up and test of a sample preparation line for ^{14}C measurements on aerosol samples carried out jointly with the LABEC-INFN research group. Literature studies showed ^{14}C as a good tracer for the separation of natural and anthropogenic carbonaceous contributions to PM [Szidat et al., 2006]. In this PhD work, a sample preparation line was designed and realised, matching the constraints for the analysis of the organic and elemental carbon fractions (OC and EC, respectively). It was the most innovative, important, and demanding part of the PhD work (it is noteworthy that only another group in the world measures ^{14}C in both OC and EC fractions). New technical solutions were developed during this PhD work and inserted in the final line, and many tests on fractions separation were carried out. First tests on isolated carbon fractions were performed and a preliminary source apportionment was carried out, evidencing limits and perspectives of the approach.

Introduction

Atmospheric aerosol is an ensemble of solid and liquid particles suspended in atmosphere. Anthropogenic aerosol contributes to air pollution, together with other gaseous anthropogenic pollutants.

Aerosol has great importance both at local and global scale. In fact, it impacts at local scale on:

- human health [Dockery et al., 1993; Pope et al., 2002; Seagrave et al., 2006];
- air quality and visibility [Watson, 2002; EPA, 2004; CEN, 2008];
- cultural heritage degradation [Bonazza et al., 2005; Nava et al., 2010];

and at global scale on:

- radiation balance, acting both on radiation scattering and absorption (direct effect) and on cloud formation (indirect effect) [Storelvmo et al., 2006; IPCC 2007; Stier et al., 2007].

These effects depend on aerosol size, composition, and life-time in atmosphere. All these parameters depend on or are influenced by the following processes:

1) aerosol formation,
2) aerosol removal/deposition,
3) aerosol transport,
4) chemical reactions in atmosphere.

Aerosol can be directly emitted in the atmosphere (primary aerosol) by anthropogenic and natural sources or it originates in the atmosphere by natural or anthropogenic gas-to-particle transformations (secondary aerosol). Aerosol size and composition are strictly related to aerosol origin; as examples, big particles with irregular shapes and composed by Al, Si, and Ca are typically of natural origin (re-suspended dust); small, spherical, carbonaceous particles are usually emitted by combustions; big particles mainly composed by organic natural compounds can be ascribed to plant debris.

Once emitted/formed, aerosol can stay in atmosphere for hours/days, depending on particle size and atmospheric conditions. During its residence time, atmospheric aerosol can be transported from a few km (regional scale) to very long distances

(continental scale). Moreover, chemical reactions can modify its composition, depending both on aerosol composition and meteorological conditions (i.e. solar radiation can activate photochemical reactions, or condensation of volatile compounds can occur at low temperatures) and condensation/coagulation processes can change aerosol size-distribution.

Different processes can cause aerosol removal:

a) small particles (0.001-0.1 μm) are mainly removed by coagulation processes: few small particles stick together to form a new particle with a larger diameter. Moreover, the brownian diffusion is very efficient for these particle sizes and allows both dry and wet deposition;
b) particles in the range (0.1 - 5 μm) usually have the longest life-time in atmosphere: they are too large for brownian diffusion and too small for gravitational settling. They are mainly removed by rain out (in-cloud removal) or wash out (particles are intercepted by rain drops and are consequently removed);
c) big particles (> 5 μm) are mainly removed by gravitational settling.

Thus, it can be noticed that aerosol is a very complex atmospheric component and it is generated and governed by many different factors.

In the recent European legislation on atmospheric pollution [CEN, 2008], the monitoring of PM10 and PM2.5 (particles with aerodynamic diameter lower than 10 μm and 2.5 μm, respectively) on 24-hour basis is prescribed and daily and annual limit values are set. At rural background sites, ionic and carbonaceous (organic and elemental carbon) speciation is prescribed for PM2.5. The importance of identifying emission sources and the need of implementing efficient abatement strategies both at local, national, and European scale are also stressed.

However, the only implementation of the legally prescribed monitoring can limit the possibility to identify sources and processes involved in the atmospheric aerosol pollution problem, as well as to correctly assess the effects of airborne particles. In fact, limited chemical speciation and 24-hour temporal resolution is required, and no size-segregated measurements are prescribed.

To gain a deeper knowledge on atmospheric aerosols, more extensive researches

have to be carried out, aimed to obtain detailed information about particle physical/chemical properties with high temporal and size-segregated resolution, and to better understand the processes previously mentioned. Models can be then applied to identify and quantify (source apportionment) different sources contributions to the measured concentrations.

In this work different techniques were designed and realised (when not available), set-up (if already available), and applied to gain new and detailed information on atmospheric aerosol properties.
More in detail, the attention was mainly focused on the following topics:

- ***set-up of an Energy-Dispersive X-Ray Spectrometer (ED-XRF) for the analysis of size-segregated aerosol samples***. Size-segregated PM composition is commonly measured in the 0.01-10 μm range by multi-stage cascade impactors [Hillamo and Kauppinen, 1991; Marple et al, 1991; Maenhaut et al., 1996]. In this work, an ED-XRF spectrometer was set-up to quantify the elemental concentration on the peculiar samples obtained by a multi-stage cascade impactor. The use of ED-XRF for the analysis of cascade impactor samples is not common due to problematic features of the collected deposits (inhomogeneous samples with a different deposition pattern on each stage, and small amount of PM collected on each stage/sample). The methodology to suitably set-up the ED-XRF spectrometer for the analysis of size-segregated aerosol samples was developed and the ED-XRF sensitivity curve to quantify elemental concentrations was determined. An inter-comparison with Particle Induced X-Ray Emission technique (PIXE: the most widespread technique for elemental analysis of size-segregated aerosol samples) was carried out and a good agreement between the techniques was obtained. Therefore, the set-up methodology developed in this work can be used to obtain reliable results on impactor samples analysed by ED-XRF. This is important when considering that the access to accelerator facilities is not always possible and that the available beam time is usually quite limited. In summary, the possibility to carry out

an ED-XRF analysis on multi-stage cascade impactor samples can be important for a widespread use of these samplers. In this work, a wintertime campaign was also carried out in Milan to test our set-up and examples of elemental concentration on size-segregated aerosol are presented. However, further work is needed to perform source apportionment using impactor data. Details on ED-XRF set-up methodology and final configuration, as well as data presentation can be found in Chapter 2.

- ***Source apportionment by Positive Matrix Factorization (PMF) on high-time resolved data***. PMF is a receptor model, i.e. the source apportionment is carried out using the aerosol components (i.e. elements, ions, carbonaceous fractions) measured at a receptor as input data. In this work, PMF was applied to an already available PM10 dataset with high temporal resolution, to obtain information on chemical profiles and high time-resolved temporal trends of the sources influencing the area of interest. Moreover, PMF sources temporal trends were analysed together with number distribution in the range 250 nm – 10 μm using a methodology developed jointly with the group of the University of Genoa [Mazzei et al., 2007] to obtain indication on the size distribution of the different sources (see Chapter 3 for details). Moreover, in joint collaboration with the group of the University of Genoa, the above mentioned methodology was developed during this work to obtain elemental size distribution without multistage impactor. The XRF set-up developed in this work and previously mentioned was used for model validation.
- ***Design and set-up of a new sample preparation line for ^{14}C measurements in aerosol, aimed at the separation of natural and anthropogenic contributions to carbonaceous fractions***. In an urban area like Milan, total carbon (TC) alone may account for about 30% of PM mass, therefore strongly influencing air quality. Carbon is present in atmospheric aerosol in three main different forms: organic carbon (OC, either directly released in the atmosphere as particles or formed in the atmosphere by gas-to-particle conversion of anthropogenic or biogenic precursor gases), elemental carbon (EC, produced by the incomplete combustion of fossil and biomass fuels in

an oxygen–poor environment), and carbonate carbon (CC, in urban areas at mid-latitudes accounts only for few per-cent of TC [Chow and Watson, 2002] and will be neglected in the following). Anthropogenic carbon sources of both OC and EC can be divided in two main categories: fossil fuels and biomass burning. On the contrary, natural sources (plant debris and secondary particles from biogenic gas emissions) contribute only to the OC fraction, at least at our latitudes where spontaneous forest burning is quite rare. Thus, the EC fraction has only an anthropogenic origin and a radiocarbon analysis on this carbon fraction can separate fossil fuel ($^{14}C/^{12}C=0$) from biomass burning ($^{14}C/^{12}C\sim10^{-12}$) contributions. Once these components are identified in EC fraction, and knowing the respective OC/EC emission ratio, their contribution can be also identified in the OC fraction and, by difference, the natural OC component can be estimated. A detailed description of the role of carbonaceous particles in atmosphere and of the problems concerning carbon fraction separation and ^{14}C analysis can be found in Chapter 4.

In this work, a new sample preparation line for radiocarbon analysis on OC and EC separated fractions was designed and set-up. It was the most innovative, important, and demanding part of the PhD work. Problems concerning the small carbon quantities available and the OC and EC separation had to be faced. Original solutions for some parts of the line were developed and implemented. A complete description of the line, of the test for data quality assurance and of the first results obtained in this work is presented in Chapter 5.

Chapter 1: Atmospheric aerosol

Atmospheric aerosol (often called particulate matter, PM) is a polydisperse ensemble of liquid and solid particles suspended in the atmosphere. An atmospheric particle is a molecular ensemble which does not vary its physical-chemical properties for long enough to be measured. The ensemble is polydisperse because particles have many different physical-chemical and geometrical properties.

The interest in atmospheric aerosol is due to its strong impact on environment and human health. In fact, atmospheric aerosol:

- changes the optical properties of the atmosphere (scattering and absorption of visible and IR radiation), influencing visibility and Earth radiation balance (direct effect) [Watson, 2002; Stier et al., 2007]. It can also act as cloud condensation nucleus for clouds and fog, influencing precipitation and radiation balance (indirect effect) [Ramanathan et al., 2001]
- catalyses chemical reactions in the atmosphere [Andreae and Crutzen, 1997; Jacob, 2000; Volkamer et al., 2006]
- can pollute soil and water because of dry (sedimentation) and wet (rain, snow) deposition [Textor et al., 2006];
- can damage materials and cultural heritage [Rodriguez-Navarro and Sebastian, 1996; Bonazza et al., 2005; Nava et al., 2010].

Moreover, atmospheric particles can affect human health: they can be inhaled, and they can enter other organs through the respiratory apparatus. Their negative effects can be different depending on their physical-chemical properties [Dockery et al., 1993; Pope et al., 2002; Seagrave et al., 2006].

Particles are formed by two main processes [Jaenike, 1980]:

- disintegration and/or dispersion of bulk material, such as the weathering of crustal material, the production and dispersion of sea-salt droplets or the emission and dispersion of particulate matter from combustion (primary aerosol);
- modification of airborne substances forming new particles or a varying size-distributions (secondary aerosol). Such processes are gas-to-particle

conversions by condensable gaseous species and the evaporation of cloud elements and rain droplets leaving aerosol particles. More in detail, we refer to:

- homogeneous nucleation or auto-nucleation: gas molecules can aggregate in small clusters, due to attractive electrostatic forces (e.g. Van der Waals). Once formed, clusters sudden disintegrate. The higher is gas saturation and the more these clusters collide before disintegrating. If the dimension of the clusters exceeds the Kelvin radius (i.e. the radius of a particle in equilibrium with gas at a definite super-saturation value) a particle is stably generated. Once stable, the particle can further grow by condensation. Homogeneous nucleation of particles requires high super-saturation ratios (2-10);
- heterogeneous nucleation (or nucleated condensation): it is a process of particles formation or growth promoted by the presence of condensation nuclei or ions. This nucleation requires super-saturation of few percents and it is the main responsible for cloud formation. Particles on which water vapour condenses to give origin first to droplets and then to clouds are called cloud condensation nuclei (CCN): they are particles that grow because of supersaturated water vapour condensation, becoming fog or cloud droplets. It is noteworthy that super-saturation has always to be indicated when CCN concentration is given [Seinfeld and Pandis, 1998];
- coagulation: it is a growth process. Aerosol particles collide one another, because of their relative motion. The result (in absence of other aerosol sources) is a continuous reduction in the number concentration and an increase in the particle sizes. It is extremely efficient for small molecules, which tend to stick because of collisions.

In table 1.1 estimates of global emissions of aerosol are reported in Tg/yr [Monks et al., 2009]. It is noteworthy the importance of secondary particles, especially of anthropogenic origin (50-60% of total anthropogenic particles).

	Mass emission "Best" Tg a^{-1}	Mass emission Min Tg a^{-1}	Mass emission Max Tg a^{-1}	Mass Burden Tg
Carbonaceous aerosols				
Primary organic (0–2 μm)	95	40	150	1.2
Biomass burning	54	26	70	–
Fossil fuel	4	3	9	–
Biogenic	35	15	70	0.2
Black carbon (0–2 μm)	10	8	14	0.1
Open burning & biofuel	6	5	7	–
Fossil fuel	4.5	3	6	–
Secondary organic	28	2.5	83	0.8
Biogenic	25	2.5	79	0.7
Anthropogenic	3.5	0.05	4.0	0.08
Sulphates	200	107	374	2.8
Biogenic	57	28	118	1.2
Volcanic	21	9	48	0.2
Anthropogenic	122	69	214	1.4
Nitrates	18	12	27	0.49
Industrial/Road Dust	100	40	130	1.1
Sea salt				
$d < 1$ μm	180	60	500	3.5
d=1–16 μm	9940	3000	20,000	12
Total	10,130	3000	20,000	15
Desert/Soil dust				
d <1 μm	165	–	–	4.7
d =1–2.5 μm	496	–	–	12.5
d =2.5–10 μm	992	–	–	6
Total	1600	1000	2150	18 ± 5
Anthropogenic total	312	158.1	467	3.1
Biogenic total	117	45.5	267	2.1

table 1.1: major type, source and mass burdens of aerosol at global scale [Monks et al., 2009]

Besides the origin (natural/anthropogenic or primary/secondary), two other parameters are of great importance for particles classification: size and composition. Particles size can span a range from a few nanometres to tens micrometers. The definition of particles size is complicate because particles can have many different shapes (e.g. spherical, cubic, based on crystal lattice... see figure 1.1).

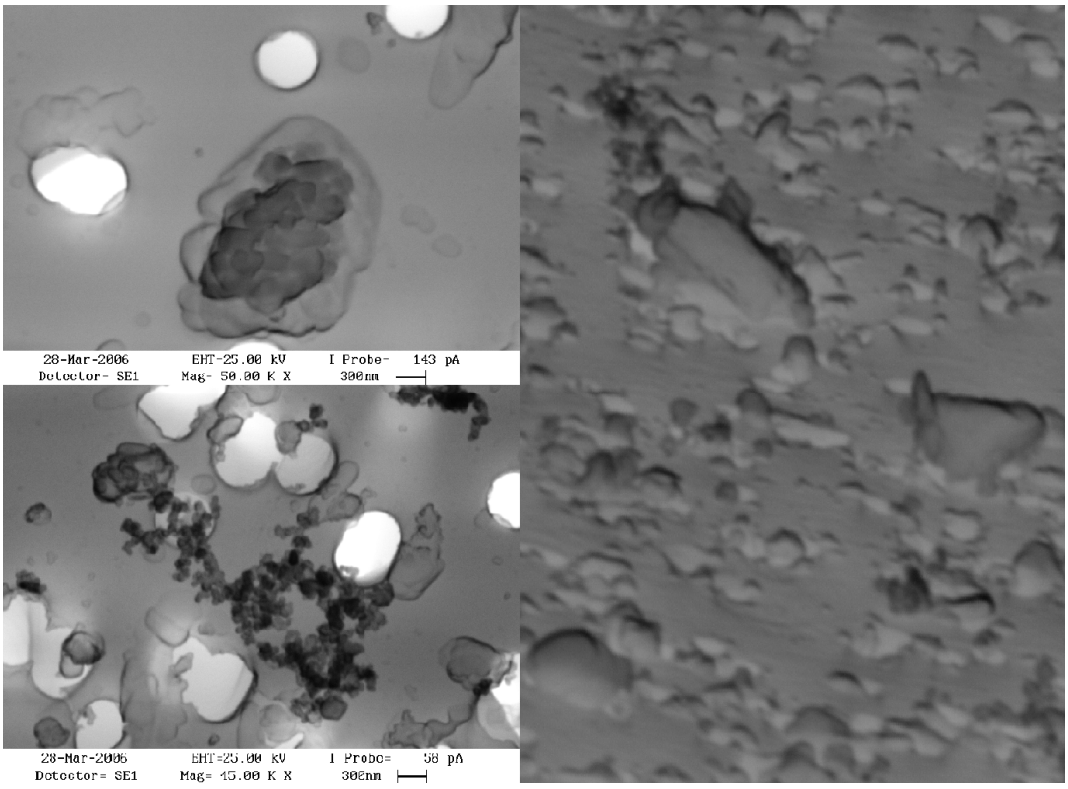

figure 1.1: atmospheric particles as detected by an electronic microscope. Right: PM10 on filter; Left up: core made of soil elements surrounded by Ce; left down: soot particles

Thus, it is necessary referring to "equivalent diameters" (according to specific parameters) to define particles size.

There exist equivalent diameters referring to particles properties and others based on their behaviour (figure 1.2) [Hinds,1999]. In this work, two main equivalent diameters will be considered:

- aerodynamic diameter (d_{ae}): diameter of a spherical particle, of unitary density (1 g/cm^3), having the same inertial properties (terminal velocity of settlement) of the analysed particle;
- optical diameter: diameter of a spherical particle with known refraction index that scatters at a specific angle the same light amount as the analysed particle.

There exists a relationship between the shape and size of particles and their origin: natural particles of primary origin are generally in the range 5-50 μm (except for marine salt, which is in the 1-5 μm range) with irregular shapes. As for anthropogenic emissions, high temperature combustions generally emit very fine, spherical particles, while tyre and brake wear or some industrial processes (e.g. ceramic factory) lead to bigger primary, irregularly shaped anthropogenic particles

[Viksna et al., 2004]. Secondary aerosol has usually small dimensions: $d < 0.5$ μm. However, some nitrates can be in the $0.5\ \mu m < d < 5\ \mu m$ [Querol et al., 2001].

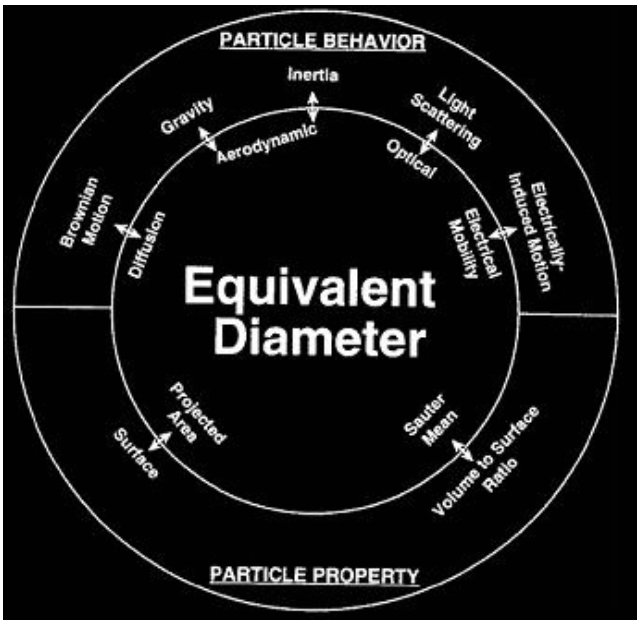

figure 1.2: equivalent diameters

Particle size distribution can be expressed as a function of different parameters:

- number (number distribution)
- surface (surface distribution)
- volume (volume distribution)
- mass (mass distribution).

In 1978, Whitby analysed about 1000 particle size distributions and singled out a tri-modal pattern of the size distribution [Whitby, 1978]. The three modes were called:

- Aitken mode: $0.01\ \mu m < d_p < 0.1\ \mu m$. They are mainly produced by high-temperature combustions; their diffusion is mainly due to Brownian motion and they are mainly removed by coagulation;
- accumulation mode: $0.1\ \mu m < d_p < 1\ \mu m$. In this mode, particles of different origin (e.g. combustion, chemical reaction, coagulation of smaller particles) can be found. They are subjected to Brownian motion too, even if it is less efficient because of their higher mass. Also gravitational settling is not so efficient, therefore they have the highest residence time in atmosphere (see figure 1.3). They are mainly removed by wash-out or rain-out;

– coarse mode: $d_p > 1$ μm. Particles in the coarse mode are mainly of natural origin. They are not subject to Brownian motion and their removal is due to gravitational settling. Their residence time is very short; as a consequence, they are transported only at local scale and this transport is strongly affected by local turbulence.

The development of the measuring techniques has allowed the measurement of particles with dimensions down to few nanometres and the discovery of a fourth mode (see figure 1.4), consisting in ultra-fine particles [EPA, 2004]. It was called

– nucleation mode: 0.001 μm < d_p < 0.01 μm: particles are formed by nucleation and can be measured only next to their source because they rapidly coagulate, increasing their size. The lower limit between cluster of molecules and particles is not well defined. Up to now, however, there exists a technical limit of detection at about 3 nm diameter.

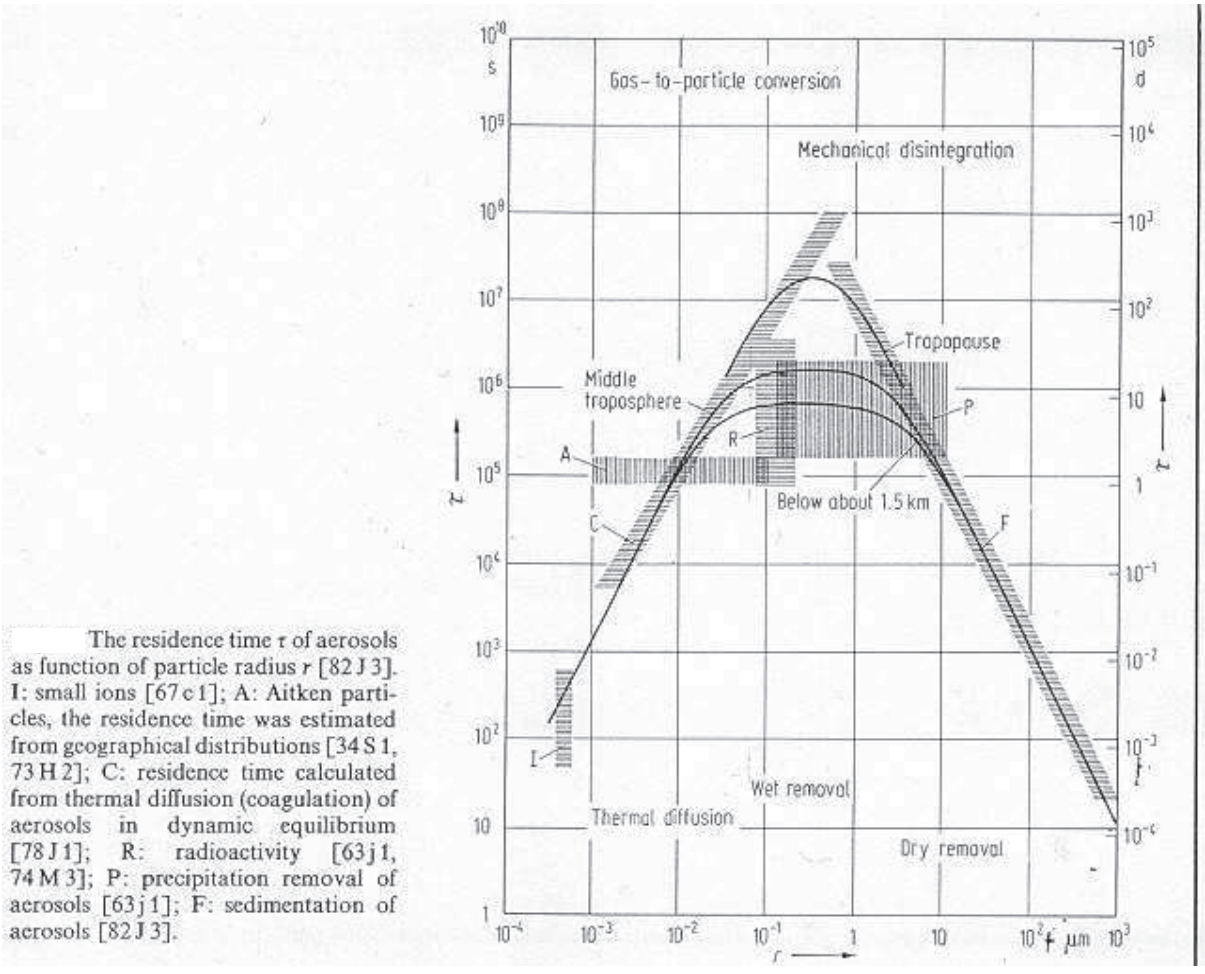

The residence time τ of aerosols as function of particle radius r [82 J 3]. I: small ions [67 c 1]; A: Aitken particles, the residence time was estimated from geographical distributions [34 S 1, 73 H 2]; C: residence time calculated from thermal diffusion (coagulation) of aerosols in dynamic equilibrium [78 J 1]; R: radioactivity [63 j 1, 74 M 3]; P: precipitation removal of aerosols [63 j 1]; F: sedimentation of aerosols [82 J 3].

figure 1.3: residence time of particles as function of their diameter in low and medium troposphere and in the tropopause **[*Jaenicke, 1986*]**

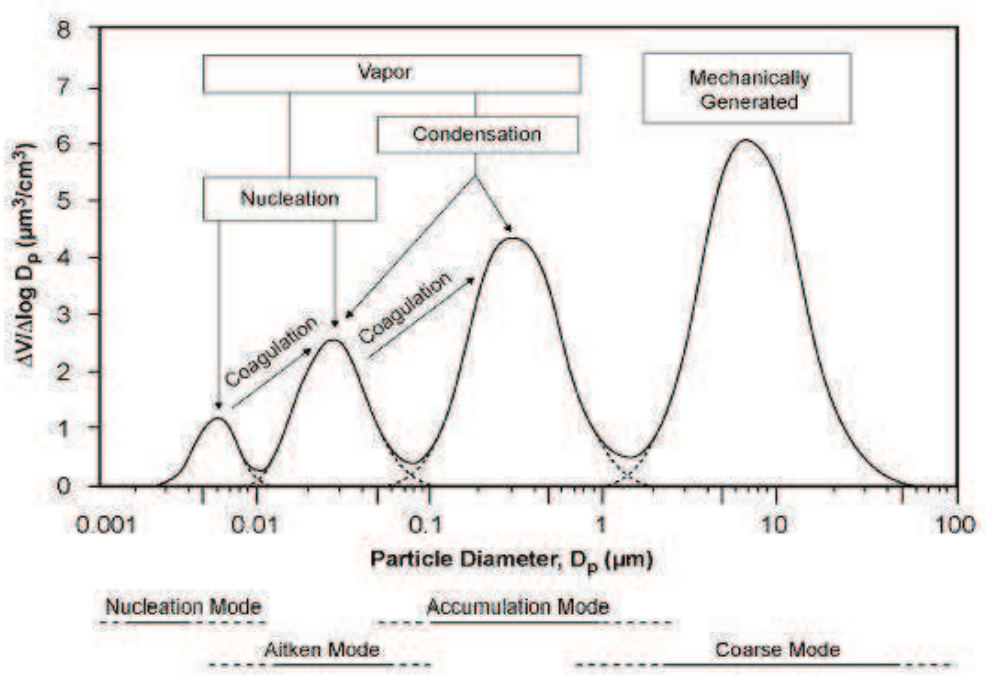

figure 1.4: particle size distribution

Whitby also found that the best curve fitting experimental data was a sum of log-normal functions. The log-normal function is defined as:

$$\frac{dn(r)}{dr} = \frac{n_0}{r \cdot \ln\sigma_g \cdot \sqrt{2\pi}} e^{-\left(\frac{\ln r - \ln r_m}{2 \ln\sigma_g}\right)^2} \qquad (1.1)$$

where:

n(r) = number of particles per unit volume as function of their size (part/cm^3)

n_0 = number of particles per unit volume (part/cm^3)

σ_g= geometric standard deviation ($\sigma_g = e^{\sigma\{\log x_i\}}$)

r_m= median distribution radius (usually in μm)

It is usually represented in bi-logarithmic scale because the parameters to be represented span different orders of magnitude.

If number distribution is available (e.g. measured using Optical Particles Counters, which select particles depending on their optical diameter), area and volume distribution can be easily calculated considering spherical particles:

$$\frac{dS}{d\log D} = \frac{dN}{d\log D}\pi D^2 \quad \text{and} \quad \frac{dV}{d\log D} = \frac{dN}{d\log D}\frac{\pi}{6}D^3 \text{ (see figure 1.5).}$$

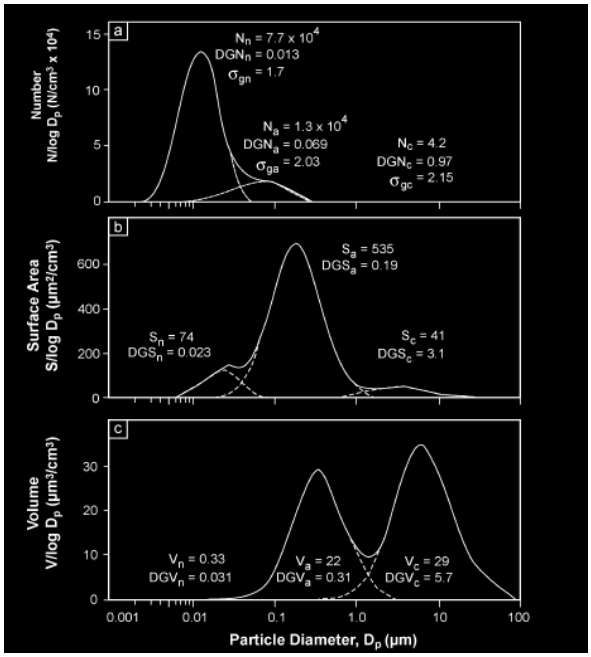

figure 1.5: distribution of coarse, accumulation and nuclei mode particles by: a) number, b) surface, c) volume for average continental size distribution. DGV/DGS/DGN= geometric mean diameter by volume/surface area/number

It is also noteworthy that ultra-fine particles dominate in the number distribution, while volume (and thus mass) distribution is strongly affected by coarse particles, because the mass is directly related to the volume, which depends on r^3. As ultra-fine particles contribution to the measured mass is very low, it can be useful to carry out number concentration measurements, even if, up to now, available epidemiological studies do not report the number concentration as a better indicator for particulate health effect than the mass concentration [Harrison, 2004].

Starting from volume distribution and assuming a hypothetical (but realistic!) value for the average particles density, a rough estimate of the mass distribution can be obtained multiplying the volume distribution times the density. It is noteworthy that the density of particles forming atmospheric aerosol is usually in the range 0.5-6.5 g/cm^3, with an average value usually of about 2 g/cm^3. Thus, the hypothesis on the density value is very strong as it can negatively affect the calculated distribution. On the contrary, direct measurements of mass distribution can be obtained sampling the aerosol on suitable substrates, which can be weighed before and after the sampling to have information about the mass of the particles collected. Furthermore, analytical techniques can be applied to determine particles composition.

In the last decades, atmospheric aerosol has been studied after size-segregation to

understand particle-health interaction. Size cuts have been chosen depending on the capability of particles with different sizes to penetrate the respiratory system. Moreover, chemical composition is considered important in health effect evaluation. In particular, water soluble components can have a role because they can release metals or other highly toxic compounds, when they come in contact with water inside the body [Viksna et al., 2004].

The human respiratory system can be divided in three main parts: higher (nose, mouth, larynx, and pharynx), tracheal-bronchial region and alveolar region. Particles penetrate respiratory system at different extent depending on their aerodynamic diameter (d_{ae}): particles with 2 μm < d_{ae} < 5 μm reach tracheal-bronchial region, while those with d_{ae} < 1 μm can reach alveoli (see figure 1.6). Standard sampling cut-off diameters were chosen and legislative restrictions were developed for two important classes of particles, i.e. PM_{10} e $PM_{2.5}$ [EPA, 2004; CEN 2008].

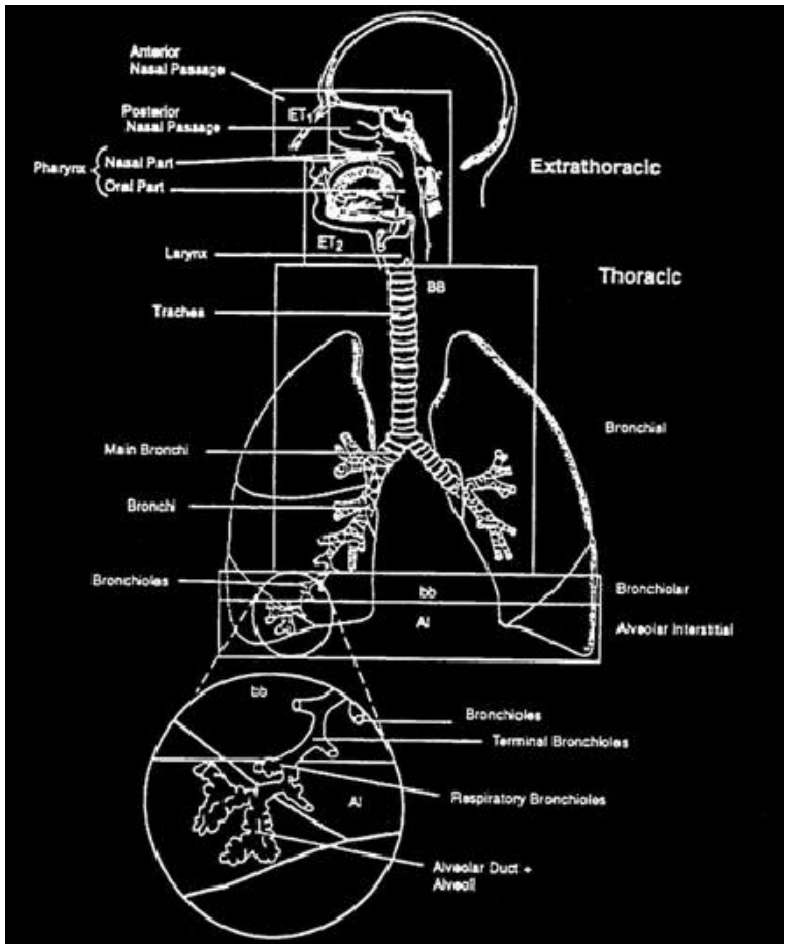

figure 1.6: anatomical regions of respiratory tract

PM_x refers to particles collected by a sampling device that collects 50% of x μm aerodynamic diameter particles. However, size fractions are defined not merely by the 50% cut point, but by the entire penetration curve. Examples of penetration curves are given in figure 1.7. Samplers with the same 50% cut point, but differently shaped penetration curves, would collect different fractions of PM.
In the USA, rules establishing limit values for both PM_{10} and $PM_{2.5}$ exist since 1997. In Europe, the EN12341 [CEN, 1998] and EN14907 [CEN, 2005] technical notes indicate sampling and data analysis methodology; limit values for PM_{10}. Limit values for PM10 and $PM_{2.5}$ are reported in the 2008/50/EC directive [CEN, 2008].

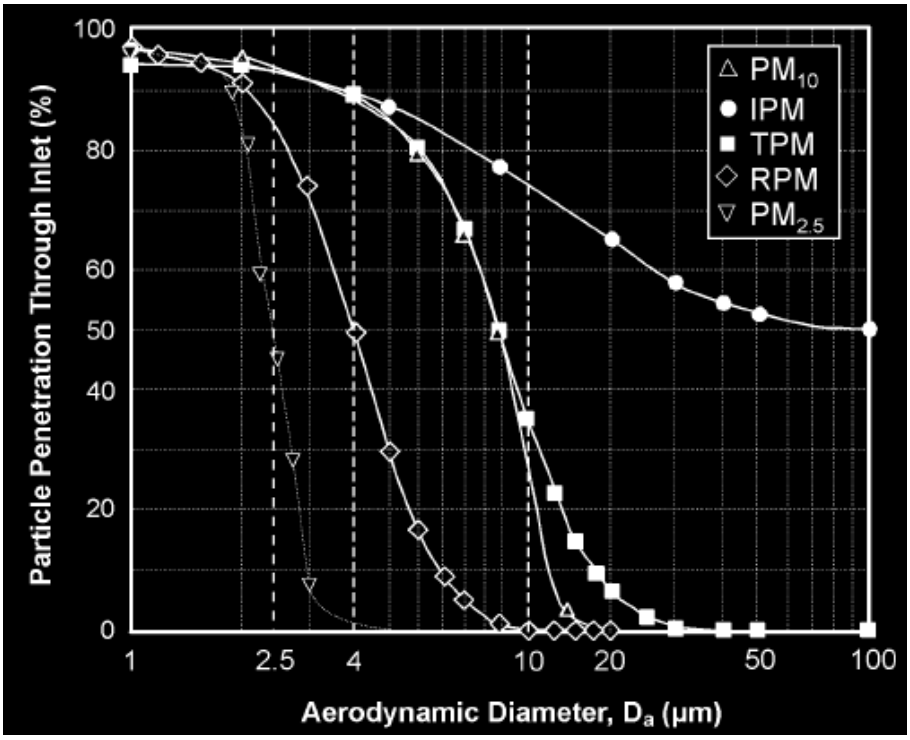

figure 1.7: particle penetration (size-cut curves) through an ideal (no-particle-loss) inlet for five different size-cut selective sampling criteria: PM2.5, PM10, inhalable particulate matter (IPM), thoracic particulate matter (TPM) and respirable particulate matter (RPM) size cuts

Aerosol can also be sampled using multistage cascade impactors: these instruments select particles depending on their aerodynamic diameter in different size ranges. The separated particles can be then analysed for their mass (see figure 1.8) or for their composition (e.g. elemental composition, ionic content). These samplings and the following analyses are of particular interest because all aerosol effects depend both on particles size and composition.

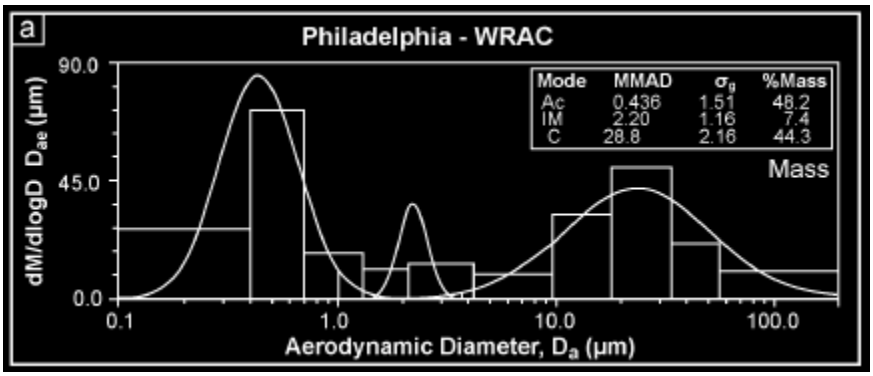

figure 1.8: example of impactor mass size distribution and log-normal fitting

Aerosol composition is another parameter of great interest. Composition is strongly influenced by emission sources. They can be mainly divided into natural and anthropogenic.

Among natural sources, the most important are [Seinfeld and Pandis, 1998]:

a) *erosion and re-suspension of the lithosphere:* this component is due to atmospheric agents (wind, rain) and its importance depends on atmospheric phenomena intensity. These processes usually generate big particles, with irregular shapes and containing typical crustal elements (Al, Ca, Fe, Si, Ti, Sr, Mg…), as well as traces of organic compounds, Th and REE (Rare Earth Elements);
b) *marine aerosol:* it is mainly composed by inorganic salts (NaCl and other sea water trace elements, i.e. Mg, Ca, K, Br, I); an important secondary contribution can be ascribed to DMS (Dimethyl sulfide) conversion into sulphates, iodine oxidation, and formation of secondary organic aerosol [O'Dowd and de Leeuw, 2007];
c) *volcanoes emission*: volcanoes emit many gaseous species in the atmosphere. They can then undergo chemical reactions and be converted into solid compounds (e.g. SO_2 to sulphate). Moreover, also metal emissions are characteristic, especially Cu, Zn, Pb;
d) *forest combustion*: usually small particles are emitted. They contain elements such as K, Mg, Na, Ti, Ca and organic compounds (such as levoglucosan).

Among anthropogenic sources, the following should be mentioned:

a) *energy production*: particles emitted by power plants based on combustion oils are typically composed by S, V, Ni, and they have a strong negative effect on human health [Ghio et al., 2002]. Sulphur is mainly emitted in gaseous form (SO_2), but it rapidly converts into sulphate, generating fine particles [Seinfeld and Pandis, 1998]. Primary sulphate emissions, on the contrary, are usually in the coarse fraction [Berresheim et al., 1995]. As regards power plants fuelled with coal, the main combustion product is C, emitted together with other elements (e.g. S, As, Fe, Se…) due to fuel combustion impurities.

b) *industry*: typical combustion products (containing carbon and nitrogen) are coupled to other tracers specific for different industrial processes. As an example, iron and steel industry usually emit Fe, Pb, Zn, C, Si, Ca, Mg; chemical and petrochemical industries usually emit organic sulphur compounds, heavy metals and hydrocarbons; metallurgic industry produces metal oxides, while cement factory and glass and ceramic industry emit particles containing silicates and carbonates as well as sulphur gases. Ceramic industry emits also heavy metals like Hf, U e Th, but they have only a very local influence [Querol et al., 2001];

c) *domestic heating*: usually it generates small particles, with variable composition depending on the fuel used and on its impurities. The most common elements are C, S, V; however, the widespread use of methane as domestic fuel has fostered an important reduction in particles emission.

d) *transports*: combustion in the engines generates small particles, whose composition depends on the fuel. Diesel vehicles emit 90% of carbonaceous material; vehicles equipped with catalytic converters typically emit Pt, Pd, Rh, hydrocarbons and other carbonaceous species, while in the past vehicles powered by leaded petrol mainly emitted Pb, Br, nitrates, non-combusted hydrocarbons and other organic compounds.

   Besides emissions by engines, also re-suspended dust as well as brake and tyre wear particles have to be considered. Traffic contribution to dust re-suspension has been evidenced by the correlation between Pb peaks (when

leaded petrol was still used) and crustal elements peaks often verified during rush hours, and by the reduction of the contribution of mineral dust to atmospheric aerosol during the weekends [Marcazzan et al., 2002]. As regards brake wear, they contain elements like Fe, Cu, Cr, Sb, Ba, Mo [Weckwert, 2001; Sternbeck et al., 2002; Lough et al., 2005]. Also tyre wear leads to the formation of particles (in the coarse fraction) mainly composed of carbon compounds and inorganic material containing Zn, Ca, Fe, S, Al, Ti, K, Pb, Mg [Salma and Maenhaut, 2006]

e) waste incinerators: they produce small particles (generally < 2 μm) principally made of Zn, K, Cl, together with other elements, depending on the material burnt.

It is noteworthy that the existence of a physical-chemical fingerprint for the different sources is the basis for the application of receptor models for source identification and apportionment starting from in-situ measured data.

Chapter 2: Set-up of an ED-XRF spectrometer for size-segregated aerosol analysis.

As already mentioned, aerosol effects at both local and global scale depend on particles size and chemical composition. In fact, their ability to penetrate into the airways depends only on their size, but their impact on health is strongly related to reactivity and toxicity of the particle components [Pope et al., 2002]. At global scale, particles size and composition play a key role in light scattering and absorption as well as in clouds formation [Ramanathan et al., 2001]. In addition, a detailed chemical characterisation of size-segregated aerosol can be useful for accurate source identification and apportionment. Indeed, the same aerosol component can be emitted by sources with different size-profiles, and the analysis of size-segregated aerosol composition can help in resolving the contribution given by different sources.

Thus, the knowledge of size segregated elemental concentrations in atmospheric particulate matter (PM) can be a useful contribution to the complete chemical characterisation and to a more detailed source apportionment. Size-segregated PM composition is commonly measured in the 0.01-10 μm range by multi-stage cascade impactors [Hillamo and Kauppinen, 1991; Marple et al, 1991; Maenhaut et al., 1996]. In the literature, different techniques are reported to detect trace elements deposited on impactor substrates; among the most diffused there are PIXE (Particle Induced X-Ray Emission), which is not-destructive but can be performed only at an accelerator facility [Johansson and Campbell, 1988], and ICP-MS (Inductively Coupled Plasma Mass Spectrometry), which needs sample pre-treatment and it is completely destructive [Grohse, 1999].

In this work, an ED-XRF (Energy Dispersive X-Ray Fluorescence) spectrometer was set-up to quantify the elemental concentration on the peculiar samples obtained by a Small Deposit Impactor (SDI) – Dekati multi-stage cascade impactor. Some peculiar features of the samples obtained by this impactor (a different deposition pattern in each stage, an enclosing deposit area of about 0.5 cm^2, and the small

amount of PM collected in each stage/sample) required the development of a specific methodology to suitably set-up the ED-XRF spectrometer. The application of this methodology allowed the determination of the ED-XRF sensitivity curve necessary to quantify elemental concentrations. As ED-XRF is not commonly applied to this kind of samples, an inter-comparison with PIXE was carried out and a very good agreement between data obtained with these two techniques was obtained.

ED-XRF is easier-to-manage than PIXE; moreover, the access to accelerator facilities is not always possible and the available beam time is usually quite limited. In summary, the possibility to carry out an ED-XRF analysis on multi-stage cascade impactor samples can be important for a widespread use of these samplers.

In this work, a wintertime campaign was also carried out in Milan and the data of elemental concentration on size-segregated aerosol were obtained as a first test of the methodology on real samples. However, further work is needed to perform source apportionment using impactor data.

2.1 Theoretical background and experimental devices

2.1.1 Aerosol dynamics

A particle moving in a viscous fluid with $\vec{u}_0$ is subject to a drag force that can be calculated starting using the Navier-Stokes equation referred to incompressible fluid ($\mathrm{div}\,\vec{u} = 0$):

$$\rho \frac{D\vec{u}}{Dt} = -\mathrm{grad}\, p + \eta \nabla^2 \vec{u} \tag{2.1}$$

where ρ is the fluid density, $\vec{u}$ is the velocity field, p is the fluid pressure and η is the fluid viscosity [Vincent, 1989]. It is noteworthy that incompressible condition does not requires that the air is uncompressible, but that it is not significantly compressed when moving around a particle.

The Navier-Stokes equation is derived from the application of the Newton's second law to a fluid element. It is a balance of body, viscous, and pressure forces acting on a unit volume of the fluid.

Defining the characteristic fluid velocity u_0, the characteristic dimension of the system (i.e. the particle diameter D_p), and the characteristic pressure of the system (p_0), the equation 2.1 can be re-written as:

$$\frac{D\vec{U}}{D\tau} = -\text{grad}_{\chi} P + \frac{1}{Re}\nabla_{\chi}^{2}\vec{U}, \tag{2.2}$$

where $\vec{U} = \frac{\vec{u}}{u_0}$, $\vec{\chi} = \frac{\vec{x}}{D_p}$, $\tau = \frac{t\,u_0}{D_p}$, $P = \frac{pD_p}{\rho u_0^2}$, and $Re = \frac{\eta}{\rho D_p u_0}$ is the Reynolds number of the system. It represents the ratio between viscous and inertial forces acting on the fluid element.

Stokes solved the equation in the following conditions:

a) Re<<1: viscous forces dominate inertial forces,
b) the particle can be assumed as a rigid sphere,
c) the motion of the particle is constant with $|\vec{u}| = u_0$
d) there is no slipping on the particle surface.

Solving the equation 2.2 under these conditions it can be found:

$$\left|\vec{F}_{Drag}\right| = -3\pi\eta D_p u_0 \tag{2.3}$$

It should be noticed that Re<<1 is nearly always true for particles lower than 10 μm (e.g. for 10 μm particles falling with their terminal velocity in air @ 25°C Re=0.0025). It is also noteworthy that when particle size is comparable to the mean free path of air λ (about 65 nm @ 25°C), the no-slipping condition cannot be considered satisfied anymore and the effective F_{Drag} is lower than predicted. A slip correction factor C_c is thus included in the formula 2.3:

$$\left|\vec{F}_{Drag}\right| = -\frac{3\pi\eta D_p}{C_c} u_0 \tag{2.4}$$

where $C_c = 1 + \frac{2\lambda}{D_p}\left[1.257 + 0.4\exp\left(-\frac{1.1 D_p}{2\lambda}\right)\right]$.

If a particle falls in a still fluid, it is subject only to gravity and F_{Drag}. So it can be written [Hinds, 1999]:

$$m\frac{d\vec{v}}{dt} = m\vec{g} - \frac{3\pi\eta D_p \vec{v}}{C_c}. \tag{2.5}$$

Defining the relaxation time T_0

$$T_0 = \frac{m C_c}{3\pi\eta D_p} \tag{2.6}$$

and time-integrating 2.5 in the vertical direction considering $v_0=0$ it can be found

$$v_z(t)=T_0 g[1-\exp(-t/T_0)]. \tag{2.7}$$

Furthermore, if the particle is moving in a fluid ($v_0=V$) and it is subject only to F_{Drag}, the maximum travelled distance (named Stopping Distance) is

$$S=VT_0 \tag{2.8}$$

So far, we considered a particle moving in a still fluid. If the fluid is moving, higher-order approximations have to be considered.

Small particles with negligible inertia will follow the fluid motion. On the contrary, large and heavy particles will continue their motion on a straight line. It is interesting the analysis of the motion of particles laying between these extremes. To this aim, it is necessary to define the fluid motion around an obstacle. The analysis is usually numerically performed, except for very regular shapes (spherical, cylindrical). Curvilinear motion is characterised by a dimensionless number called Stokes number (Stk). It is represented by the ratio between the stopping distance (S, see formula 2.8) and a characteristic dimension of the obstacle L.

$$Stk = \frac{S}{L} = \frac{T_0 V}{L}. \tag{2.9}$$

When Stk<<1 the particle will easily follow the streamlines; on the contrary if Stk >>1 the particle will move on a straight line when the gas turns around the obstacle. The Stokes number is useful to characterise the inertial impaction (i.e. the inertial transfer of a particle to a surface).

2.1.2 The inertial impactor

The inertial impactor operates on the following principle: the air (including the suspended particles) is passed through a nozzle and the output stream (jet) is directed against a flat plate (impaction plate). The impaction plate deflects the flow and 90° streamlines are formed. Particles with small inertia will follow the streamlines, while bigger, heavier particles will impact on the impaction surface (and it is assumed they stick on it) (see figure 2.1) [Hinds, 1999].

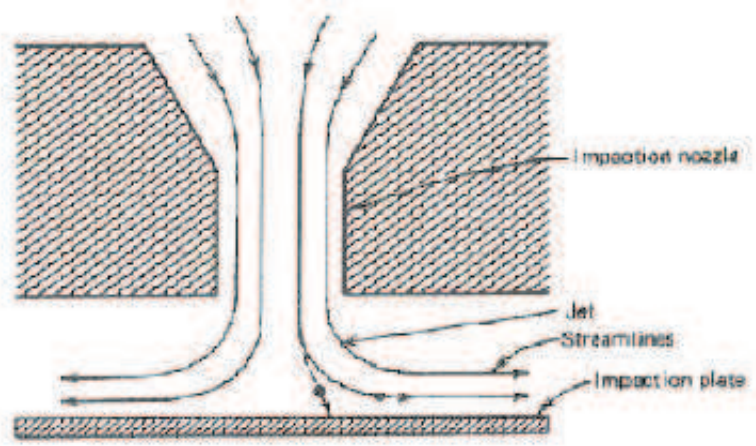

figure 2.1: cross-sectional view of an impactor

The parameter governing collection efficiency is Stk, in this case defined as the ratio of the particle stopping distance at the average nozzle exit velocity (U) and the jet radius ($D_j/2$):

$$Stk = \frac{\rho_p d_p^2 U C_c}{9\eta D_j} \tag{2.10}$$

Impaction efficiency E_I is function of Stk (and thus of d_p^2), but no simple relationship can be found between these parameters. For a given particle size, particle trajectories are determined by Navier-Stokes equation for each streamline. The efficiency for a specific particle size is thus dependent on the fraction of trajectories intercepting the impaction plate. Collection efficiency for a plate is usually plotted as a function of $(Stk)^{1/2}$ (see figure 2.2). Experimental calibration requires efficiency measurements carried out using mono-disperse aerosols.

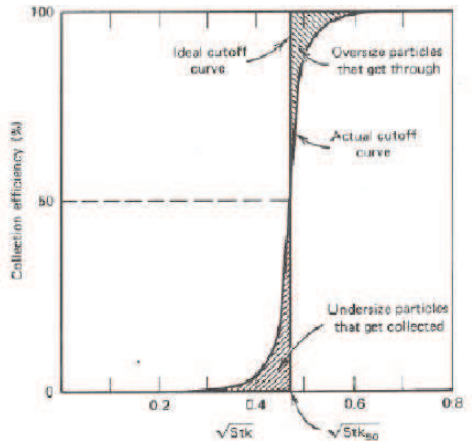

figure 2.2: Actual and ideal cut-off curve

It is noteworthy that streamlines at the nozzle exit are not strongly influenced by the

spacing between the nozzle and the plate because the jet of aerosol expands only slightly until it is at about one jet diameter distance from the impaction plate.

For most impactors, when cut-off curve is sharp enough to approach the ideal step-function efficiency curve for particle classification (all the particles greater than a specific aerodynamic size are collected and all the smaller particles pass through), only the cut-off size of the ideal curve is indicated. Thus, the efficiency curve of well-designed impactors can be described by a single number Stk_{50} (0.24 for a circular jet). From the previous equation, the cut-off aerodynamic diameter (d_{50}) can be expressed as:

$$d_{50}\sqrt{C_c} = \left(\frac{9\eta D_j (Stk_{50})}{\rho_p U}\right)^{1/2} \tag{2.11}$$

There are design criteria to produce a sharp cut-off curve with an impactor. Reynolds number of the gas flow in the nozzle should be between 500 and 3000. The ratio of the separation distance between the nozzle and the impaction stage should range from 1 to 5 for circular nozzles.

Sub-micrometer cut-off diameters require small diameter nozzle operating at high velocity. Another approach, which allows to reach cut-off d_{50} down to 0.05μm, is the low-pressure impactor. It operates at very low pressure (3-40 kPa). This strongly increases the slip correction factor, thus allowing a strong reduction in cut-off diameters.

2.1.3 Cascade impactor

The inertial impactor separates particles in two fractions. If a more detailed size-segregation is needed, several impactors can operate in series (multistage cascade impactor), provided that they are arranged in order of decreasing cut-off sizes (obtained varying nozzles width). The sequential impaction separates particles in contiguous groups of particles according to their aerodynamic diameters.

If cut-off sizes for the different stages are far enough for cut-off curves not to overlap, sharp separation between different size-classes will be obtained and the different parameters can be directly plotted as a function of the cut-off size. On the contrary, data inversion will have to be carried out as explained in paragraph 2.1.5.

2.1.4 SDI-Dekati Low Pressure Impactor

In this work a Dekati Low Pressure-Small Deposit Area Impactor (SDI) multistage sampler was used to collect size-segregated samples [Maenhaut et al., 1996]. This multistage impactor allows the separation of the particles in 12 size classes from 45 nm to 8 μm (in our impactor real cut-off diameters (d_{50}) are 0.0479, 0.0897, 0.1548, 0.235, 0.349, 0.598, 0.804, 1.07, 1.68, 2.70, 4.12, and 8.57 μm). Low-size cut-off diameters can be obtained using reduced pressure and high jet velocities [Hillamo and Kauppinen, 1991] (in our impactor: 135 mbar at the lowest stage @ 11 l/min). Samples were collected on coated Kapton foils (actually, other thin materials as polycarbonate films can be also used), which are supported by 25 mm rings. Kapton foils are coated by a suitable grease (Apiezon) to avoid particle bouncing on the impaction surface during the sampling, thus negatively affecting the measured size distributions. Using SDI impactor, PM is collected in non-uniform, point-like deposits enclosed in an 8 mm-diameter area (e.g. figure 2.3).

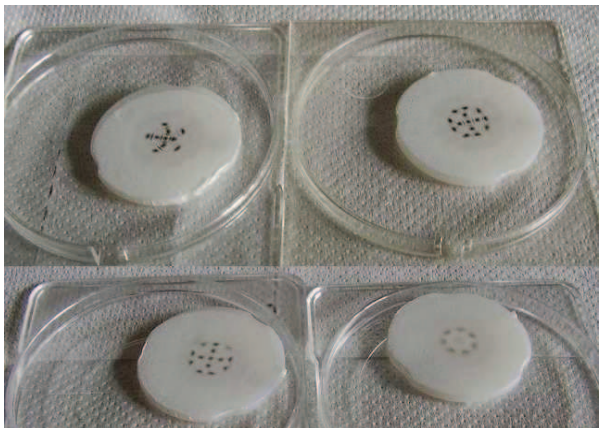

figure 2.3: examples of deposits collected by SDI impactor on different stages

As deposits are non-uniform, our ED-XRF spectrometer had to be suitably set-up to allow elemental analysis (see par. 2.2)

2.1.5 Cascade impactor data representation and inversion

When a set of samples from a cascade impactor is analysed, the results are first represented as histograms of $\Delta m/\Delta(\log D_{50})$ vs. D_{50}, where m is the mass concentration (in ng) of an element on each impactor stage and D_{50} is the cut-off diameter of the stage (see figure 2.4).

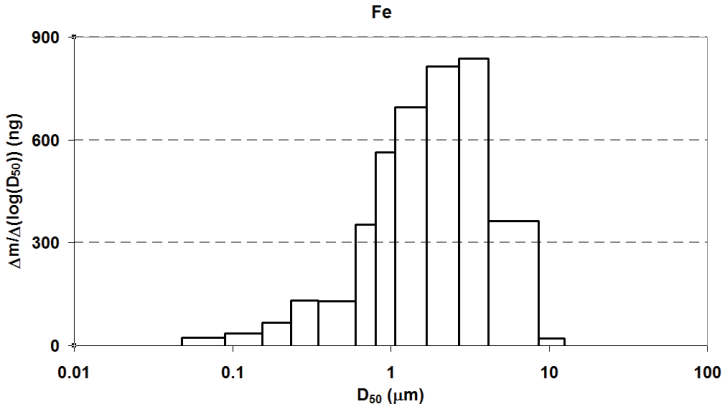

figure 2.4: example of histogram representation of SDI data

However, it must be considered that cut-off curves are not ideal and they partially overlap (see figure 2.5); thus, on each stage also particles of sizes nominally belonging to other stages can be collected. Therefore, data inversion is needed to give the correct representation of the measured data.

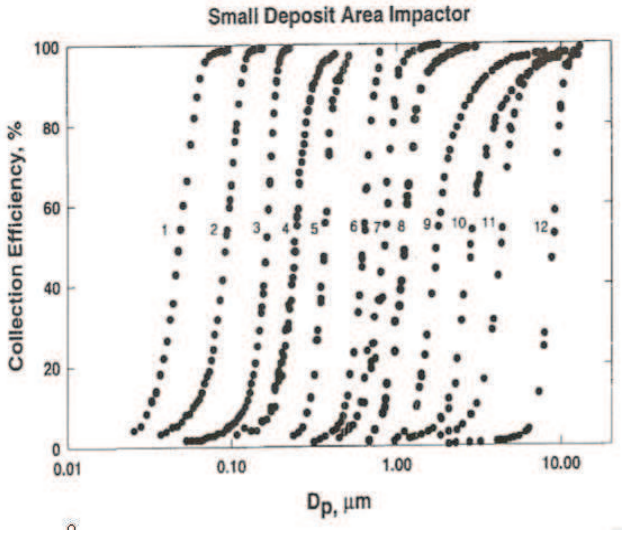

figure 2.5: SDI cut-off curves

In this work, data inversion was carried out using the program MICRON [Wolfenbarger and Seinfeld, 1990]. It is an inversion algorithm based on regularisation, enabling to obtain smoothed size distributions that are faithful to the measured data. Uncertainties on the measured data and cut-off curves are also taken into account to perform a more reliable inversion.

An example of the inverted function is presented in figure 2.6. In the figure, D_{50} was changed into a more generic particle diameter D_p, as the inverted function is semi-continuous.

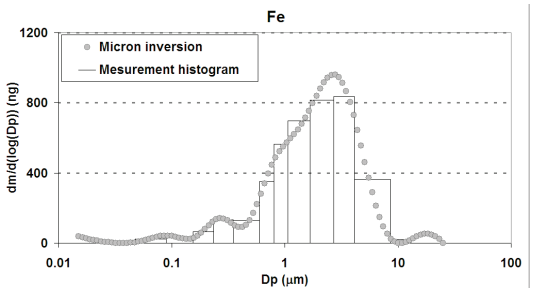

figure 2.6: example of SDI data and inversion by MICRON

The inversion function is then further interpolated using log-normal functions, in order to reproduce the standard aerosol representation based on modes (see figure 2.7). Indeed, with reference to formula 1.1, the log-normal mass distribution can be defined (as function of particle diameter D_p) as:

$$\frac{dm(D_p)}{d\log(D_p)} = \frac{m_0}{\ln\sigma_g\sqrt{2\pi}} e^{-\left(\frac{(\ln D_p - \ln D_m)^2}{2(\ln\sigma_g)^2}\right)}$$

where:

m (D_p)= particle mass concentration as function of their size

m_0 = particle mass concentration

σ_g= geometric standard deviation ($\sigma_g = e^{\sigma\{\ln D_p\}}$). It is dimensionless, and ≥1.

D_m= median distribution diameter (usually in μm)

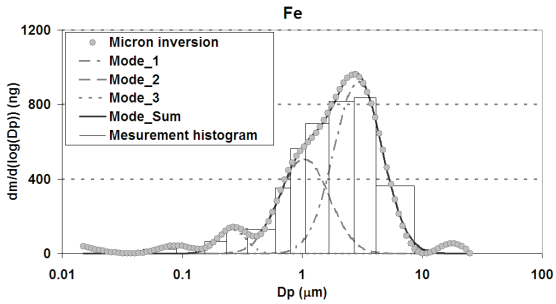

figure 2.7: interpolation of the inverted function using log-normal curves

2.1.6 ED-XRF technique

Energy Dispersive X-Ray Fluorescence (ED-XRF) is an analytical technique used in this work for elemental analysis of atmospheric aerosol. The main advantages of this technique are:

1) it is multi-elemental (for Z > 11 elements)
2) it is highly sensitive (< 10 ng/cm^2 for most elements)
3) no sample pre-treatment is required
4) it is not destructive.

The last two features are particularly useful when more than one type of analysis has to be carried out on the sample.

The ED-XRF analyser is based on the emission of characteristic rays by an atom, after it is ionised by an incident radiation (in our case X-ray beam generated by Coolidge tube with an Ag anode). Once ionised, the atom returns to the original configuration by electronic cascade transitions from some higher shell to the vacant electron site. Such electron transitions imply a well defined loss of energy of the atomic system, therefore X-rays are emitted with characteristic energies which depend on the energy difference between the atomic levels of the transition. As atomic levels (and the probability for a transition to occur) are well defined for each atom, the emitted photons are characteristic for each atom and they allow the identification of the elements in the sample. All X-ray emissions as well as relative intensities are known, thus the elements in the sample can be easily identified once the instrument is calibrated in energy.

ED-XRF instrumentation is mainly composed by a primary X-ray source for sample excitation and by a detector (and electronic chain) for characteristic X-ray detection. A standard electronic chain processes the signal and allows spectra visualisation.

The X-ray spectrometer used in this work (an ED2000 spectrometer by Oxford Instr. available at our laboratory at the Physics Department of the University of Milan) uses a Coolidge tube as excitation source (ΔV_{max}=50 kV, I_{max}=1mA, Ag anode).

The detector is a Si(Li) detector which converts the energy of the incident photons into current pulses, which are suitably converted, amplified, and analysed by the electronic chain.

The geometry of the analysis is 45° between the Coolidge tube and the sample and 45° between the sample and the detector (90° geometry to minimise the Compton contribution to the spectrum). In front of the detector an 8 μm Be window separates the detector from ambient air. The Be window reduces to 41% of the incident

intensity the X-ray with energy about 1 keV (which corresponds to the highest energy of Na fluorescence emissions, thus preventing the detection of elements lighter than Na) and that is the reason why no X-ray from elements with Z < 11 can be detected.

2.1.7 Quantitative ED-XRF analysis on thin and uniform samples.

Once an element has been identified by the energy of its emission lines, quantification can be carried out. If the sample can be considered a thin sample, i.e. $m\,(g/cm^2) \leq \frac{0.1}{\mu_i\,(cm^2/g)}$ where m is the sample mass and μ_i is the average massive coefficient, matrix effect and secondary/tertiary fluorescence effects can be neglected. In this case, a linear relation between the concentration of an element in the sample and the number of primary fluorescence photons produced per second is found, once the geometry and the characteristics of the incident excitation radiation are set:

$$P_i = m_i G_i,$$

where m_i is the mass of the i^{th}-element and G_i is a factor depending only on experimental setup conditions and on the considered element [AA.VV., 2002].

The quantitative analysis on thin layers requires the determination of the sensitivity curve of the instrument (i.e. the G_i factor), which is performed using suitable standards. In our laboratory, MICROMATTER standards are usually used to this aim. They are prescribed by an EPA protocol [EPA, 1999a] for XRF analyses. They are certified at ±5% and they can be mono or multi-elemental (in our case they contain two elements at most to avoid secondary fluorescence phenomena).

Once the sensitivity curve is determined, it can be validated using a suitable particulate matter standard (SRM2783, Air particulate matter on filter media, i.e. PM2.5 on polycarbonate), whose elemental content is certified by the National Institute for Standard and Technology (NIST). The analysis of the NIST standard in the same conditions used for both calibration and sample analyses and the comparison of the obtained results with certified values allow the validation of the

sensitivity curve.

2.2 Results

2.2.1 Set-up of an ED-XRF spectrometer for quantitative analysis on SDI samples.

Aerosol deposits obtained by the SDI impactor are not uniform, thus the ordinary calibration technique could not be carried out. However, it is noteworthy that all the deposits are enclosed in the same area (in the following called "enclosing area"). Thus it was considered that if all the points of the enclosing area give the same count-contribution to the detector, the sample can be considered as it is uniformly distributed on the enclosing area. This was the starting point for the development of the set-up procedure that followed different steps:

a) identification of the irradiated area in different geometric conditions using GAFCHROMIC dosimetry films;

b) scanning of the irradiated area using a point-like probe material to evaluate the uniformity of the contribution by different points in the sample to the total counts;

c) sensitivity curve determination using suitable elemental standards and validation by NIST standard;

d) inter-comparison between ED-XRF and PIXE results on real size-segregated samples.

So, first of all, different collimators (4, 8, 10, 12 mm diameter, some of which properly realised for this work) were mounted on the tube, and the irradiated area in each condition was identified using GAFCHROMIC foils (generally used for personal dosimetry) (see figure 2.8).

Once the conditions to fully irradiate the enclosing area were identified, a small Ca marker was used to verify the uniformity of the contribution by a single point of the irradiated area to the measured counts (figure 2.9). This was realised scanning the irradiated area with 1x1 mm^2 spatial resolution using the point-like Ca marker and using different collimator on the X-ray tube and the detector until an area with (at

least) 8mm diameter showed a 20%-uniformity in Ca counts (figure 2.10).

figure 2.8: example of a GAFCHROMIC foil after irradiation. The collimator with 10 mm diameter was mounted on the X-ray tube side.

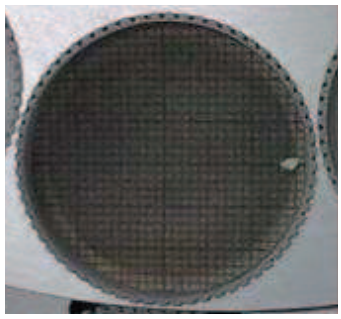

figure 2.9: Ca marker used to determine the counts-uniformity of the irradiated area

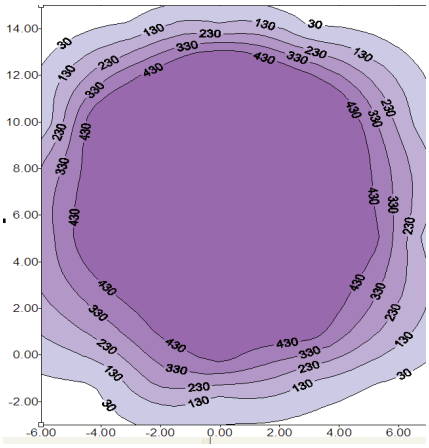

figure 2.10: map of Ca counts for the definitive configuration

figure 2.11: Millipore mask for sample positioning

Once the uniformity area was identified, masks for the reproducibility of sample positioning in this area were realised. To this aim, a mixed cellulose esters filter (Millipore, AAWP type, pore size: 0.8 µm) was punched (hole diameter 8 mm) and suitably marked (see figure 2.11) to act as sample holder. Many blank masks were first irradiated to account for their contribution to the X-ray spectrum.

Also in this case, MICROMATTER standards were used to obtain the sensitivity curve. However, they were punched at 8.8 mm diameter to allow the positioning on the 8 mm hole in the sample holder mask, and then analysed taking into account the possible attenuation due to the mask covering a small part of the standards. The sensitivity curve was validated by the analysis of the SRM2783 particulate matter standard by NIST suitably punched at 8.8 mm diameter. Minimum Detection Limits (MDLs) for polycarbonate filters (NIST blanks) were evaluated in µg per sample (see table 2.2).

All elements with concentrations higher than MDLs (K, Ca, Ti, Cr, Mn, Fe, Ni, Cu, Zn, Pb), except for Mn, were in agreement with the certified concentrations (see figure 2.12) and the regression curve shows a very good correlation between NIST certified and measured concentrations (figure 2.13).

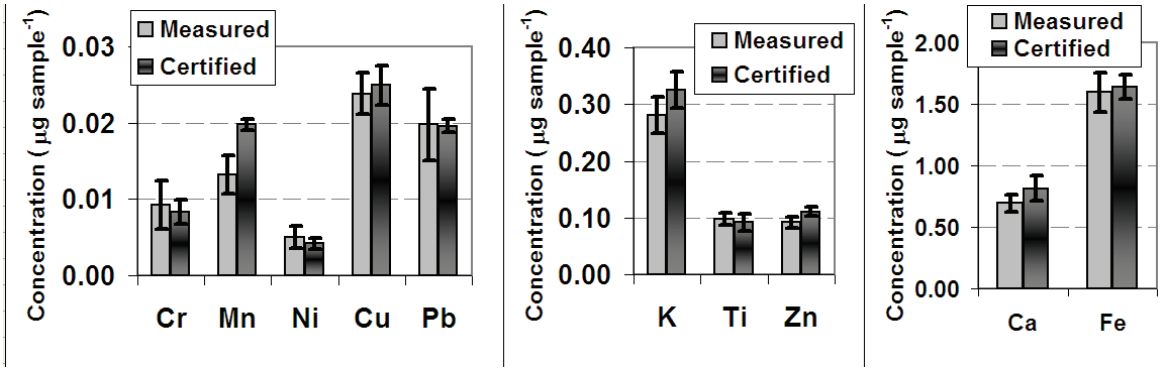

figure 2.12: check on sensitivity curve using NIST standard

The analysis of Kapton foils used in SDI sampling was carried out separating the foils from the supporting rings using a cutter: this was necessary to avoid contaminations in the background spectrum induced by the interaction of the X ray beam halo with the supporting ring. Once separated from the supporting ring, both blank foils and foils with aerosol deposits were analysed (I=800 µA, HV=30 kV, t=3000 s, in vacuum analysis with a thin Ag primary filter) using the sample holder

mask for correct positioning. In this work, ten blank Kapton foils were analysed to obtain an average blank value to be subtracted to sampled Kapton foils. Average values and other statistical parameters for the ten blank foils analysed with this ED-XRF set-up are reported in table 2.1. MDLs were evaluated from the whole counts area in the average blank spectrum and values in μg per sample are reported in table 2.2.

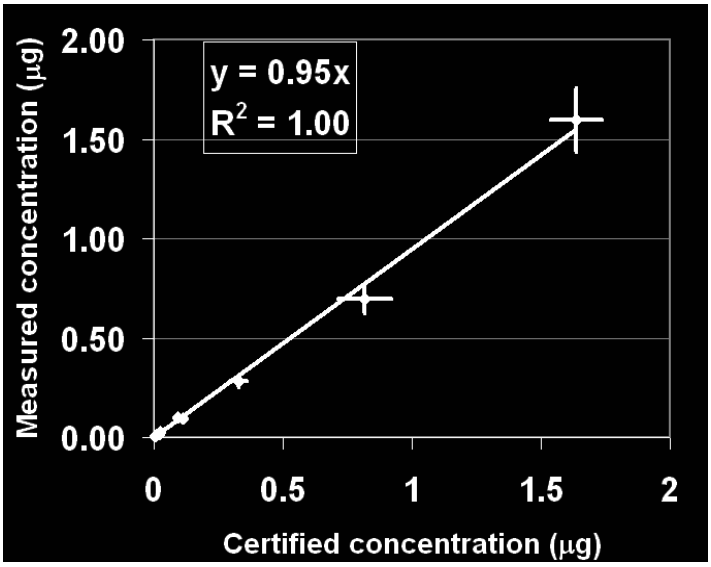

figure 2.13: Certified vs. measured NIST concentrations

	μg per sample			
Element	**Average**	**St. Dev**	**Min**	**Max**
Cl	0.246	0.022	0.219	0.282
K	0.069	0.008	0.055	0.081
Ca	0.443	0.075	0.378	0.603
Ti	0.011	0.002	0.008	0.014
V	<MDL	<MDL	<MDL	<MDL
Cr	0.067	0.004	0.061	0.073
Mn	0.026	0.002	0.023	0.028
Fe	0.120	0.010	0.111	0.141
Ni	0.012	0.000	0.011	0.013
Cu	0.016	0.005	0.012	0.025
Zn	0.041	0.004	0.035	0.047

table 2.1: statistics on the 10 coated Kapton® supports measured for blank evaluation in SDI configuration

	ED-XRF SDI configuration		PIXE SDI configuration
	MDL NIST (µg per sample)	MDL Kapton (µg per sample)	MDL Kapton (µg per sample)
S	0.053	0.070	0.013
Cl	0.045	0.059	0.013
K	0.015	0.021	0.015
Ca	0.015	0.020	0.012
Ti	0.006	0.007	0.005
V	0.004	0.005	0.004
Cr	0.005	0.006	0.002
Mn	0.003	0.004	0.002
Fe	0.005	0.006	0.001
Ni	0.002	0.002	0.001
Cu	0.002	0.002	0.001
Zn	0.002	0.003	0.001
Br	0.003	0.004	0.001
Pb	0.003	0.005	0.002

table 2.2: MDLs evaluated in SDI configuration for polycarbonate (NIST) and Kapton foils for ED-XRF configuration, and for Kapton foils in PIXE configuration (par. 2.2.2)

2.2.2 XRF-PIXE inter-comparison.

To further verify the results obtained in our ED-XRF configuration, an inter-comparison with PIXE analysis was carried out. PIXE measurements were performed at the 3 MV Tandetron accelerator of INFN-LABEC laboratory in Florence. The incident beam (10 nA average) consisted in 3.06 MeV energy protons. Average time of analysis was 1200 s per sample. The beam was collimated to dimensions of 2 x 1 mm^2 and it was homogeneous. A suitable scanning mode for the SDI samples was set up in order to fully analyse the deposit enclosing area. X-rays were collected by two detectors: a Silicon Drift Detector for light elements (Na-Ca), and a Si(Li) optimised for the detection of X-rays in the range 4–20 keV (see figure 2.14); energy resolutions were 145 and 190 eV FWHM at 5.9 keV, respectively. The experimental set-up is described in detail elsewhere [Calzolai et al., 2006]. PIXE spectra were analysed with the GUPIX software [Maxwell et al., 1995].

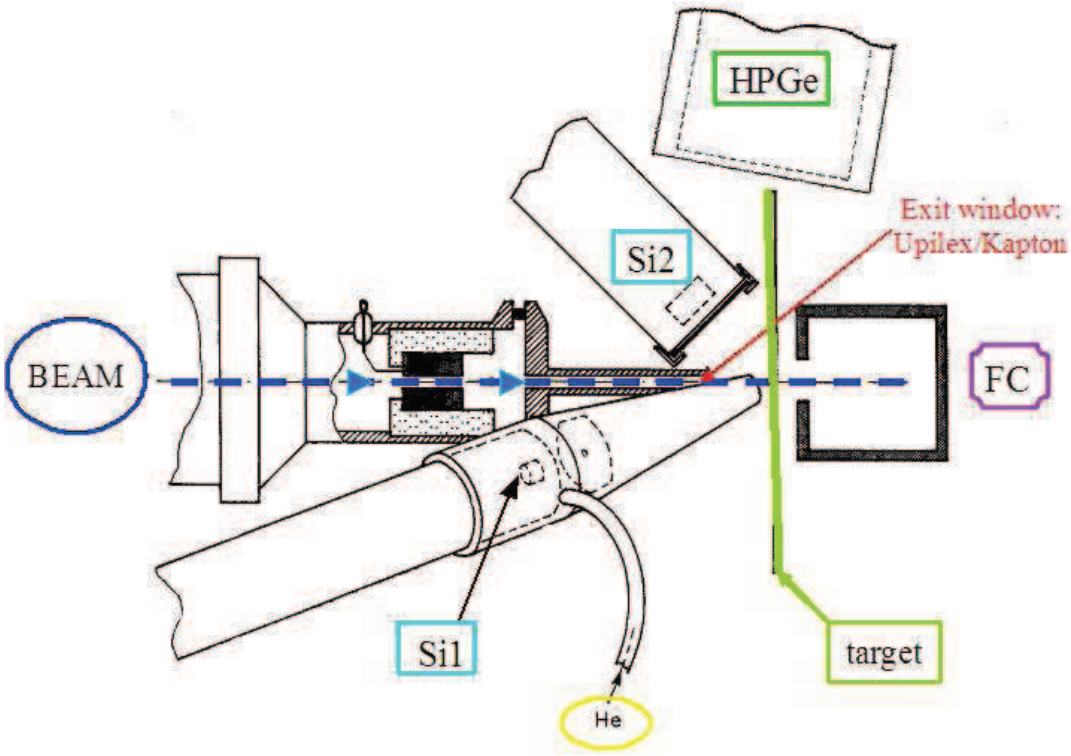

figure 2.14: PIXE set-up scheme @ LABEC-INFN

The inter-comparison with PIXE analysis was carried out on four SDI series (stages 1-12 for a total of 48 aerosol samples) collected in Florence. They were analysed first at LABEC-INFN by PIXE and then in our laboratory by the ED-XRF spectrometer in the SDI configuration. The results obtained in the two laboratories were in good agreement (better than 10%) for most of the detected elements (see figure 2.15).

In figure 2.15, a good agreement between the concentrations measured using ED-XRF or PIXE technique on SDI samples can be noticed. Only elements detected in very low concentration (e.g. V and Ni) show a lower correlation, although ED-XRF and PIXE values are often comparable if error bars are considered. In fact, for low concentrations significant uncertainties on measured values are always registered due to the low statistics in measured counts. The ratio between ED-XRF and PIXE concentration values is generally 1.0 ± 0.1; since the MICROMATTER standards used by the two laboratories to calibrate their set-up belong to different batches, each certified within 5%, this indicate that no significant systematic discrepancy affects the ED-XRF results. The agreement between ED-XRF and PIXE for Mn

data is also noteworthy, indicating that disagreement between ED-XRF and certified Mn values for NIST standard (see figure 2.13) cannot be ascribed to problems in ED-XRF analysis.

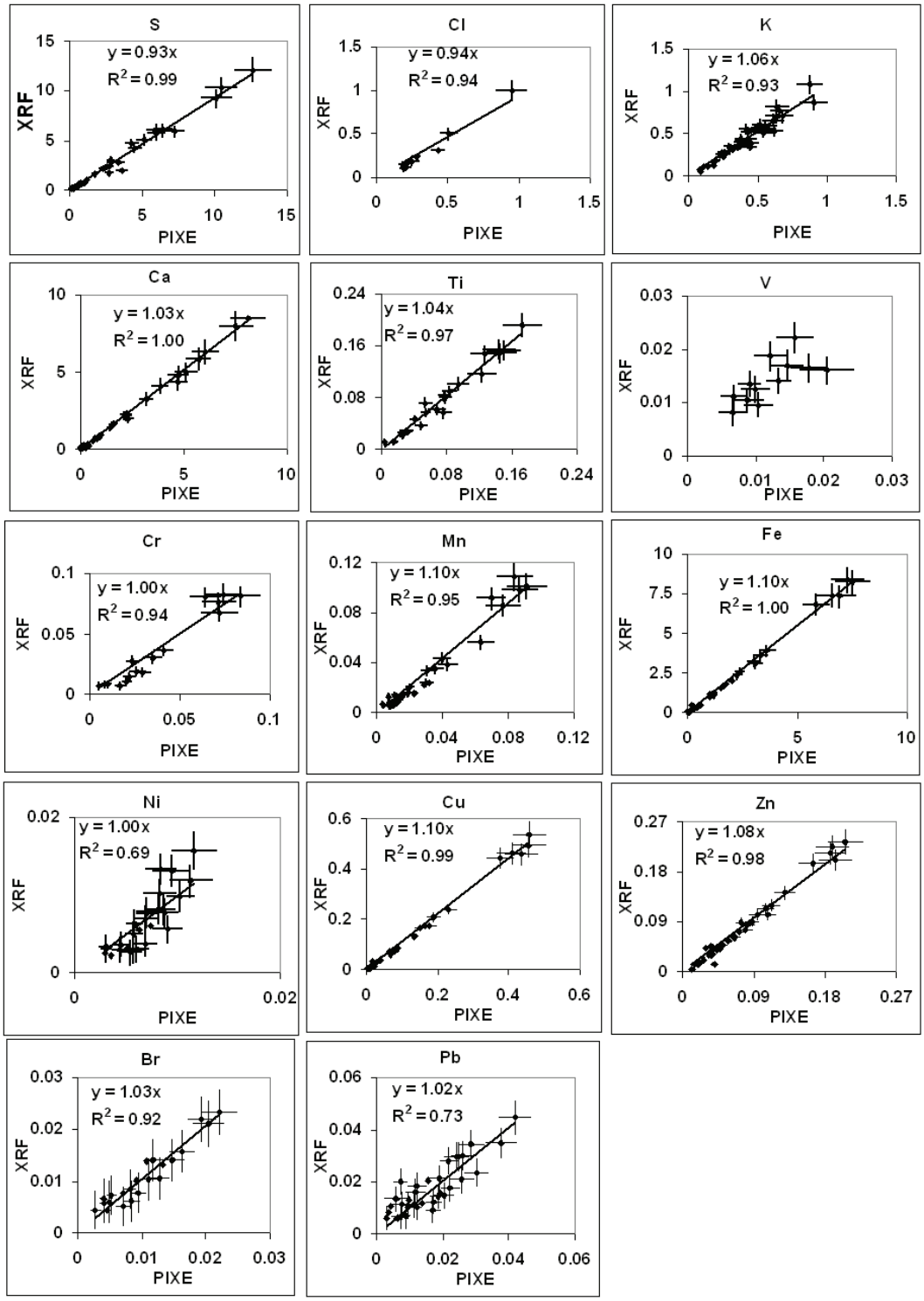

figure 2.15: XRF-PIXE inter-comparison on four SDI series (stages 1-12). On both axis, concentration in µg per sample are represented**.**

In table 2.1, the variability of blank SDI Kapton supports was reported. It could

give problems especially for Ca evaluation. In this case, the advantage of PIXE on ED-XRF analysis is the possibility to analyse not-sampled parts of the Kapton supports for a better blank correction (ED-XRF can not be carried out on small parts of the support). However, good agreement in the inter-comparison results was found and blank variability had a not-significant effect on results; it should be also considered that Ca is one of the elements detected in the highest concentration, so that blank variability had small influence on the final results.

It is noteworthy that PIXE MDLs were lower than ED-XRF, especially for $Z<20$ and PIXE analysis requires shorter times (1200 s) to detect simultaneously elements with $Z>11$ in SDI samples. However, ED-XRF can be considered a good alternative to PIXE in the analysis of size-segregated samples, considering that the results obtained with the two techniques are in very good agreement and that ED-XRF is much more widespread, cheap and easy to use.

Future developments will face the problem of $11<Z<16$ elements, focusing on self-absorption coefficient determination.

2.2.3 Examples of elemental size distributions in Milan

In winter 2009 (21st November - 4th December) a sampling campaign was carried out in Milan at the urban background station located on the roof of the Department of Physics in the University campus.

PM10 daytime (09-18) and night-time (21-06) samplings were performed to obtain a complete chemical characterisation (elements, ions, and organic and elemental carbon); moreover, an SDI impactor was used to carry out 7 measurements of size-segregated particulate matter in Milan. SDI supports were analysed using the ED-XRF spectrometer set-up previously described.

In the following, examples of measured elemental size distributions and inverted data for the 24 hours sampling will be presented. The presented elements have been identified as tracers for some important sources in Milan (see par. 3.3.2).

In table 2.3, data concerning the identified modes for the selected elements are shown. It is noteworthy that at least one mode for $d > 1$ μm was detected for all the elements. No mode in the sub-micron range was identified for Ca and Ti.

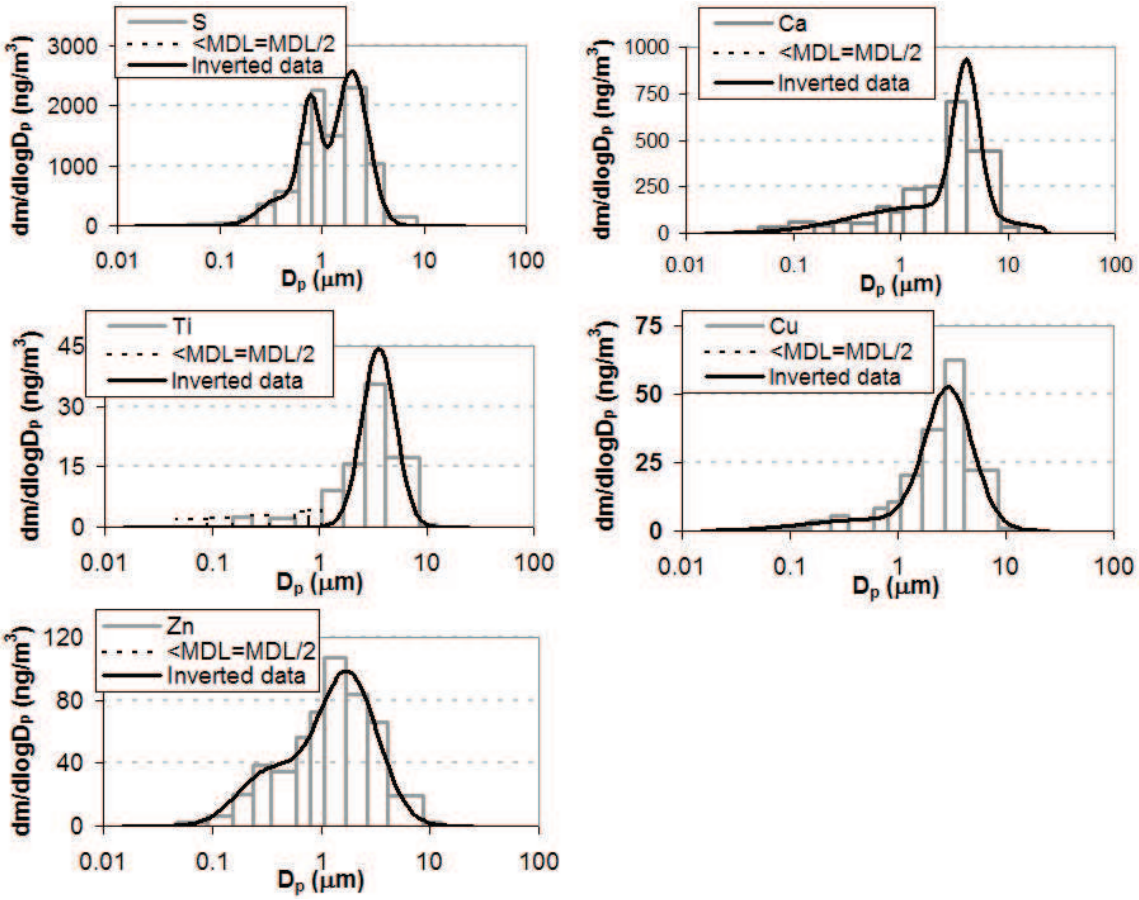

figure 2.16: examples of 24-hours size distributions obtained by SDI cascade impactor in winter 2009

Element	Series 7 (24 hours sampling)		
	diameter (µm)	sigma	amplitude (ng/m^3)
S	0.40	1.59	455
	0.77	1.25	1927
	1.97	1.44	2585
Ca			
	1.58	4.35	141
	4.10	1.31	826
Ti	3.58	1.43	45
Cu	0.58	4.05	4
	2.95	1.66	50
Zn	0.33	1.93	34
	1.75	1.87	97

table 2.3: 24-hours mode data for the selected elements

This was the first study in Milan area on size-segregated aerosol composition down to 40 nm and these samples were useful to test the ED-XRF methodology set-up. Further campaigns have to be carried out in order to gain complete information on

elemental size distributions and on their link to emission sources and atmospheric processes in Milan area. In fact, is useful recalling that differences in the modal distributions have to be ascribed to different particle sources or atmospheric processes involved in particle formation.

It is also noteworthy that the set-up of the ED-XRF spectrometer for cascade impactor analyses allowed to test a new methodology for the determination of elemental size distribution [Cuccia et al., 2010]. It is based on the combination of receptor modelling and number size distribution analysis (see Chapter 3). Up to now it has been tested on a dataset of samples collected in Genoa. The comparison between the data obtained by our model and real cascade impactor data showed good agreement, provided that source profiles for at least three main PM classes (PM10, PM2.5, and PM1) are available (see par. 3.3.3).

Chapter 3: Source apportionment by Positive Matrix Factorization (PMF) on high-time resolved data

The identification and quantification of source contributions to the measured PM concentration (source apportionment) is one of the main topics of interest in aerosol science.

Three main source apportionment approaches can be applied [Viana et al., 2008 and therein literature]:

a) basic numerical analysis of monitoring data (e.g.: correlation of wind direction with levels of measured components to identify source locations, correlation between gaseous pollutants and PM components to identify source associations...). The main advantage of this approach is the low impact of mathematical artefacts due to the simplicity of the data analysis;
b) simulation of aerosol emission, formation, transport and deposition, based on emission inventories and/or dispersion models. A limitation of this approach is due to the request of detailed emission inventories (not always available) and to the low accuracy of available emission inventories, especially when natural emissions are important. The main advantage consists in the possibility using these methods in scenario studies to evaluate the impact of emission abatement strategies on the anthropogenic contribution to ambient PM concentrations;
c) statistical evaluation of PM chemical data acquired at receptor sites (receptor models). Receptor modelling is based on the assumption that mass and species conservation can be assumed and a mass balance analysis can be used to identify and apportion sources of airborne PM in the atmosphere. A wide range of statistical models and modelling approaches are currently available in the literature, requiring a different degree of knowledge on the pollution sources prior to the application of receptor models. The two main extremes of receptor models are chemical mass balance (CMB: detailed sources chemical characterisation is required) and multivariate models (no or

limited information on the emission sources is required).

Among the three approaches mentioned above, receptor models are of great interest because they allow the source apportionment starting from in-situ measurements of aerosol components. More in detail, the model input data are the aerosol components measured at a receptor site.

Positive Matrix Factorization (PMF) is a receptor model widely applied in aerosol sciences to obtain information on the aerosol sources influencing a specific area. It was developed by Paatero and Tapper (1994). In this work, PMF2 was applied to 4-hour time-resolved PM10 composition, to gather information on source apportionment, source profiles, and high time-resolved temporal trends of the sources influencing the area of interest.

In this work, PM measured components used for PMF analysis included elements measured by ED-XRF, ions (sulphate, nitrate, ammonium) detected by ion chromatography (IC), organic and elemental carbon measured by thermal-optical transmittance method (TOT), and levoglucosan concentrations determined by high-performance anion-exchange chromatography coupled with pulsed amperometric detection (HPAEC-PAD).

Once PMF results were obtained, a methodology developed by Mazzei et al. (2007) was applied, to identify of the contribution of the detected sources to the measured particle number in different size-bins. This was obtained by the application of multiple linear regression among PMF source temporal trends and particle number distribution in 10 classes in the range 250 nm – 10 μm.

3.1 The applied model: Positive Matrix Factorization

3.1.1 PMF index convention

Samplings of particulate matter are usually aimed at mass concentration determination and/or chemical speciation. During a sampling campaign, N samples are analysed for M chemical species determination. Chemical speciation is important both for the assessment of aerosol effects on human health and

environment, and for source identification. It is noteworthy that the more detailed is the chemical speciation, the more complete and correct will be the source identification. Indeed, if a source is characterised by a specific tracer but it is not measured, this source cannot be identified by receptor modelling.

Data for the M chemical species from the N samples can be organised in an NxM data matrix (index i=1...N for samples and index j=1...M for chemical species):

$$\mathbf{X} = \begin{bmatrix} X_{11} & X_{21} & ... & X_{1M} \\ X_{21} & X_{22} & ... & X_{2M} \\ ... & ... & X_{ij} & ... \\ ... & ... & ... & ... \\ X_{N1} & X_{N2} & ... & X_{NM} \end{bmatrix},$$

where each X_{ij} in the matrix represents the concentration of the j^{th} species measured at the receptor site in the i^{th} sample.

The aim of PMF is the factorisation of the matrix X as follows:

$$X_{ij} = \sum_{k=1}^{P} G_{ik} F_{kj} + e_{ij},$$

where the k index indicates one of the P sources to identify, G_{ik} represents the contribution of the source k to the sample i, and F_{kj} is the contribution of the chemical species j to the source k. Each e_{ij} represented by

$$e_{ij} = X_{ij} - \sum_{k=1}^{P} G_{ik} F_{kj} = X_{ij} - Y_{ij}$$

is the residual between the concentration X_{ij} measured at the receptor site and the concentration Y_{ij} reconstructed by the model. In matrix form it can be re-written:

$$\mathbf{X}=\mathbf{GF}+\mathbf{E},$$

where **G** is the "factor scores" matrix (the columns are the temporal contributions of the sources to the receptor), **F** is the "factor loadings" matrix (i.e. its rows represent the chemical profiles of the sources), and **E** is the residual matrix.

3.1.2 Physical constraints for the apportionment

PMF has to satisfy the following constraints for the solutions to be physically consistent (thus limiting the choice among the possible solutions):

a) the model has to reproduce experimental data;

b) $G_{ik} \geq 0 \ \forall$ i, k: indeed, negative elements would represent an aerosol sink and not a source;

c) $F_{kj} \geq 0 \ \forall$ k, j: indeed, a source is expected to emit, not to absorb, elements;

Conditions a), b), and c) are directly implemented into the PMF algorithm (see the following paragraph). However, further physical constraints can be identified:

d) $F_{kj} \leq 1 \ \forall k = 1, \ldots, P$, i.e. the measured species cannot explain more than 100% of the source composition

The a-posteriori check on conditions d) is the first criterion for results validation.

3.1.3 PMF mathematical model

PMF is a bilinear factor model factorising the X matrix as

$$\mathbf{X}=\mathbf{GF}+\mathbf{E}.$$

G and **F** are non-negative matrices that minimise the object function Q:

$$Q=\sum_{i=1}^{N}\sum_{j=1}^{M}\left(\frac{e_{ij}}{s_{ij}}\right)^2,$$

where s_{ij} are the weights associated to the j species in the i sample (evaluated from analytical uncertainties) and e_{ij} are the residuals between measured and reconstructed concentrations. Thus, PMF solves the factorisation problem using the weighed least-squares minimisation method. The minimisation algorithm directly includes non-negative constraints for the elements of **F** and **G**. In fact, it minimises a $\overline{Q}$ function, in which Q is summed to terms for non-negativity implementation and for rotational control. Non-negativity implementation ensures physical significance to the solutions.

Variables were selected according to the signal to noise ratio criterion [Paatero and Hopke, 2003]. We used the procedure of Polissar et al. (1998) to obtain the estimates for data and weights to be used as input for PMF for all the measured, missing and below MDL (Minimum Detection Limit specific for each component) data combining experimental values, uncertainties and MDL as explained in the following. Briefly, be v_{ij} the measured value, u_{ij} the analytical uncertainty, and d_{ij}

the MDL for sample i and species j. Moreover, be $\tilde{v}_j$ the geometric mean of the measured concentrations for element j and $\bar{d}_j$ the arithmetic mean of the MDLs for the species j. Then X_{ij} and s_{ij} for each sample i and chemical species j are calculated as shown in table 3.1.

	$\mathbf{X_{ij}}$	$\mathbf{s_{ij}}$
Determined values	$X_{ij}=v_{ij}$	$s_{ij}=u_{ij}+v_{ij}/3$
Values below MDL	$X_{ij}=d_{ij}/2$	$s_{ij}=\bar{d}_j+d_{ij}/3$
Missing values	$X_{ij}=\tilde{v}_j$	$s_{ij}=4\,\tilde{v}_j$

table 3.1: Polissar approach for X_{ij} and s_{ij} estimation in PMF analysis.

The output factors **G** and **F** have to be normalised, to represent the temporal trends and the profiles of the identified sources. The normalized **G** factors were obtained as those reconstructing the receptor-measured mass concentrations c_i at the receptor site, according to the Multi-Linear Regression (MLR) model: $c_i = \sum_{k=1}^{P} b_k g_{ik} + \varepsilon_i$. The quantity $b_k g_{ik}$ represents the contribution due to the k-source to the i-th PM concentration registered at the receptor; ε_i represents the i-th residual of the regression model. The intercept was set to zero, as otherwise it would have represented a not meaningful constant contribution at the receptor as already done by Polissar et al. (1998).

Among the outputs of the model, important parameters to consider are the explained variations (EV). They indicate to what extent a source explains the temporal trend of an element. The higher is the EV of an element in a source, the more this element is specifically contained in that source if compared to the others. Thus, high EV for an element in a source identify that element as a good tracer for the source.

PMF, as well as other receptor models (e.g. Absolute Principal Component Analysis), is affected by the rotational ambiguity problem [Paatero et al., 2002]. Opposite to other models, in which central solutions are rotated a-posteriori, PMF directly implements rotations in the minimisation algorithm. They are controlled using the parameter FPEAK [Paatero, 1997], which influences one of the regularisation terms of the object function $\overline{Q}$. The rotation tool FPEAK, for its

mathematical structure, does not allow a-posteriori rotation of the solution after the choice of the 'correct' number of factors. On the contrary, the selection of a reasonable range for the number of factors is performed analysing conventional output parameters (e.g. Q, IM, IS, see Lee et al. (1999) for details) and, for each selected number of factors, the exploration of all the solutions corresponding to the rotational range -1 < FPEAK < +1 has to be carried out, looking for the best rotated solution.

Every other a priori physical condition about the problem can be translated into mathematical constraints to reduce the ambiguity in the choice of the best solution (e.g. points d in paragraph 3.1.2).

The robust mode based on iterative re-weighting of data points [Paatero, 1997] was also selected to control and limit the influence of outliers (i.e. data in the tail of the log-normal distribution) on the solutions.

Estimates of the errors on the source apportionment were obtained from the error propagation on **G** and **F** elements given as output by the model.

3.1.4 PMF peculiar features

Summarising, PMF is characterised by some peculiar features:

1) the minimisation algorithm directly implements non-negative constraints on **F** and **G** matrices;
2) PMF allows to associate a specific weight to each datum, determined first of all by its analytical uncertainty. Thus, less uncertain data have higher importance in the fit; moreover, it allows the maximisation of the number of input data, as missing data or data below the MDL can be inserted after suitable estimations, always down-weighed, differentiating the quality of their information from that given by more robust data;
3) PMF gives the possibility to limit the influence of outliers data in the fit working in robust model, which allows a reduction of the weight of possible outliers;
4) PMF output includes also the estimation of the uncertainties on **F** and **G** matrices, thus allowing the determination of the uncertainties on the obtained

apportionment;

5) PMF (as all receptor models) is affected by rotational ambiguity. The model allows to iteratively perform global rotations instead of the a-posteriori rotation of the central solution, as usually done using other models. Rotational ambiguity can be further reduced introducing the control on further physical constraints to be satisfied by the solution.

3.2 The analysed dataset.

PMF analysis was applied to a dataset already available; general features will be reported in the following.

PM10 samples were collected with 4-hour resolution in 2006 (two weeks during summertime and two weeks during wintertime) in parallel on PTFE and quartz fibre filters (total: 180 samples per substrate). Elemental composition was determined on all PTFE filters by ED-XRF. The main inorganic ions (sulphate, nitrate and ammonium) were determined after water extraction of half quartz fibre filter by IC. TOT method (see paragraph 4.3.1) was applied to a 1.5 cm^2 quartz fibre filter punch to obtain organic and elemental carbon quantification. Levoglucosan (produced by cellulose pyrolysis and thus marker for biomass burning) was measured only on wintertime samples by HPAEC-PAD, following the procedure described in Piazzalunga et al., 2010.

Additional measurements included the determination of the number size distribution with high temporal resolution using an optical particle counter (OPC) and (only during wintertime) a condensation particle counter (CPC), and information on meteorological and atmospheric dispersion conditions (using ^{222}Rn as tracer for the Mixing Layer condition). Moreover, a *streaker sampler* was used to obtain element concentrations with hourly resolution by PIXE analysis in two size fractions: fine (<2.5 μm), and coarse (> 2.5 μm).

Details on the experimental techniques, results on the concentrations and temporal trends, and the identification of specific episodes are reported in Vecchi et al. (2009a). A peculiar feature of this database was the possibility to identify episodes as long-range transports, or local production of atmospheric particles. Moreover, the

high-time resolution allowed to identify periods dominated by primary contribution, and to give information about primary and secondary contributions to the measured PM.

It is noteworthy that the high degree of detail of the database made it ideal also for the application of PMF analysis to apportion the contribution of the different sources to the measured PM, as carried out in this PhD thesis.

3.3 Results

3.3.1 Dataset features

Nineteen chemical species were considered for PMF analysis: Al, Si, sulphate, Cl, K, Ca, Ti, Mn, Fe, Ni, Cu, Zn, Br, Pb, nitrate, ammonium, OC, EC, and levoglucosan. Sulphate concentration was inserted as $3 \cdot S_{ED\text{-}XRF}$ due to the good inter-comparison between ED-XRF and IC results and the lower uncertainties affecting ED-XRF determination [Kim and Hopke, 2006].

Input weights were evaluated using the Polissar approach. Basic uncertainties used for Polissar method application were those determined by ED-XRF for the elements; as for ions and carbon fractions, 10% uncertainty on the measured value was used for ions and 15% for carbon fractions both due to higher uncertainties in these determination techniques and to underestimate their weight of these species in the fit, thus limiting the influence of the high concentration values and accounting for the possible variability of the source profiles from which they are expected to derive (mainly secondary compounds and combustion) [Kim et al., 2004].

3.3.2 Identified sources

The analysis of conventional output parameters (i.e. the Q, IM and IS) allowed to restrict the range of the number of factors to be studied to P=7, 8, 9.

P=9 was immediately rejected, as for all rotation the sum of the contributions in at least one source profile exceeded 100% (i.e. the components explained more than the total mass emitted by the source).

For P=7, the resolved factors were identified as construction works, re-suspended

dust, secondary sulphates and organics, traffic, industry, secondary nitrate, and wood combustion.

For P=8, a source containing mainly OC and without specific tracers appeared and it was decided not to consider it.

Focusing on the seven factorial solution, the rotations with FPEAK $\geq$ 0.3 were rejected, as for one source the sum of the contributions in the source profile exceeded 100%. In the range -0.4 $\leq$ FPEAK $\leq$ 0.2 the ratios between Al/Si in construction works source, and Levoglucosan/OC and EC/OC in wood combustion source are stable. The main differences among the considered rotations are the nitrate and ammonium contents in wood combustion source. These contributions are completely negligible in the range 0 $\leq$ FPEAK $\leq$ 0.2, while nitrate contribution grows from 8% to 15% (ammonium from 1% to 3%) with FPEAK varying in the range -0.1 to -0.4. As levoglucosan is a tracer for primary wood combustion emissions, the range 0 $\leq$ FPEAK $\leq$ 0.2 was only considered. In this range the solutions were comparable within the errors for all the analysed parameters, thus FPEAK=0 was chosen as final solution.

As previously mentioned, the seven sources were identified as construction works, re-suspended dust, secondary sulphates and organics, traffic, industry, secondary nitrate, and combustion.

Average seasonal source apportionment and estimated uncertainties are shown in table 3.2. It is noteworthy that the two secondary sources account for about 37% of the measured mass during summertime and 49% during wintertime: thus, secondary sources are main contributors to PM10 mass in both seasons. Another major contributor during summertime is re-suspended dust (28% on average). In figure 3.1, 4-hour resolved average apportionments during summer and winter are represented. In the following, each source will be presented in detail.

		Construction works	Re-suspended dust	Secondary sulphate	Traffic	Industry	Nitrate	Wood combustion
Summer	Average	9%	28%	30%	14%	11%	7%	1%
	Uncertainty	1%	2%	3%	1%	1%	1%	1%
Winter	Average	4%	8%	24%	16%	8%	25%	14%
	Uncertainty	0%	1%	3%	1%	1%	2%	1%

table 3.2: source apportionment and uncertainties on source contributions.

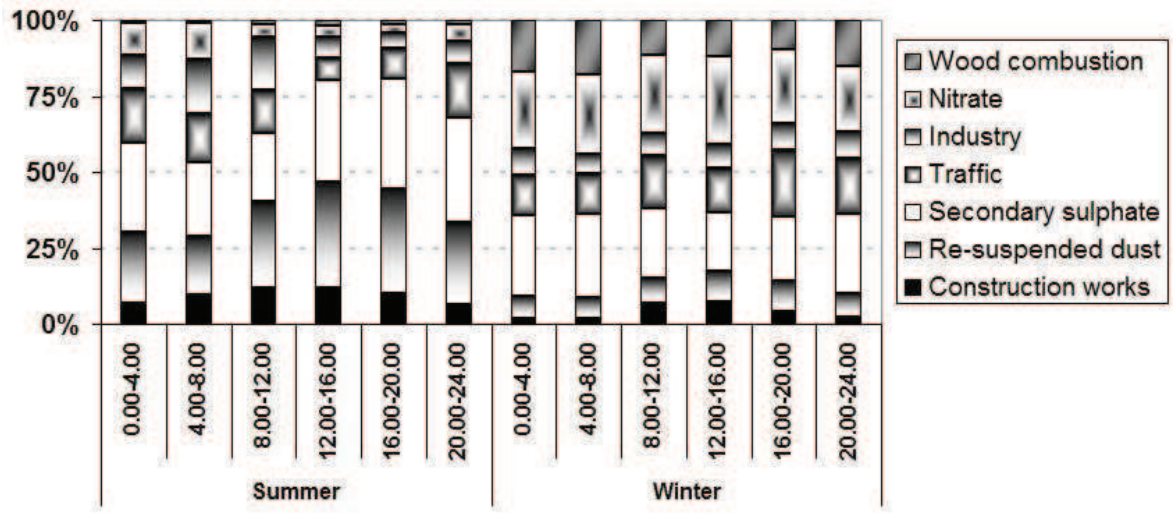

figure 3.1: 4-hour resolved average source apportionment by PMF during summertime and wintertime

Construction works

The construction works source (see details in figure 3.2) represents re-suspended construction material (i.e. cement, dust, gypsum) and machineries exhausts. Ca is considered the main tracer for this source, and it is responsible for a considerable mass fraction of this source (nearly 20%). Other important components for construction works source are OC, Si, and sulphate. Ca and sulphate can be ascribed to the gypsum used for construction activities. The possible presence of gypsum in Milan urban area was mentioned by Vecchi et al. (2009a): in that work, a relation between Ca and S concentration in the coarse fraction ($d > 2$ μm) with 1 hour resolution was found (see figure 3.3).

In construction works source, Al/Si ratio registered by our PMF analysis is 0.3, which is the ratio expected for crustal matter. In fact, particulate matter in this source includes soil directly lifted up from the ground nearby the receptor site, thus a contamination by the soil is expected. The highest peaks in this source temporal pattern are due to construction works sporadically carried out (and directly observed) in the garden of the Department of Physics during the periods of the field campaigns. The relative contribution of this source was higher during summertime (9%) than during wintertime (4%), probably due to the drier conditions during the hot season which enhance re-suspension of construction material, and to the reduced contribution of other sources (i.e. wood combustion, see later). However,

the contribution of this source during peak events (3 July, 23 November, and 27 November) rose up to 35% of the PM10 mass. The relative contribution of this source is about 5% higher during daytime than night-time in both seasons, due to the higher contribution of source emissions and to the particle size (see in the following the discussion on size-segregated apportionment), which enhances deposition processes during night-time.

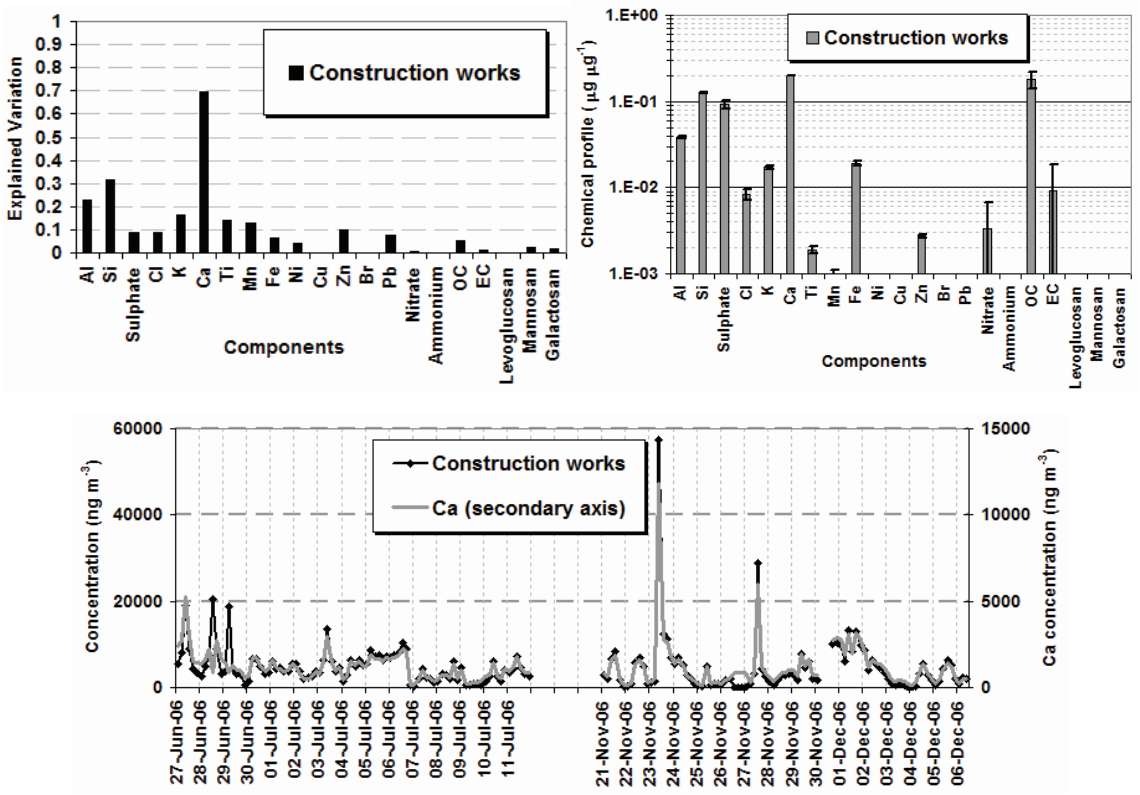

figure 3.2: explained variation, source profile and temporal trends (including a source tracer) for construction works source

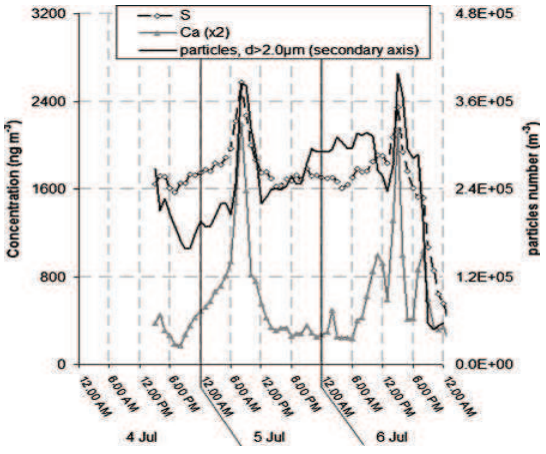

figure 3.3: S, Ca and particles number concentration (d > 2 µm) with 1-hour resolution during 4–6 July 2006 [Vecchi et al., 2009a]

Re-suspended dust

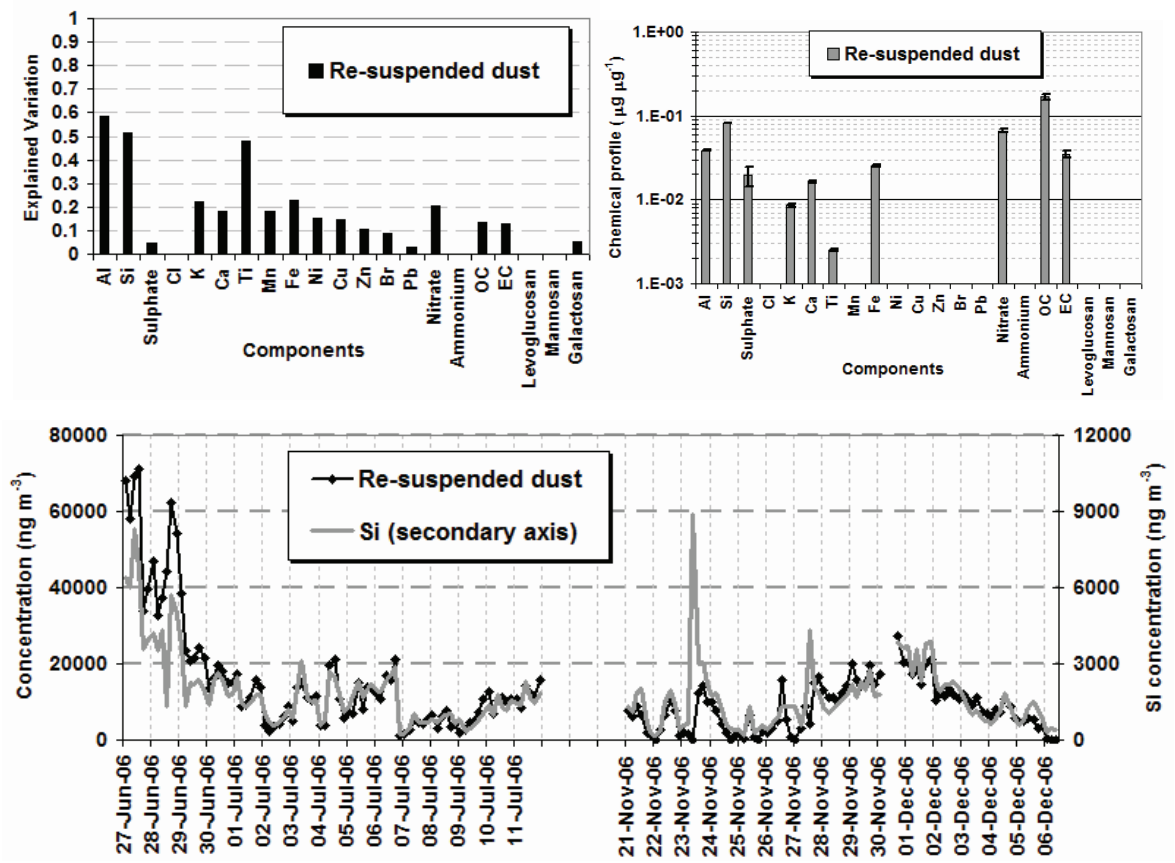

figure 3.4: explained variation, source profile and temporal trends (including a source tracer) for re-suspended dust source

Re-suspended dust (see figure 3.4) represents particulate matter deposited on the ground and re-suspended by natural (e.g. wind) or anthropogenic (e.g. traffic) agents. Specific tracers for this source are Al, Si, and Ti. The ratios for these elements are not expected to be those from soil dust, as particles coming from this source are a mixture of soil dust and other particles (i.e. coming from abrasion of mechanical parts and vehicle exhaust) previously deposited on the ground. For the re-suspended dust source resolved by PMF, Al/Si ratio is 0.45, higher than that expected for natural dust (0.3). Other important constituents of this source are OC and nitrate. The relative contribution of this source is 28% and 8% in summer and winter, respectively. As previously mentioned for construction works contribution, drier soils and higher atmospheric turbulence during summertime play a key role for the explanation of the variation of re-suspended dust contribution in the two seasons. Moreover, a high re-suspended dust contribution is registered during summer

afternoons (h. 12.00-20.00: 35% on average), while during the second part of the night (h. 0.00-8.00) it accounts only for about 20% of PM10 mass. In this case, differences in anthropogenic activities and atmospheric turbulence between daytime and night-time, and the short residence time of the larger re-suspended particles can justify this variation.

Comparing construction works and re-suspended dust temporal trends, it can be evidenced the capability of PMF in identifying of sources with similar components (e.g. Al, Si, Ti, and Fe account for similar amounts in the above mentioned source profiles). As an example, when analysing the bare elemental trends a sudden strong increase during 23 November morning was identified in Al, Si, Ti and Ca temporal trends, but it was not possible understanding the origin of these elements (see Figure 4). PMF ascribed this increase to construction works and this result is supported also by in-situ observation (e.g. analogous increase in particle number concentration with d > 2 μm by OPC), as during that day in the garden of the Department construction works were carried out.

Secondary sulphates and organics

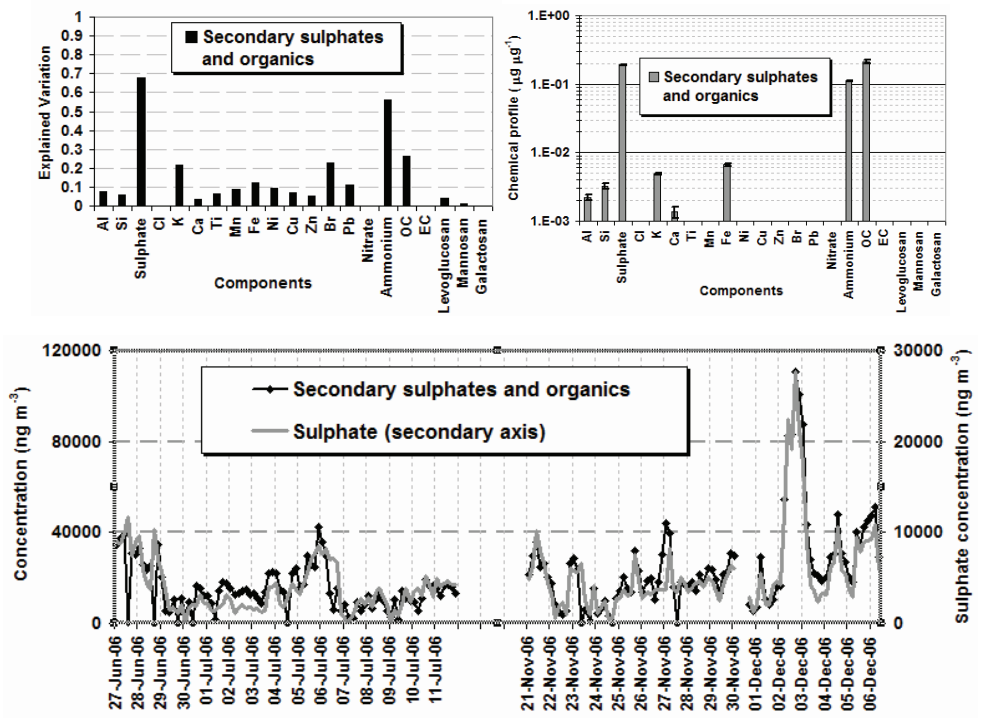

figure 3.5: explained variation, source profile and temporal trends (including a source tracer) for secondary sulphates and organics source

The source called secondary sulphates and organics is traced by sulphate (which accounts for nearly 20% mass in the profile) and ammonium. The other main contributor (20%) is OC. Thus the is a complex secondary source including sulphates and secondary organic compounds. This source gives significant and similar contributions to PM mass in both seasons (30% and 24% in summer and winter, respectively). 4-hour resolved apportionment evidences the highest contribution during summer afternoons, when photochemical activity is more efficient. During wintertime, maximum relative contribution is reached during night-time (about 27%) and it has probably to be ascribed to condensation (mainly of organic compounds).

The analysis of bare data had been coupled to back-trajectory results in a previous work [Vecchi et al., 2009a], highlighting the presence of long-range transport episodes during the two field campaigns (5-6 July and 2 December). The identification of this episodes was confirmed by back-trajectories analysis: the air mass on Milan during that periods had travelled through eastern Europe countries during previous days. Fuels containing high quantities of S are still largely used in those countries, so that sulphates and/or their precursors, together with other components (e.g. organics), are occasionally transported to Northern Italy. PMF analysis carried out in this work allowed the quantification of secondary contribution during these episodes (about 55% in both seasons).

Traffic

As for traffic (see figure 3.6), Fe, Cu, and EC are the main tracers of this source. Fe and Cu had been already identified as traffic markers in the Milan area [Marcazzan et al., 2003]. EC and OC are the main contributors to the traffic source profile. This source, representing only primary traffic emissions, accounts for 14% and 16% during summer and winter, respectively. During summertime, the relative contribution of this source is higher during the night. This can be ascribed to the rapid deposition of particles generated by other sources (e.g. re-suspended dust and construction works). During wintertime, on the contrary, rush hours are well defined. More in detail, the traffic relative contribution and the total number concentration of particles with $d > 4$ nm (measured by the CPC) were compared

during working days: maxima in the time slots 8.00-12.00 and 16.00-20.00 were detected (see figure 3.7). It is noteworthy that no class in the range 0.25-10 µm shows an analogous trend.

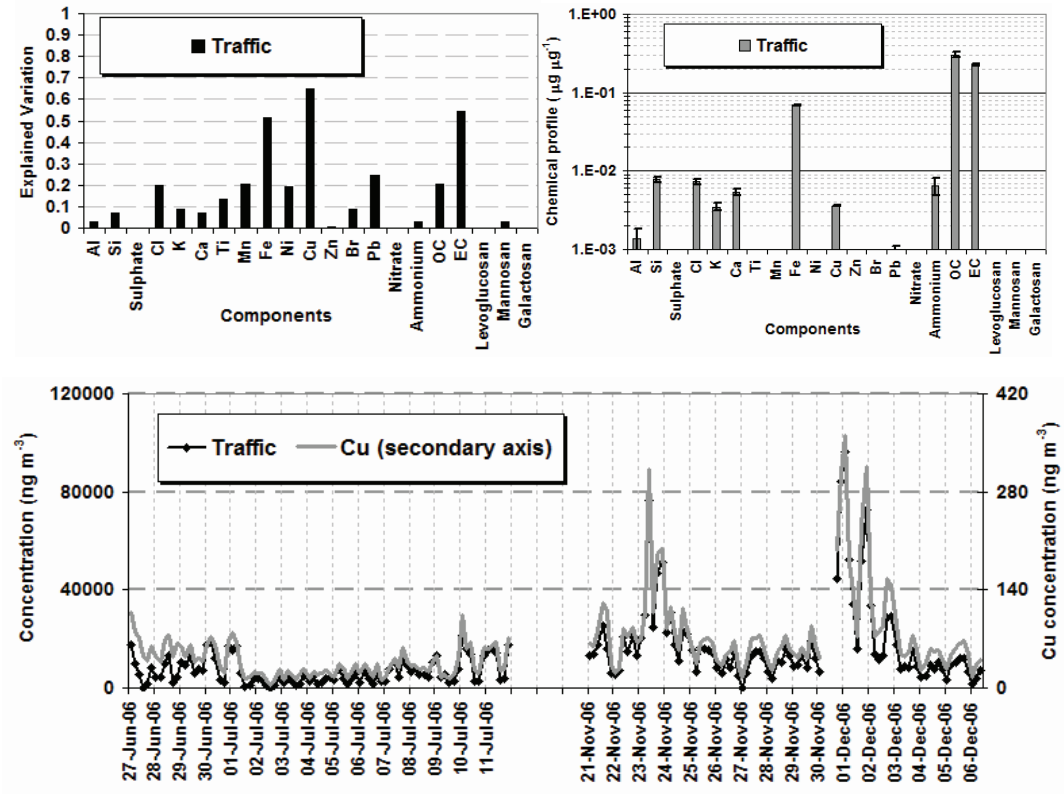

figure 3.6: explained variation, source profile and temporal trends (including a source tracer) for traffic source

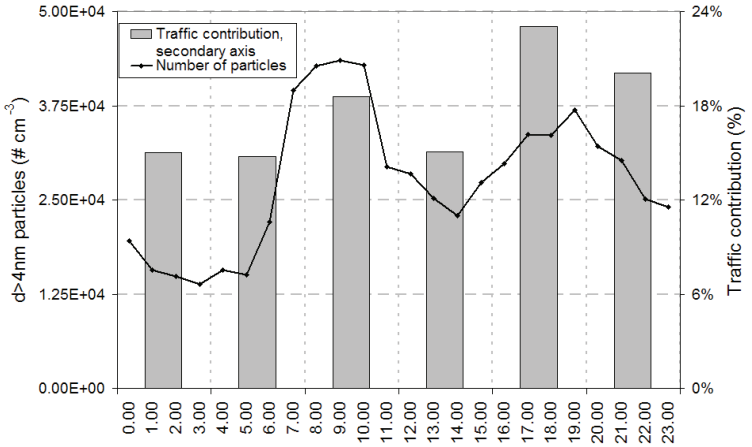

figure 3.7: representative day for traffic source relative contribution and for total particle number concentration (d > 4 nm)

Industry

In this work, Zn and Mn are the main tracers for industry source. Previous works

had identified these elements in Milan urban area as primary tracers for industrial processes including incinerators emissions [Marcazzan et al., 2003]. It should be noticed that OC, EC, nitrate, and ammonium are the main constituents of this source. figure 3.8 shows that the temporal pattern of this source is very regular during summertime, with maxima (well above 10 μg m^{-3}) during night-time and diurnal minima. During wintertime, the temporal pattern is not so clear. This might be due to strong ground-based temperature inversions typical of winter nights in the Po Valley. In fact in these conditions industrial/incinerators chimneys are above the Mixing Layer; therefore, during night-time the pollutants cannot reach the receptor point, situated at ground level. Average relative contributions for this source were comparable in summer and winter (11% and 8%, respectively).

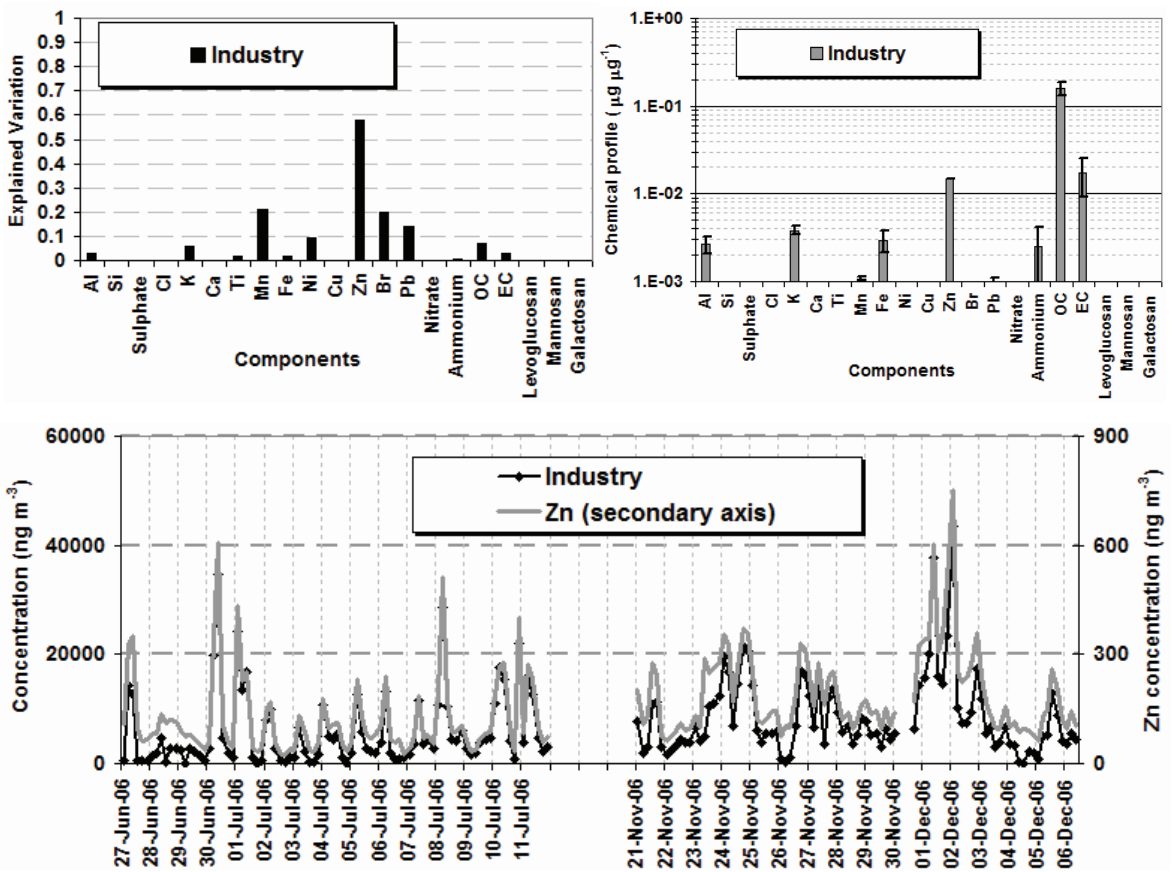

figure 3.8: explained variation, source profile and temporal trends (including a source tracer) for industry source

3.1.6 Secondary nitrate

Secondary nitrate source (figure 3.9) is characterised by nitrate as main tracer. Main

contributors are nitrate (50%) and ammonium (10%). It is characterised by a peculiar seasonal trend: during summertime it accounts only for 7% on average. On the contrary, it becomes one of the main contributors during winter season (25%). During summertime, it is also noteworthy that nitrate contribution is higher during night-time (average 11% for h. 0.00-8.00). This has to be ascribed to the lower night temperature, which allows the presence of particulate nitrate and limits sampling artefacts to occur. Organic and inorganic artefacts were estimated in Milan urban area by Vecchi et al. (2009b), and an average nitrate loss of 22% on quartz fibre filters during summertime was reported. Also a tendency of greater nitrate volatilisation with temperature increase was detected, in agreement with other literature data [Chow et al., 2005; Keck and Wittmaack, 2005].

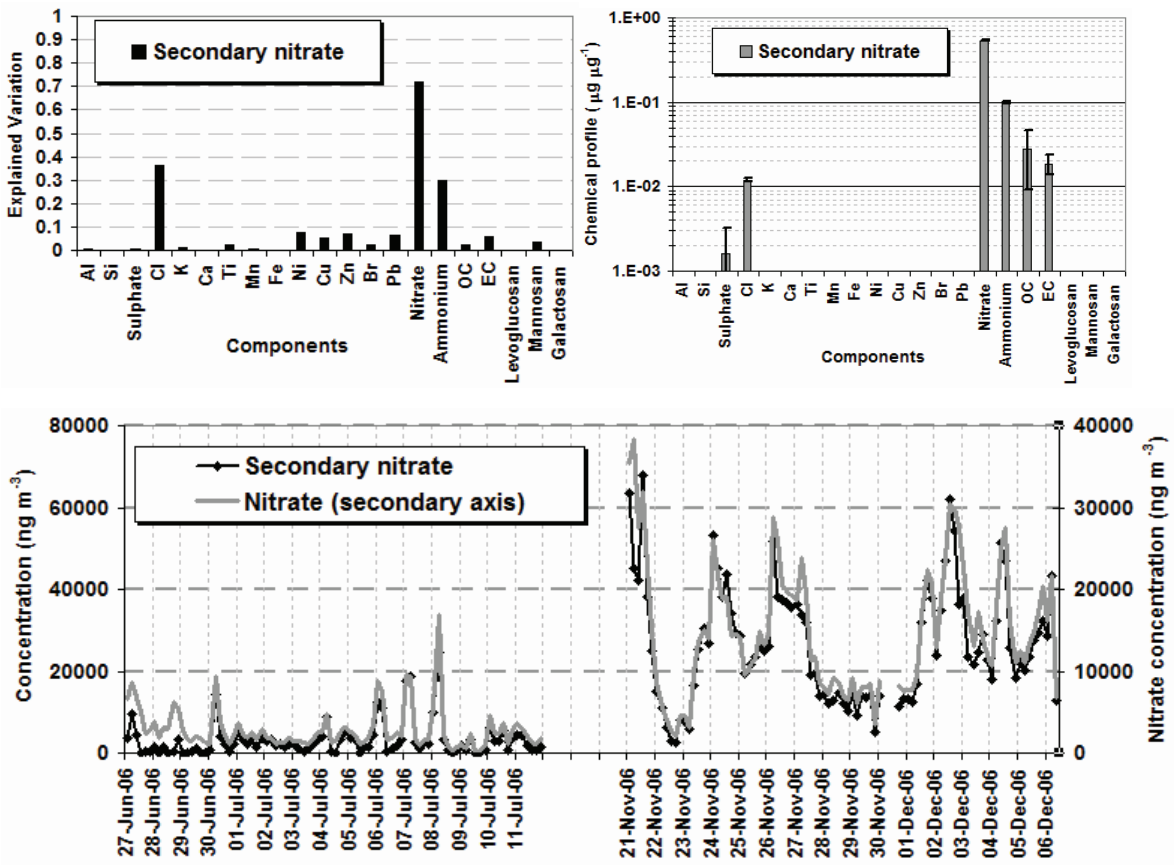

figure 3.9: explained variation, source profile and temporal trends (including a source tracer) for secondary nitrate source

Wood combustion

This source is characterised by levoglucosan and its isomers as source tracers (see figure 3.10). The main contributors to this source are OC, EC, and levoglucosan.

Levoglucosan is a specific tracer for wood combustion, and the presence of K in the source profile is a further confirmation [Kleeman et al., 1999]. This source, which represents primary wood burning contribution, accounts on average for 14% during wintertime. The relative contribution of this source is higher during night-time. In the following paragraph, size segregated apportionment is reported. It can be noticed (see figure 3.11) that wood combustion source is a main contributor for fine particles, which have the longest residence time in atmosphere, thus justifying wood combustion daily trend.

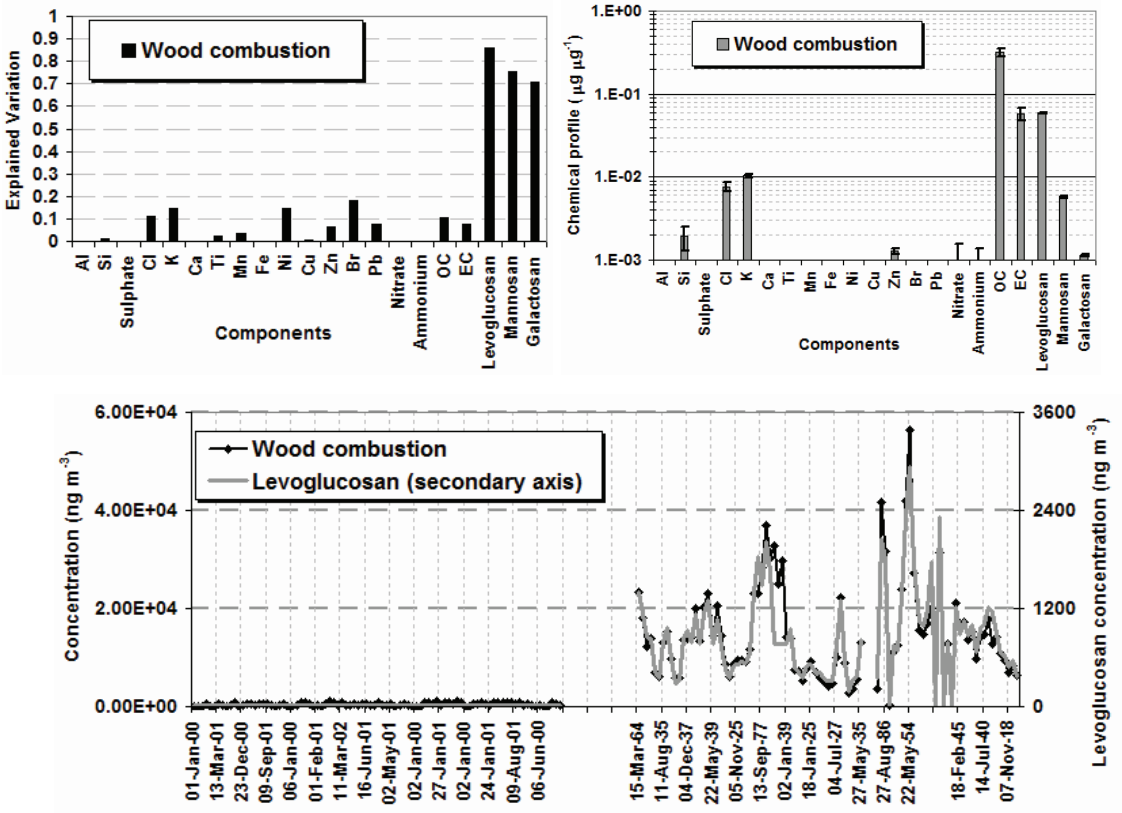

figure 3.10: explained variation, source profile and temporal trends (including a source tracers) for combustion source

3.3.3 Size-segregated particle number source apportionment

As previously mentioned (par 3.2), an optical particle counter (OPC) operated during the sampling campaign. It gave information on high-time resolved particle number concentration in 31 size bins from 0.25 to 32 µm. Our analysis was limited to the range 0.25-12 µm. Size bins with similar temporal patterns were summed together. 4-hour averages were calculated to make particle number temporal trends

directly comparable to PMF sources temporal trends.

Multi-linear regression was performed between particles number in each size range and PMF sources temporal trends. This allowed the apportionment of source contributions to the particle number distribution. Multi-linear regression was separately performed during summer and winter, due to the strong seasonal variation of some sources contribution. The results for both seasons are presented in figure 3.11. It is noteworthy that wood combustion was not considered in the analysis during summertime, as the tracer for this source was not measured in this season.

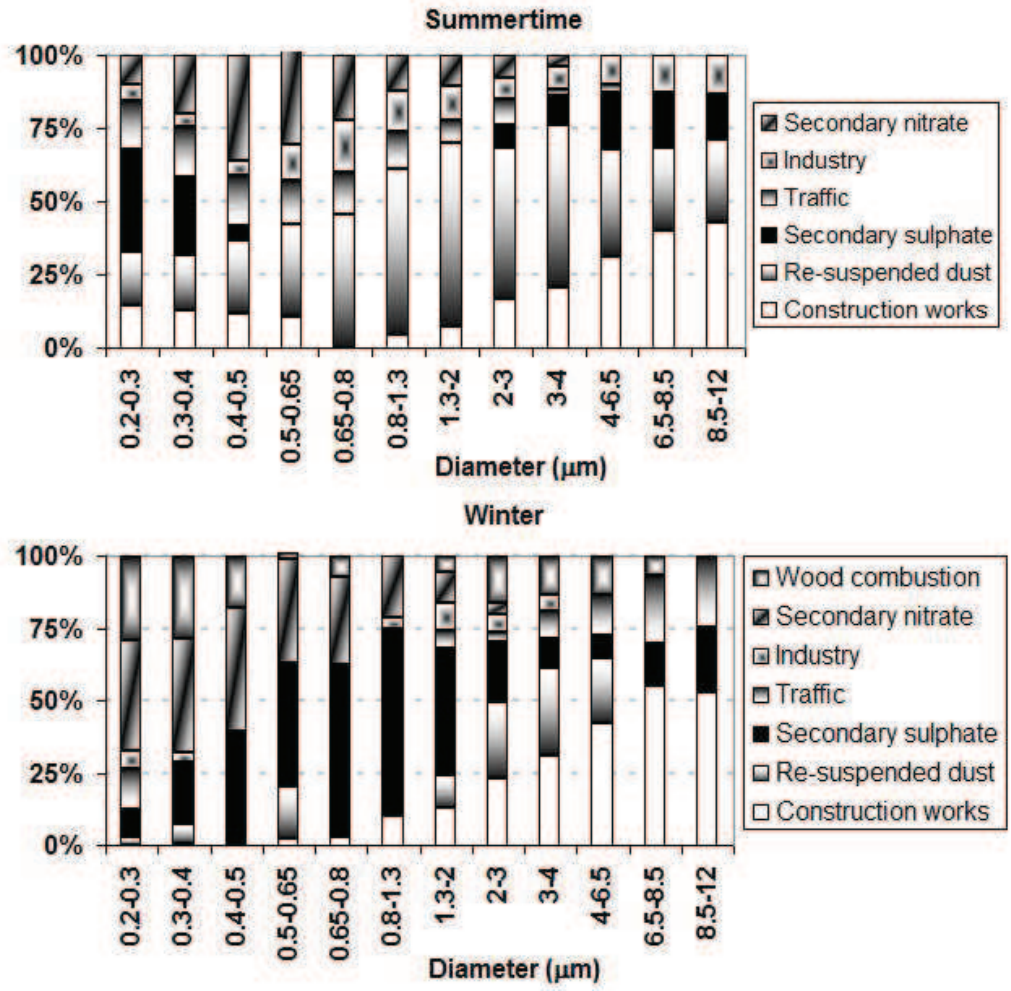

figure 3.11: particle number distribution source apportionment during summer and winter.

In figure 3.11, it is noteworthy that construction works contributes mainly to particles with d > 2 µm (> 30% for d > 4µm), while re-suspended dust gives a more significant contribution to lower size bins especially during summertime. In this season, re-suspended dust contribution accounts for more than 25% in almost all

size bins (more than 50% in 0.8-4 μm range). Indeed, as previously mentioned, re-suspended dust is composed not only by soil, but it also includes a contribution from smaller particles (e.g. vehicle exhausts particles), which can deposit on the ground and then be re-suspended by traffic or by atmospheric agents (e.g. wind, thermal-driven turbulence). It is also interesting that there is no contribution of re-suspended dust to particles with d > 6.5 μm during wintertime. This can be due to the lower atmospheric turbulence and wind speed during the cold season that limit the strength of re-suspension forces, as well as to high relative humidity that enhances particle sticking on the ground. On the contrary, the contribution of construction works to larger particles is observed also during wintertime because of machine excavation of the ground leading to important soil lift up.

A strong variation of the relative contribution of secondary sulphates and organics source to the different classes in the two seasons was detected. During summertime, highest contributions are registered for particles with d < 0.5 μm (up to 35% for 0.25-0.30 μm diameter particles). Moreover, a contribution to particles with d > 2 μm is observed, correspondent to the increase in construction works contribution. However, it has been supposed that this can be ascribed to PMF analysis. In fact, sulphate is one of the main components of the secondary compound source, but it is also present in the construction work source (gypsum). Therefore, it is possible that uncertainties on the sulphate apportionment by PMF lead to the detected increase. During wintertime, the size distribution of secondary sulphates and organics source is completely different. It becomes the dominant component in the 0.5-2 μm diameter range. This can be ascribed to the different processes leading to secondary formation in the two seasons (i.e. photochemistry during summertime and condensation during wintertime), to the higher relative humidity during the cold season leading to particle hygroscopic growth, and to the reduction of the contribution importance of other sources (e.g. there is no re-suspended dust contribution during wintertime in the range 0.8-1.3 μm).

Traffic contributes for 8-17% in all classes up to 3 μm during summertime, while during wintertime the main contributions are given to small particles (< 0.4 μm) and to particles greater than 1 μm (probably due to the increase of other sources

contribution in the intermediate classes).
As for industry, the contribution is higher than 5% in all classes during summertime; maxima values are registered in the 0.4-0.8 μm range, where industry accounts for about 17% of the measured particle number. During wintertime the contribution is much lower in all OPC classes.
Secondary nitrate gives a high contribution for sub-micrometric particles during both summer (up to 40% in the 0.4-0.65 μm range) and winter (about 40% in the 0.2-0.5 μm range).
As for wood combustion contribution, it is noteworthy that it is the main primary contributor in the 0.25-0.50 μm during the winter season (> 20%).

It is noteworthy that the information given in this last paragraph has to be considered just as an indication of the importance of the identified source contributions to the different size bins. In fact, our research group in close collaboration with the research group of the University of Genoa, recently further developed this technique to gather information on elemental size distribution [Cuccia et al., 2010], thus limiting the need to use multi-stage cascade impactors (see Chapter 2) whose application in field campaigns is always highly time consuming. In that work, applied to Genoa samples, we proved that reliable results on elemental size distribution can be obtained only if source profiles are available in at least three main size fractions (PM10, PM2.5, PM1). This can be noticed by the comparison of figure 3.12 and figure 3.13: in figure 3.12, where only PM10 profile is used for size distribution reconstruction, the reconstructed data (grey) can be considered only indicative, as the general trend is similar to that obtained by cascade impactor (black), but the differences between the two are significant. On the contrary in figure 3.13, where PM10, PM2.5 and PM1 profiles are available, measured and reconstructed data are nearly always comparable within the estimated errors.
During the Milan field campaign considered in this chapter, only PM10 samplings were available. Future measurement campaigns will be carried out allow further steps of our analysis.

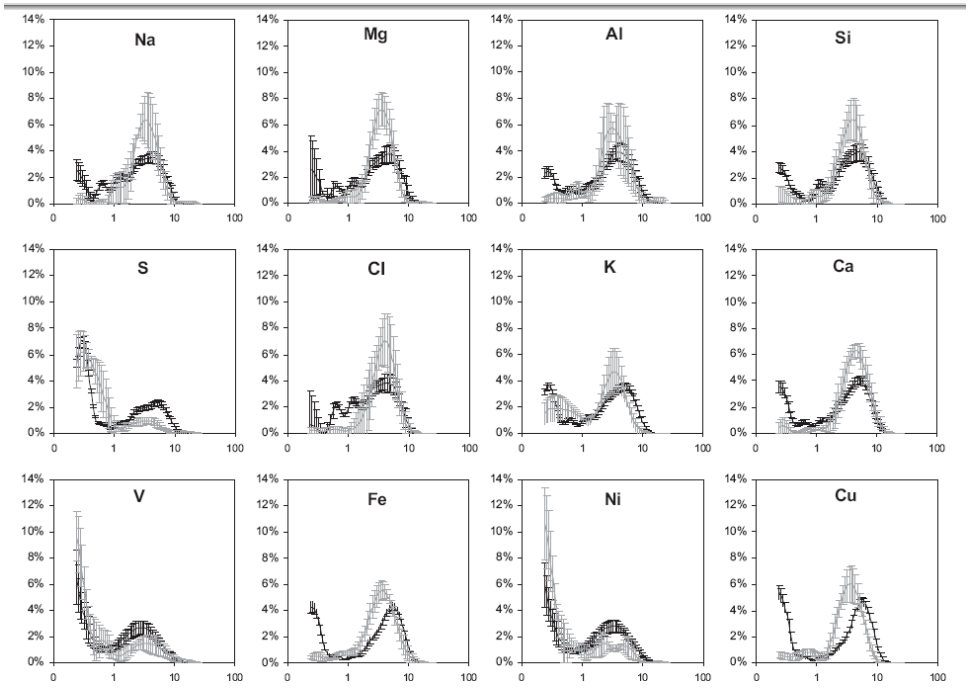

figure 3.12: elements size distribution obtained by multistage impactor (grey) and by the combination of PMF and OPC analysis (black), when only PM10 profile is available [Cuccia et al., 2010]. On the x-axis particle diameter in μm is reported, on y axis % PM concentration is reported.

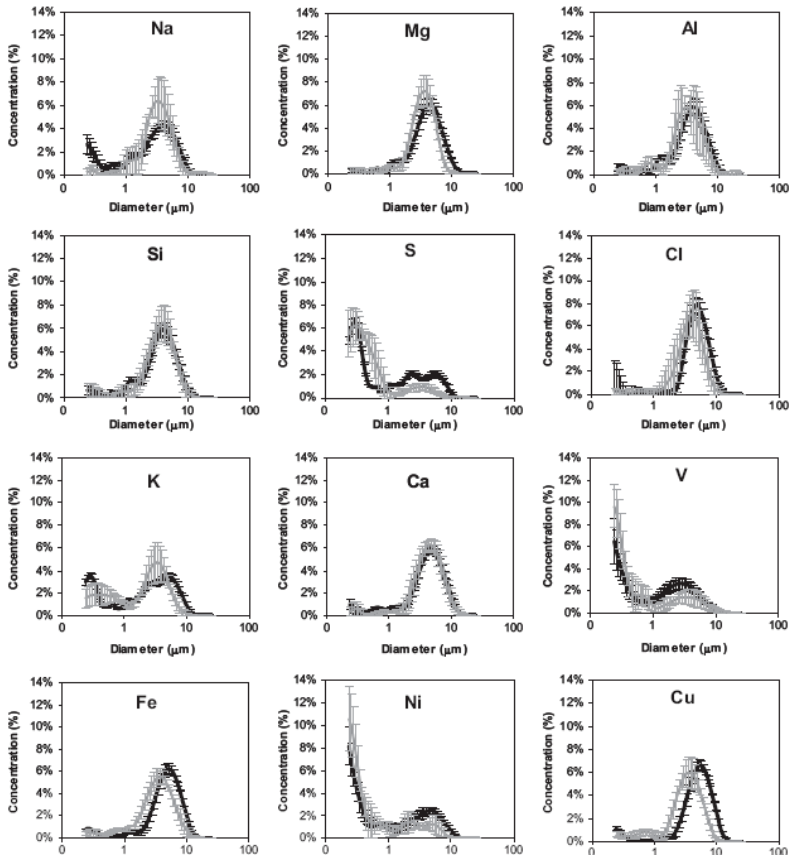

figure 3.13: elements size distribution obtained by multistage impactor (grey) and by the combination of PMD and OPC analysis (black), when only PM10, PM2.5 and PM1 profiles are available [Cuccia et al., 2010]

Chapter 4: Carbonaceous particles and the role of ^{14}C in source apportionment

4.1 Introduction.

Carbon is one of the major components of atmospheric aerosol, especially in the fine fraction.

Carbonaceous particles affect the atmosphere properties at both local and global scale (see par 4.1.3). They can have either natural or anthropogenic origin; in both cases, they can be of primary or secondary origin. For example, primary carbonaceous particles of natural origin are plants debris, spores, pollens, virus, and bacteria. Secondary particles of natural origin are formed by biogenic VOCs-to-particle conversion (e.g. VOCs like terpens emitted by trees). Primary carbonaceous particles of anthropogenic origin are mainly originated by combustion processes (e.g. traffic, industry, biomass burning), while secondary carbonaceous particles are formed by organic gas-to-particle conversion, mainly resulting from oxidation due to hydroxyl radical ($OH^{\bullet}$), ozone (O_3) and nitrate radical ($NO_3^{\bullet}$) [Jacobson et al., 2000] or from aqueous–phase oxidation [Haywood and Boucher, 2000].

4.1.1 Organic and elemental carbon.

Total carbon in the aerosol (TC) consists of two main fractions: elemental (EC) and organic (OC) carbon. Another small contribution from carbonate carbon (CC) may also exist; Chow and Watson (2002) consider it always negligible in PM2.5 or lower size particles. Also in PM10, it can be neglected except in regions near carbonate deposits. In this work carbonate will be considered as negligible in our PM samples.

EC has only primary origin and it is produced by the incomplete combustion of fossil and biomass fuels in an oxygen–poor environment; it is a complex three dimensional polymer and it is not present in atmosphere in its purest form (graphite): it is composed by randomly oriented crystals of 2–3 nm in diameter, interspersed with other elements (mainly oxygen, hydrogen, sulphur and nitrogen), in less than 10% of elemental carbon content [Chow et al., 2001]. Moreover, it is the main light

absorber material in atmosphere [Novakov, 1997].

OC, which is the most abundant fraction in carbonaceous aerosol, is either directly released in the atmosphere in the particulate form or it is formed in the atmosphere by gas-to-particle conversion of anthropogenic or biogenic precursor gases [Novakov, 1997]. It consists of thousands of chemical constituents belonging to many compound classes, such as aromatics or alcohols alkanes, and it covers a wide range of molecular forms, solubilities, reactivities, and physical properties which make a complete characterisation extremely difficult. In many areas, organic compounds represent the majority of particulate matter [Jacobson et al., 2000] and a lot of organic species have been recognised as biologically toxic [Chow et al., 2007]. It is noteworthy that the analytical separation of OC from EC using thermal protocols is, at the state of art, ambiguous because some of the EC thermally evolves in presence of oxygen, and part of OC can change to EC (this process is called pyrolysis or charring) in an oxygen–poor atmosphere [Watson et al., 2005], so the two fractions are operationally defined (see more details in paragraph 4.3.1). The definition of OC and EC is further complicated by a number of different methods (based on thermal or optical properties) used to quantify them. Results of round–robin tests carried out on samples of atmospheric aerosol show good agreement (better than 10%) for TC concentrations obtained by different instruments and techniques, while discrepancies up to a factor 2 are commonly found in EC measurements carried out with different methodologies (i.e. optical, thermal) [e.g. Schmid et al., 2001; Watson et al., 2005 and therein literature]. Further problems have to be ascribed to the absence of commonly accepted standards and reference materials that can be used to quantify EC as it appears in the atmosphere [Chow et al., 2001], thus it is impossible to characterise the EC thermal behaviour under different thermal analysis conditions [Yu et al., 2002]. In the last years, work on the realisation of a suitable reference material has been carried out [Popovicheva et al., 2010].

4.1.2 Global primary emission inventory of OC and EC from combustion

Bond et al. (2004) reported a new global inventory of black carbon (BC, which can

represent elemental carbon resulting from optical measurements) and organic carbon, as well as the uncertainties in these estimates.

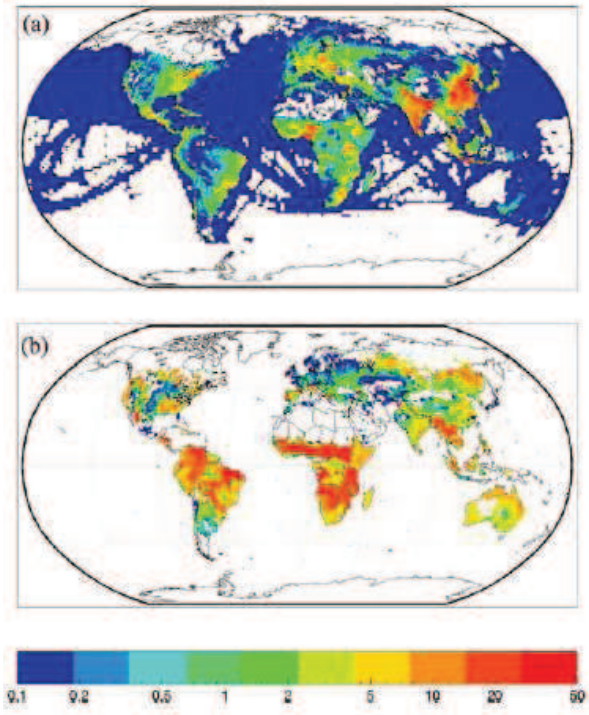

figure 4.1: Emissions of primary organic carbon aerosol based on 1996 activity data. (a) Contained combustion, based on 1996 activity data. (b) Open burning, annual average. The colour variation is approximately logarithmic and is the same as in figure 4.2. Units are ng/m^2/s [Bond et al., 2004].

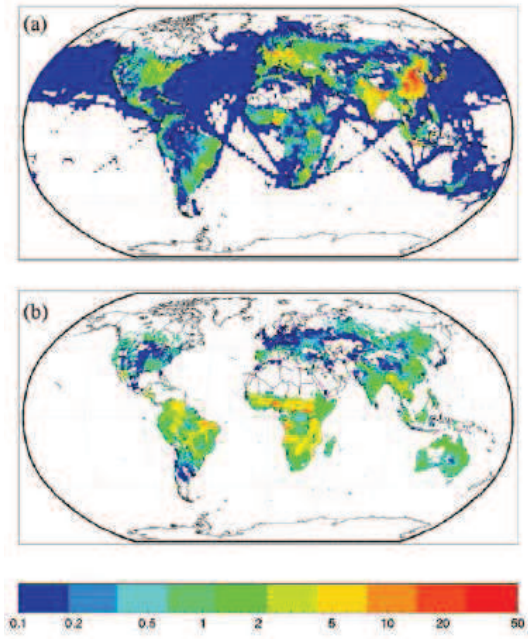

figure 4.2: Emissions of black carbon aerosol. (a) Contained combustion, based on 1996 activity data. (b) Open burning, annual average. The colour coding is an approximately logarithmic scale. Units are ng/m^2/s (1 ng/m^2/s = 32 kg/km^2/yr) [Bond et al., 2004].

The calculation procedure is based on combining fuel consumption data, application of combustion technologies, and emission controls. Bond et al. (2004) estimated primary organic carbon emissions from contained combustion of fossil fuels and biofuels in the range 5-17 TgC yr^{-1}, while open burning OC was estimated in the range 12–57 TgC yr^{-1} (see figure 4.1). As for BC emissions, Bond et al. (2004) estimated contained combustions in the range 3–10 TgC yr^{-1}, while open fires contribution was estimated in the range 1.6–3.8 TgC yr^{-1} (see figure 4.2). It is also worth noting that Ito and Penner (2005) report an increase of a factor three from 1870 to 2000 for BC emissions.

4.1.3 Importance of carbonaceous particles

Carbonaceous particles have great importance at both local and global scale.

In fact at the local scale:

- they account for a large part of PM concentration. For example, in the Milan urban area, they explain about 40% of PM10 (particles with aerodynamic diameter lower than 10 μm) mass during both summer and winter (see figure 4.3) [Vecchi et al., 2009a];
- there is evidence for a relationship between the presence of carbonaceous PM components and cardiovascular diseases and mortality. Recent studies indicate that OC and EC can have health importance equal to, or greater than, the other commonly measured pollutants. On the contrary, no evidence for a relationship between OC or EC and respiratory mortality was found [Mauderly and Chow, 2008 and therein literature];
- carbon interacts with light, removing it from a sight path and thus influencing visibility. Currently, visibility monitoring is mandatory in the US [EPA, 1999b; Watson, 2002 and therein cited literature], while no systematic monitoring is statutory in the EU;
- carbonaceous particles, together with sulphates, are the main responsible for the damage of monument surface in urban area. Both OC and EC are present in surface crusts, in different relative quantities depending on the analysed site [Bonazza et al., 2005]. The dark component of carbonaceous aerosols (EC) plays a key role in surface soiling and black crust formation.

Furthermore, carbonaceous particles, because of their high specific surface and the possible heavy metal content (especially when formed due to condensation processes), act as catalytic support to the heterogeneous oxidation of SO_2, thus fostering the transformation of carbonate calcium (marble, of which many monuments are made) into gypsum [Ghedini et al., 2000].

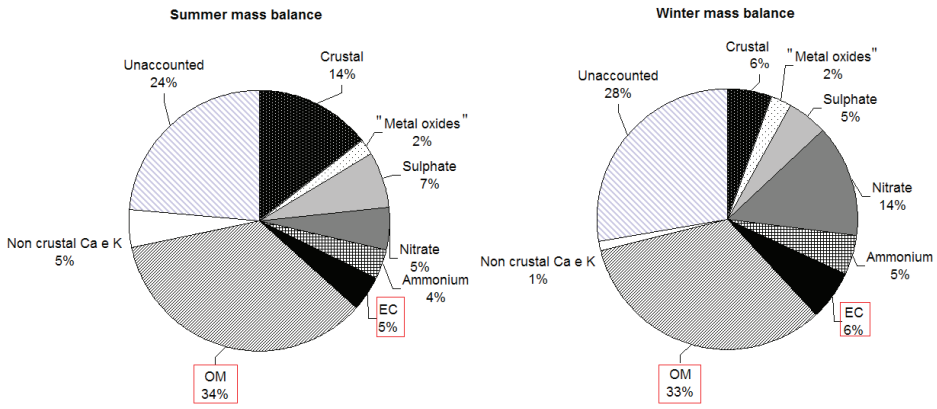

figure 4.3: chemical mass closure as reported in Vecchi et al., 2009a

At the global scale carbonaceous particles influence the radiative budget of the Earth–Atmosphere system in two different ways: they can scatter and absorb solar and thermal infrared radiation (direct effect), and they modify the microphysical properties of clouds with effects on their interaction with the radiation and lifetimes [Haywood and Boucher, 2000].

The Intergovernmental Panel on Climate Change reports a radiative forcing estimation of -0.05 ± 0.05 W m^{-2} for fossil fuel OC, 0.20 ± 0.15 W m^{-2} for fossil fuel BC and 0.03 ± 0.12 W m^{-2} for the whole biomass burning aerosol (see figure 4.4) [IPCC, 2007]. It should be noticed that central values for fossil and biomass carbon contribution are quite different and an improvement in the quantification of these two contributions may be important for the assessment of global scale effects.

Great uncertainties are associated to these estimates and they are due to different reasons. For example, BC has different effects if modelled as external or internal mixture (see figure 4.5): in the last case the radiative effect may be considerably enhanced. Moreover, the BC radiative effect depends on the reflectance of the underlying surface or if BC is above or below clouds.

As for OC, direct measurements are difficult and secondary production processes as

well as the presence of the natural component further complicate the correct estimation [Haywood and Boucher, 2000]. Moreover, a considerable fraction of OC is water soluble and at low relative humidity more water is often associated to organic fraction than to inorganic material, while at higher relative humidity the hygroscopicity of organic carbon is considerably less than that of sulphate aerosol [IPCC, 2007], modifying particle–radiation interactions. Therefore, also local meteorological conditions play an important role in the assessment of direct radiative forcing.

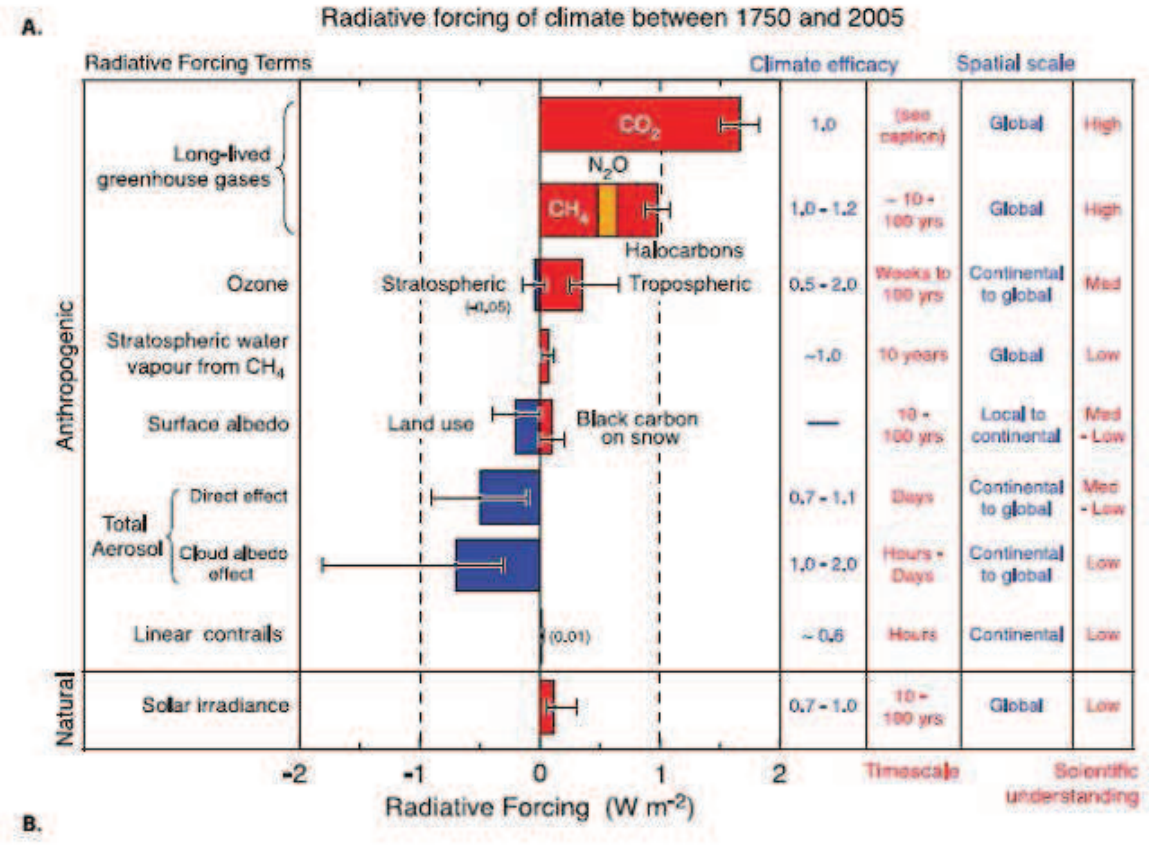

figure 4.4: radiative forcing of different atmospheric components as reported in IPCC (2007)

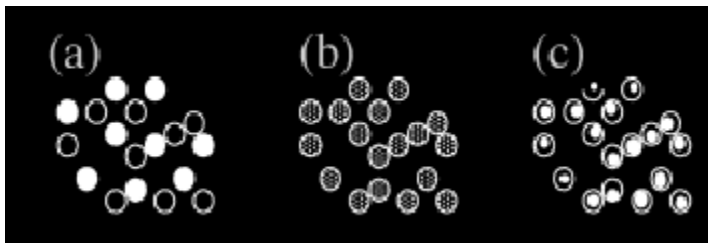

figure 4.5: a) external mixture; b) internal homogeneous mixture ; c) internal heterogeneous mixture

As regards the indirect effect, different aspects can be considered [Lohmann and Feichter, 2005 and therein cited literature] (figure 4.6):

a) the Twomey effect, which refers to the enhanced reflection of solar radiation due to more but smaller cloud droplets, whose liquid water content remains constant. In fact, anthropogenic aerosol can act as CCN, reducing the dimension of droplets in clouds;
b) the higher number of smaller droplets reduces the precipitation efficiency and therefore enhances the cloud lifetime and hence the cloud reflectivity (second indirect effect or cloud lifetime effect)
c) absorption of solar radiation by aerosol (especially BC) can lead to an air heating, which can result in cloud droplets evaporation with a dependence on the relative vertical position of clouds and BC (semi–direct effect).

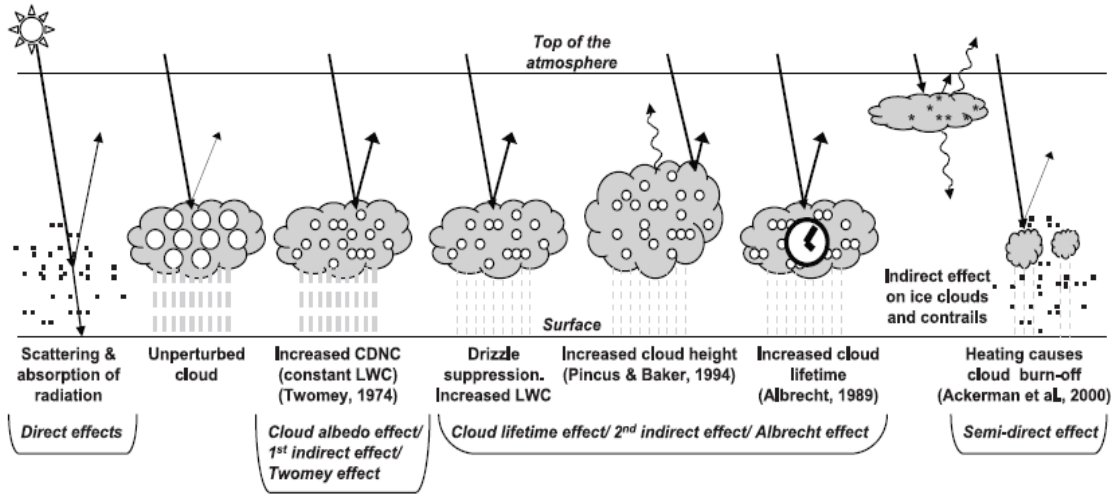

figure 4.6: direct and indirect aerosol effect

The average forcing due to anthropogenic aerosol influence on cloud albedo is estimated to be –0.7 W m^{-2} (ranging from –1.8 to –0.3 W m^{-2}) [IPCC, 2007], but the degree of scientific understanding is still considered low. Moreover, effects linked to cloud lifetime and precipitation were not considered in this estimation because potential cloud–dynamic feedbacks complicate the calculation of this effect [Pierce and Adams, 2009].

In this context, source apportionment gains great importance, as the possibility to correctly separate anthropogenic and natural components would allow the

assessment of human activities contribution to the locally measured carbonaceous PM. Moreover, among anthropogenic contributions, the apportionment between fossil fuels and biomass burning contribution would lead to the development of efficient abatement strategies and a better estimation of the effects at global scale of anthropogenic carbonaceous aerosol. The detection of specific chemical tracers (e.g. organic species) for the identification and quantification of the sources contributing to carbonaceous particles in atmosphere is a hard task. Indeed, a detailed carbon chemical speciation requires many analyses, and organic species identification is not completed yet. Moreover, high reactivity of organic species in atmosphere and temporal variation of emission factors further enhance uncertainties on source contribution estimates. Thus, another tracer for the separation of natural and anthropogenic carbon contribution is needed: ^{14}C measurements on aerosol samples (see paragraph 4.2) have a key role to achieve this goal.

4.2 ^{14}C in atmospheric aerosol and source apportionment

4.2.1 ^{14}C as a tool for apportioning natural and anthropogenic sources

^{14}C is an unstable natural carbon isotope. It is formed in the atmosphere by reactions between ^{14}N and thermal neutrons originated by secondary cosmic rays. $^{14}C/^{12}C$ ratio is about 10^{-12} and it is almost constant during time.

A very important ^{14}C feature is its half–life: 5730±40 years. As fossil fuels need millions of years to be formed, no ^{14}C is contained in these fuels anymore. Therefore, ^{14}C analyses on total carbon contained in atmospheric aerosol samples allow the discrimination between the contributions due to fossil fuels and to sources of modern carbon (i.e. biomass burning and biogenic emissions).

However, the aim of this work is separating natural from anthropogenic emissions. As biomass burning emissions at our latitudes have to be considered anthropogenic and they contain ^{14}C, the separation between fossil and non fossil contributions on the total carbon fraction does not allow the separation between natural and anthropogenic sources.

Nevertheless, ^{14}C analysis on the OC and EC fractions can be useful to achieve this separation (figure 4.7). In fact, EC is emitted only by combustion processes, thus it has two contributions: one from fossil fuels (where no ^{14}C is contained) and one from biomass burning (containing ^{14}C). Once these two contributions in the EC fraction are quantified, and knowing (from literature or experimental studies) the emission ratio $(OC/EC)_{ER,bb}$ by biomass burning, it is possible to assess the biomass burning contribution in the modern fraction of OC and, by difference in the ^{14}C–containing OC fraction, the natural contribution can be evaluated. Therefore, ^{14}C analysis on separated carbon fractions allows quantifying the contribution of natural and anthropogenic sources [Szidat et al., 2004a].

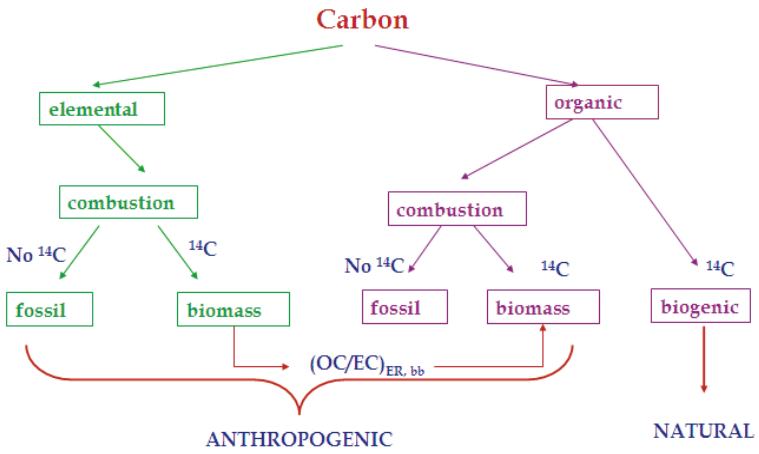

figure 4.7: scheme of ^{14}C contribution to the different carbon components and identification of natural and anthropogenic contribution

4.2.2 Fraction of modern carbon and source apportionment

^{14}C analyses are carried out using Accelerator Mass Spectrometry (AMS, see par. 4.4). This analysis gives information about the fraction of modern carbon (f_m) in the sample, which is defined as:

$$f_m = \frac{(^{14}C/^{12}C)_{sample}}{(^{14}C/^{12}C)_{1950}}$$

where $(^{14}C/^{12}C)_{1950}$ is the ratio between the concentrations of these two carbon isotopes in the atmosphere in 1950. The fraction of modern carbon is often represented also as percent Modern Carbon ($pMC = 100 \cdot f_m$).

The fraction of modern carbon is zero for fossil fuels, because of their long time of

formation. On the contrary, for biological materials originated in the last 50 years, it is higher than 1 because of the enrichment in ^{14}C atmospheric content generated by nuclear tests in the '50s; in particular:

a) for fossil fuels: $f_{m,fossil} = 0$
b) for biogenic contribution: $f_{m,bio} = 1.055 \pm 0.015$, obtained by long–term CO_2 series at rural Schauinsland, Germany [Szidat et al., 2009];
c) for biomass burning contribution the integral signal of 30–50 years old trees harvested in 2004 gives $f_{m,bb}$=1.16±0.05 [Szidat et al., 2009]. However, depending on the age of the tree, it can vary in the range 1.08-1.24 [Mohn et al., 2008].

As f_m is 1.055 in today atmospheric CO_2, the fraction of contemporary carbon defined as $f_c=1/f_{m,\,today}$ is sometimes used to represent the ^{14}C content in a sample.
The above mentioned data, coupled to AMS results on ^{14}C in the OC and EC fractions, allow the source apportionment of fossil, biomass burning and biogenic carbon contributions.
In fact, starting from the balance equations:

$$EC \cdot f_m(EC) = EC_{fossil} \cdot f_{m,fossil} + EC_{bb} \cdot f_{m,bb}$$

$$OC \cdot f_m(OC) = OC_{fossil} \cdot f_{m,fossil} + OC_{bb} \cdot f_{m,bb} + OC_{bio} \cdot f_{m,bio}$$

and recalling that the fraction of modern carbon for fossil fuels is zero, it can be derived:

$$EC_{bb} = EC\frac{f_m(EC)}{f_{m,bb}} \quad \text{and} \quad EC_{fossil} = EC - EC_{bb} = EC\left(1 - \frac{f_m(EC)}{f_{m,bb}}\right).$$

Moreover, considering a known value of $(OC/EC)_{ER,\,bb,}$ ratio in biomass burning:

$$OC_{bb} = EC_{bb} \cdot (OC/EC)_{ER,bb} \qquad OC_{bio} = \frac{OC\, f_m(OC) - OC_{bb} f_{m,bb}}{f_{m,bio}}$$

$$OC_{fossil} = OC - OC_{bb} - OC_{bio}$$

In conclusion, summing up fossil fuel and biomass burning contributions, the anthropogenic contribution to carbonaceous aerosol can be estimated (see figure 4.7).

4.2.3 Different approaches to solve the problem.

In paragraph 4.2.2, the possibility to apportion anthropogenic and natural carbon sources was shown. As mentioned, AMS measurements have to be performed to obtain the information necessary to achieve the source apportionment. It should be remembered that:

$TC=OC+EC$ and $TC\cdot f_m(TC)= OC\cdot f_m(OC)+ EC\cdot f_m(EC)$.

As these equations are linked and six parameters are indicated, it is sufficient measuring four of them to completely solve the problem. Thus, it is mandatory to evaluate which are the four physical quantities less affected by uncertainties in the experimental determination, to obtain the better solution to the problem.

It is worth noting that total carbon measurements (both TC quantification and $f_m(TC)$ evaluation) are the less affected by uncertainties as no carbon fraction separation is needed. If the interest is focused on TC quantification, the CO_2 evolving during combustion can be measured using an IR detector or a flame ionisation detector (FID) after CO_2 conversion to methane and ± 5% precision can be obtained. For ^{14}C analysis on TC, the evolved CO_2 can be separated from the carrier gas (oxygen) and it can be directly sent to the graphitisation line (see par. 5.1.6) for the production of solid samples for AMS analysis (par. 4.4). Once TC and $f_m(TC)$ are determined, the following approaches can be used to completely solve the problem:

a) the measurement of both $f_m(OC)$ and $f_m(EC)$;
b) the quantification of one carbon fraction (OC or EC) and measurement of the f_m of OC or EC.

It is noteworthy that the determination of f_m in carbon fractions does not require to completely collect the separated fractions: indeed, only part of OC and EC can be analysed by AMS, provided that it is representative for the whole fraction. Furthermore, for f_m analysis it is important that no contamination of a fraction into the other occurs.

During the set-up of the sample preparation line and to choose the definitive measurement protocol, both approaches were simultaneously tested in order to verify their consistency. In the final choice, the first approach was excluded because, as better explained in paragraphs 4.3.2 and 4.3.3, the determination of f_m for both

carbon fractions is highly time-consuming. Therefore, the simultaneous determination of both f_m(OC) and f_m(EC) will be avoided in the final measurement protocol.

4.3 The problem of carbon fractions measurement and separation

4.3.1 EC and OC quantification: the thermal approaches

As mentioned in paragraph 4.1.1, thermal analyses are widely used for OC and EC quantification. They are all based on the different evolution characteristic of the two fractions as a function of the temperature and type of atmosphere and on the quantification of the evolved CO_2 at the thermal steps chosen for the separation. Different approaches are reported in the literature for thermal analyses, but they can be divided in two main categories:

a) OC separation in inert atmosphere (He) [Chow et al., 1994; Birch and Cary, 1996; Cavalli et al., 2010];
b) OC separation in oxygen at low temperature (320–450°C) for different combustion periods [Cachier et al., 1989; Kirchstetter et al., 2001; Watson et al. 2005 and therein literature].

After the first step for OC separation, the remaining carbon is oxidised at 850–900°C and the carbon evolving during this second step is considered to be the EC fraction (possibly corrected for measurement artefacts, as explained in the following).

Thermal–optical transmittance method

One of the most widespread techniques for thermal quantification of OC and EC fraction is the Thermal–Optical Transmittance method (TOT) [Birch and Cary, 1996].

TOT analysis consists of two main steps: in the first part of the analysis the thermal evolution is carried out in inert atmosphere, up to 850°C (NIOSH 5040 protocol). During the evolution in inert atmosphere, pyrolysis of the material deposited on the filter can occur. Pyrolysis consists in the conversion of an organic compound into

one or more different compounds by thermal energy and it mainly occurs in an inert environment (lack of oxygen or catalysts). Carbonatation occurs in extreme pyrolysis to form EC [Chow et al., 2007]. In these conditions, pyrolysed OC (PyC) cannot evolve in the inert atmosphere anymore, thus an underestimation of OC and an overestimation of EC are registered if the separation of the two fractions is carried out only considering the atmosphere of evolution without any correction.

Pyrolysis leads to the variation of the optical properties of the sample as PyC is light-absorbing; thus, in the TOT analysis, the optical transmission of a laser through the filter is continuously monitored. Due to pyrolysis, the transmittance of the filter decreases during the first part of the analysis (He atmosphere). When oxygen is injected into the line, EC (both originally present on the filter and derived from OC pyrolysis) evolves causing an increase of the laser transmission. When the filter transmittance reaches the value registered at the beginning of the analysis, the method assumes that a quantity of EC equal to the one formed by pyrolysis has combusted and therefore all the carbon evolved up to this point has to be considered OC. All the remaining carbon is considered EC (see figure 4.8).

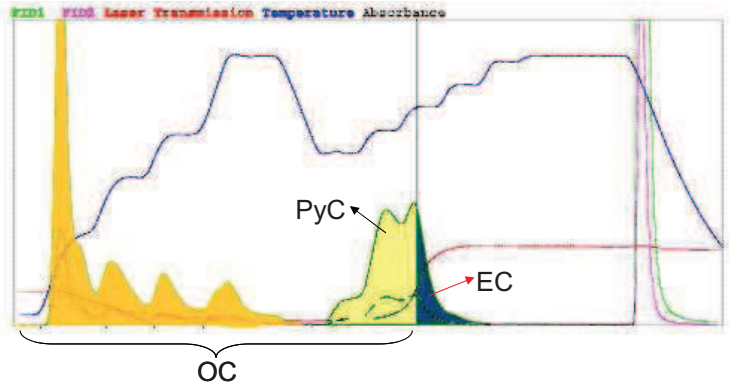

figure 4.8: example of a thermogram by TOT

It is noteworthy that this method does not physically separate the two fractions, but it simply corrects the measured concentration using EC optical properties. As AMS analysis requires the physical separation of the carbon fractions, the He atmosphere is not suitable to this aim, therefore other techniques for carbon fraction separation to obtain f_m(EC) and f_m(OC) were explored (see paragraphs 4.3.2 and 4.3.3).

Water Soluble Organic Compounds and pyrolysis

It is known that Water Soluble Organic Compounds (WSOC) are particularly prone

to pyrolysis, also in an oxygen atmosphere [Yu et al., 2002]. Thus, for a more reliable EC quantification and to limit OC transformation into EC during combustion when the two fractions have to be physically separated, the WSOC have to be removed from the sample.

Reduction in PyC formation when the analysis is carried out on washed filters is shown in figure 4.9: the laser reduction during TOT analysis on the correspondent washed filter is definitely smaller than the one registered during TOT analysis on non–washed filter. Reduction in charring leads to a more reliable EC measurement as the analytical interference is minimised. It is also noteworthy that EC is not soluble, thus EC measured on washed filters was chosen as the most reliable EC value on the filter. Once EC is evaluated on washed filters and TC is measured on the filter as-is, OC can be reliably evaluated as OC=TC–EC.

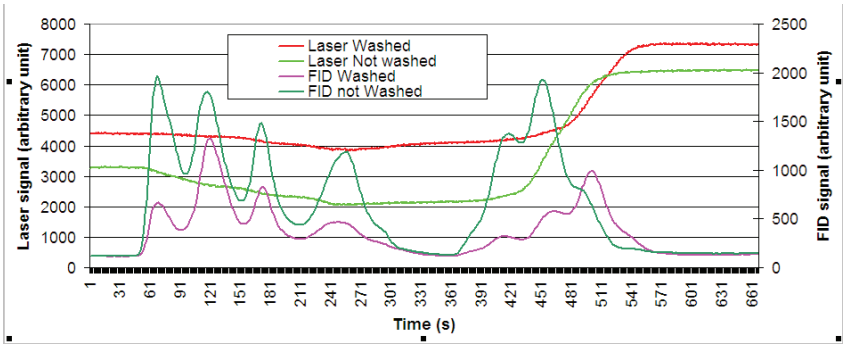

figure 4.9: laser pattern during TOT analysis on washed and non–washed filters.

4.3.2 EC separation procedure for f_m(EC) determination

As previously mentioned (par. 4.3.1), the application of TOT method does not physically separate the OC and EC, but it simply allows a quantification correcting the measured concentration using the EC optical properties. On the contrary, ^{14}C measurements by AMS analysis require solid samples of a specific carbon fraction to be analysed. The carbonaceous fractions in the sample have to be physically separated, and the CO_2 derived from each fraction has to be converted into graphitic form.

Thus, the hypothesis to carry out OC–EC separation following TOT protocol had to be abandoned due to the high PyC formation, and other techniques for the separation of EC and OC fractions, aimed at f_m(EC) and f_m(OC) determination, were explored. In figure 4.10, the laser transmittance through a filter when analysed

using different measurement procedures is shown. It is noteworthy that the smallest variation in the transmittance signal is registered when working in oxygen on a washed filter, further demonstrating the reduction in PyC formation.

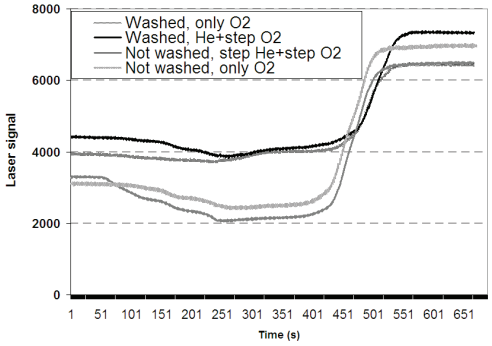

figure 4.10: comparison among laser patterns during thermal analyses carried out on washed and non–washed filter in He or He–O_2 atmosphere

Charring has to be minimised to correctly separate the two fractions, therefore the protocol for the fraction separation had to fulfil the following guidelines:

a) washing the filters for WSOC removal (see the set-up of the washing procedure in par. 5.4.1);
b) the first heating step for OC evolution has to be carried out in oxygen;
c) a rapid heating ramp (flash-heating, about 150°C/min) was chosen to further reduce pyrolysis formation following Cachier et al. (1989).

Tests carried out in this work (see par 5.4.2) showed that oxygen step is not sufficient to efficiently remove OC from the filter. Thus a further step in He at high temperature was inserted in the final protocol.

4.3.3 f_m(OC) measurement

For f_m(OC) determination, the direct measure on the whole OC fraction on not-washed filters is difficult because of the WSOC charring, which removes a significant OC fraction from the evolved OC sample. However, OC fraction may be divided into two sub-fractions: WSOC and water–insoluble organic carbon (WINSOC). The following balance equation can be written:

$$f_m(\mathrm{OC}) \cdot \mathrm{OC} = f_m(\mathrm{WSOC}) \cdot \mathrm{WSOC} + f_m(\mathrm{WINSOC}) \cdot \mathrm{WINSOC}\,.$$

WSOC can be obtained as TC–TC_{ww}, where TC_{ww} is the total carbon measured on a washed portion of the filter: indeed, the difference in total carbon content between

non-washed and washed filters is due to WSOC, as EC is not water soluble. The first term on the right hand of the previous equation can be re–written as:

$$f_m(\mathrm{WSOC}) \cdot \mathrm{WSOC} = f_m(\mathrm{TC}) \cdot \mathrm{TC} - f_m(\mathrm{TC_{ww}}) \cdot \mathrm{TC_{ww}}$$

Therefore, $f_m(\mathrm{WSOC})$ can be determined by measuring f_m(TC) and $f_m(TC_{ww})$.

WINSOC is represented by the OC measured on the washed filter. f_m(WINSOC) can be evaluated collecting the CO_2 produced at the beginning of the analysis (in our case during the first 20 minutes) burning a washed filter portion at 325°C in oxygen (as 325°C will be also the final temperature chosen for EC separation, see par 5.4.2). In this case, as no selective separation of a specific component of WINSOC is expected, the evolved CO_2 can be considered as representative of the whole WINSOC fraction.

It is worth noting that three f_m measurements are required to determine f_m(OC). However, the fractions to be analysed for ^{14}C quantification (TC, TC_{ww} and WINSOC) are easier to separate than EC. Moreover, this method allows to determine f_m(OC) independently from the f_m(EC) measurement and it gives information on the two main OC sub-fractions.

Hence, the determination of both f_m(EC) (par. 4.3.2) and f_m(OC) allows checking the reliability of the obtained results using the following equation:

$$f_m(\mathrm{TC}) \cdot \mathrm{TC} = f_m(\mathrm{EC}) \cdot \mathrm{EC} + f_m(\mathrm{OC}) \cdot \mathrm{OC}\,.$$

This is very important during the set-up of the method, in order to verify that the application of different measurement protocols gives comparable results. However in the final choice, only the f_m of one fraction will be measured, because of the time required by the samples preparation for AMS.

4.4 ^{14}C measurements: accelerator mass spectrometry

High-sensitivity analytical techniques are required to measure ^{14}C in aerosol samples as radiocarbon does not exceed one part on 10^{12} of the total carbon. Therefore, the use of Accelerator Mass Spectrometry (AMS) is mandatory to perform ^{14}C measurements.

AMS measurements were performed at LABEC-INFN (LAboratorio di tecniche

nucleari per i BEni Culturali - Istituto Nazionale di Fisica Nucleare) in Sesto Fiorentino (Fi), Italy (figure 4.11). This laboratory is equipped with a 3 MV terminal voltage tandem accelerator (Tandetron) used for both Ion Beam Analyses (IBA) and for AMS measurements.

Solid samples of the desired material have to be prepared (in our case, graphite samples from the evolved CO_2). They are inserted in the accelerator source, bombarded using positive caesium ions to produce a negative ion beam, which is injected into the line. The isotopes selection is carried out at both the low and the high energy sides of the accelerator using electrostatics analysers and suitable magnets.

At the end of the separation procedure, ^{12}C and ^{13}C ions, during the respective time windows of injection, follow inner trajectories and are collected by Faraday cups, where the current integration provides an indirect measurement of their abundance. On the contrary, ^{14}C ions are counted in a gas chamber implementing a two-stage telescope detector. Further details on the AMS line can be found in Fedi et al. (2007).

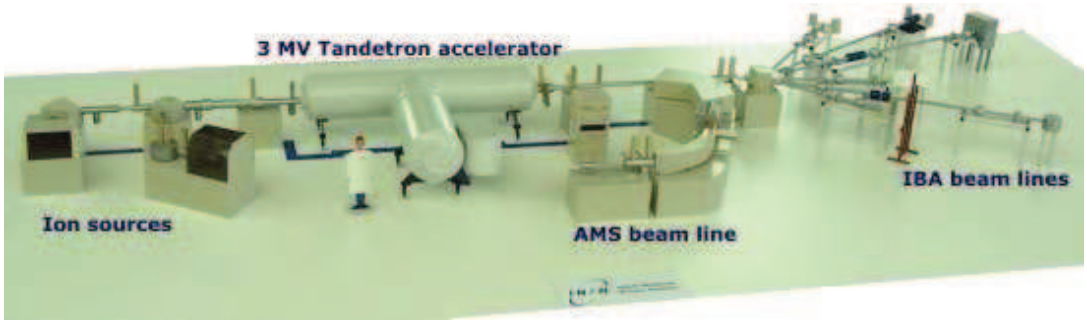

figure 4.11: Scheme of the accelerator facility at Labec-INFN

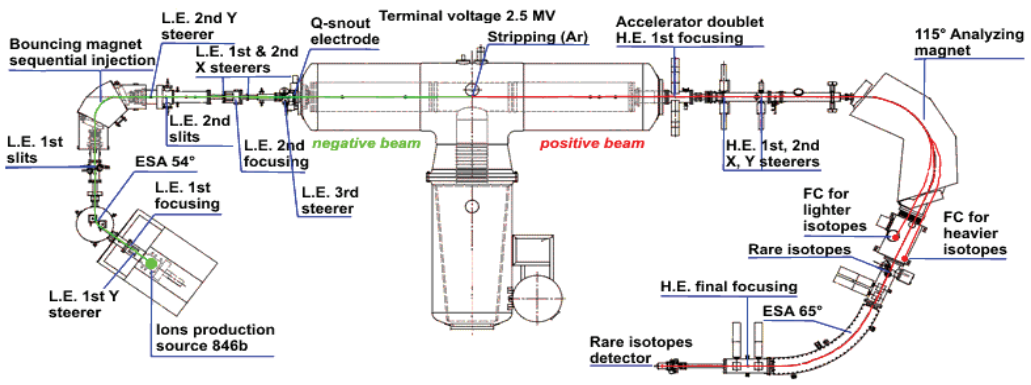

figure 4.12: AMS device (http://labec.fi.infn.it/Facilities.html**)**

Chapter 5: Set-up of a sample preparation line for ^{14}C measurements in atmospheric aerosol

In Chapter 4, problems concerning ^{14}C measurements in aerosol carbon fractions were explained. Summarising, there is the need to suitably thermally treat the sample in a combustion oven. Thermal separation requires the use of a carrier gas completely depleted of carbonaceous species (organics and CO_2), and the CO_2 produced during the thermal treatment has to be separated from other combustion gases as well as from the carrier gas because the combustion phase is carried out under gas flow. The CO_2 is then sent to the graphitisation line in order to convert it into solid samples for AMS analysis.

Thus, the sample preparation line has to match different requirements, considering the small quantities of carbon available for the analyses (usually a few hundred micrograms of carbon: μgC):

a) any CO_2 contamination from ambient air, carrier gases or parts of the line has to be avoided;
b) the CO_2 produced during the combustion phase has to be highly purified to allow graphitisation of small CO_2 quantities;
c) high efficiencies in the CO_2 separation and recovery process are needed in order to have enough material for the production of solid carbon samples (graphitisation) and for the subsequent analysis by AMS.

To this aim, a new sample preparation line was designed and set-up during this PhD thesis in close collaboration with the LABEC research group [Calzolai, 2009]. The final line is now available at the LABEC-INFN in Sesto Fiorentino, where also the AMS facility is located.

In this chapter, a description of the line realised in this PhD work and the first results are presented.

5.1 The sample preparation line.

In figure 5.1 a scheme of the sample preparation line designed and realised during this PhD thesis is shown. Even if different solutions were tested before realising the

definitive line, only the final set-up will be described in detail in the following paragraphs.

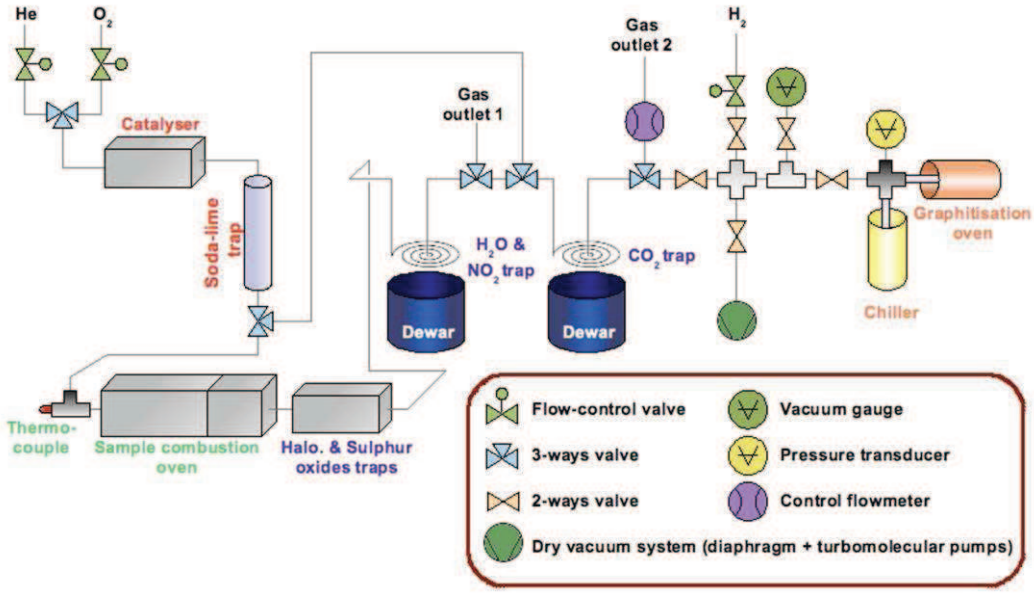

figure 5.1: scheme of the sample preparation line

The main improvements in this preparation line, when compared to the (few) others already existing for this type of measurement, consist in the sample combustion oven (see par. 5.1.2) and the system for CO_2 trapping (see par. 5.1.5)

5.1.1 Purification of carrier gases.

Helium or oxygen are used as carrier gases, to create the proper atmosphere for the sample combustion. Two thermal mass-flow controllers, placed at the entrance of the line, are used for flow regulation. The carrier gases are supplied by gas cylinders of high-purity helium (99.998%) and oxygen (99.999%).

In the first part of the sample preparation line (figure 5.1), carrier gases are purified to avoid possible contamination deriving from carbonaceous gaseous traces (CO, CO_2 and organics) in the carrier gas. To this aim, a CuO oxidiser (kept at 700°C) was inserted to convert possible carbonaceous trace gases into CO_2. The produced CO_2 is then trapped in a non-reversible soda–lime CO_2 trap, assuring that the carrier gas used for combustion is completely carbon-free.

5.1.2 Sample combustion oven and oxidising catalyst.

Once purified, the carrier gas enters the sample combustion oven (figure 5.1), which allows suitable thermal evolutions of the sample. The combustion oven is home–

made and it was designed, realised and optimised during this work. Its main features are the following:

a) it allows flash heating (150°C/min) to reduce pyrolysis during the combustion of OC for a better OC/EC separation;
b) it has a small volume and it is optimised to obtain a good temperature uniformity (≤ 3°C) inside the oven;
c) it is remote-controllable, in order to allow future line automation.

In the final configuration, a second oven is inserted in the same box of the combustion oven to lodge the CuO catalyst necessary for the complete oxidation of combustion gases.

It is interesting to note that in the first prototype of the line the main oven was completely separated from the oxidising catalyst oven. However, problems in the line were registered with this configuration. The main problem was the formation of a dark "stain" at the output of the main oven (see figure 5.2).

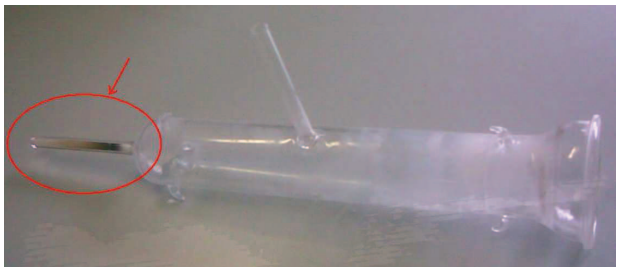

figure 5.2: stain at the output of the main oven in the prototype

The analyses of the deposit on the oven were carried out by the colleagues of Department of Inorganic, Metallorganic and Analytical Chemistry of the University of Milan, evidencing the presence of organic material and sulphates. They could result by the condensation of non-completely oxidised material: indeed, in the prototype the oxidising catalyst was about 30 cm far from the main oven, thus the gases leaving the main oven could cool before entering the catalysing oven. In this configuration, low vapour pressure gases could condense, giving origin to the observed effect.

Therefore, the main oven was re-designed and set-up. In the final configuration the two ovens are placed as near as possible (< 5 cm) in the same metallic box (see figure 5.3).

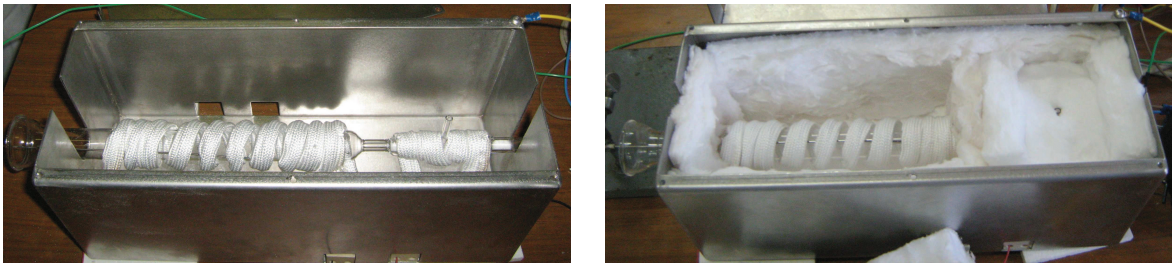

figure 5.3: the main oven: the core (left) and the final configuration with the thermal insulation (right)

The core of the final oven is composed by a double quartz furnace. The left part is the sample combustion cell and it is surrounded by a heating coil (60 Ω). The coil is inserted in a quartz fibre cloth, to ensure electrical insulation. The system is thermally insulated using quartz wool sheets, and enclosed in a metallic box. Temperature monitoring inside the combustion cell is achieved by a K-type (chromel-alumel) thermocouple inserted through the joint cap that closes the main furnace. It is positioned along the main furnace axis, in the middle of two sample boats used for sample insertion. The connection of the joint cup to the previous part of the line and to the thermocouple is realised by a Swagelok Ultra-Torr Tee connection.

The right-side of the quartz furnace is used for the CuO catalyst lodgement. It is surrounded by a small heating coil (about 110 Ω) and the temperature control, less critical than in the combustion cell, is carried out by a thermocouple inserted in a quartz finger that reaches the external surface of the furnace.

The main problem faced in this configuration was to obtain the thermal decoupling of the two ovens. In fact, the catalysing oven has to be always kept at high temperature (700°C), while the combustion oven has to rapidly increase or decrease its temperature and it has to be thermally uniform inside. It is noteworthy that the main oven has one side at room temperature (inlet) and the other at few centimetres from the catalysing oven.

Thus, to obtain good thermal decoupling the joint between the two ovens was narrowed and two layers of insulating material (quartz wool sheets) were inserted in order to limit irradiation effects. Tests were also carried out to determine the lowest operational temperature of the CuO catalyst, in order to minimise its influence on the main oven. Known carbon quantities were burnt in inert atmosphere and the

results obtained at different temperatures were compared. No significant differences in the CO_2 output was observed working with the CuO catalyst at 650°C, 750°C or 850°C. In the final setup, the CuO catalyst was kept at 700°C (figure 5.4).

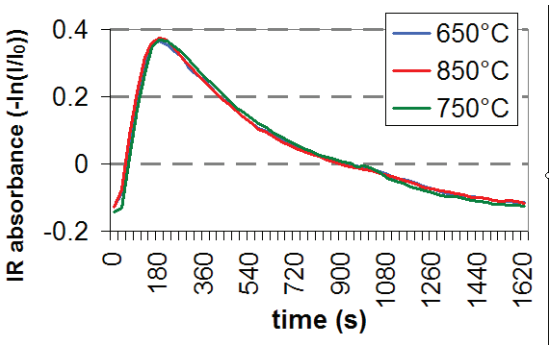

figure 5.4: IR signal during the on the catalyst temperature

Also careful optimisation of the combustion oven was needed; many tests were performed slightly moving the heating coil winds until the correct temperature ramp and temperature uniformity (at least in the central part of the cell) were obtained. In the final configuration, ± 3°C were obtained @ 400°C for 10 cm in the centre of the cell (figure 5.5).

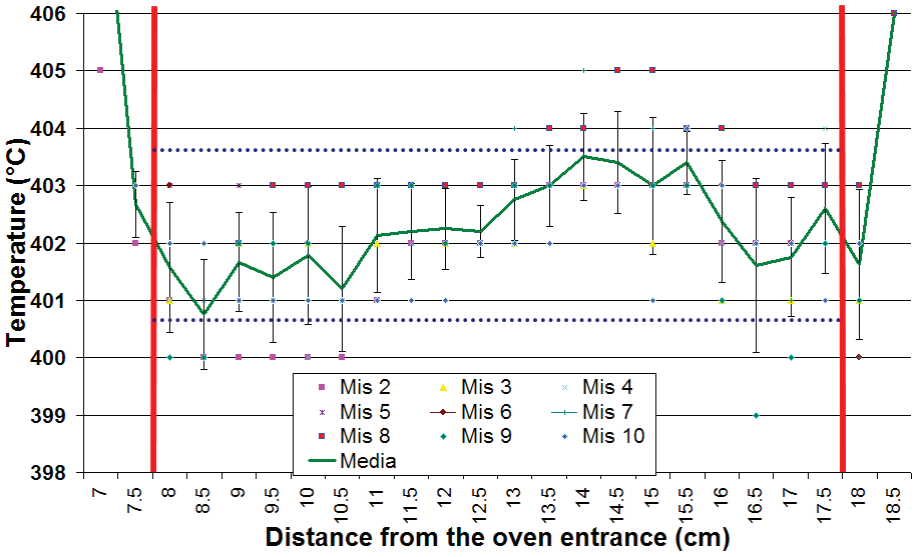

figure 5.5: temperature detected inside the furnace when a fixed thermocouple was reading 400°C

5.1.3 Sulphates and halogen traps

A fourth oven was also inserted in the line. It contained two commercial reagents (EA–1000 and Silver Vanadate from Perkin–Elmer) used to trap sulphates and halogens, respectively. All these reagents are kept at about 800°C to ensure a good trapping efficiency.

5.1.4 Water and NO_2 trap

Also water and NO_2 have to be removed from the gas flow, in order to separate CO_2 and the carrier gas from all the other combustion products. They are removed using a cryogenic trap, kept at about -55°C to obtain water and NO_2 condensation (see table 5.1), while CO_2 and the carrier gas go on flowing in the line. This trap is based on a coil inserted in a dewar partially filled with liquid N_2 as better explained in the next paragraph.

5.1.5 CO_2 trap

The CO_2 trap is necessary because the CO_2 produced during sample combustion has to be completely separated from the carrier gas. Indeed, the graphitisation process requires that only pure CO_2 enters the graphitisation line. The CO_2 trap realised in this work was designed, realised, and tested following an original idea.

Gas	Melting temperature (°C, at 1 atm)	Sublimation temperature (°C, at 1 atm)	Sublimation temperature (°C, at 1 mbar)	Sublimation temperature (*) (°C, at $2 \cdot 10^{-4}$ mbar)	Boiling temperature (°C, at 1 atm)
H_2O	0.0				100.0
NO_2	**-11.2**				21.1
CO_2		**-78.8**	**-137.2**	**-173.2**	
O_2	-218.4				**-183.0**
N_2	-210.0				**-195.9**
He					-269.0

table 5.1: phase transition temperatures of interest for the preparation line; (*) [Azreg-Aïnou, 2005]

CO_2 can be separated from the carrier gas because of the difference between CO_2 sublimation temperature (-79°C) and oxygen and helium condensation temperatures (-183°C and -269°C, respectively, see table 5.1). When the gases enter a part of the preparation line which is kept at a temperature between -183°C and -78°C, the CO_2 solidifies and it is trapped at that point, while the carrier gas remains in the gas state. In this work, the separation of the CO_2 from the carrier gas was realised starting from the following principle: in a dewar partially filled with liquid nitrogen (LN_2), a temperature gradient is established between the LN_2 surface (–196°C) and the dewar top (at room temperature) (see figure 5.6). Provided that the dewar is sufficiently deep for the temperature gradient to be smoothed enough to obtain a

good temperature resolution, it is possible to realise a thermal trap working at the desired temperature giving a spiral shape to a stainless steel tube and positioning the spiral at the proper depth into the dewar. As the spiral is connected to the line, the distance between the spiral and the liquid nitrogen can be regulated lifting up and down the dewar by a controlled elevator (figure 5.7). A resistive thermal element (PT100) connected to the coil allows the temperature monitoring.

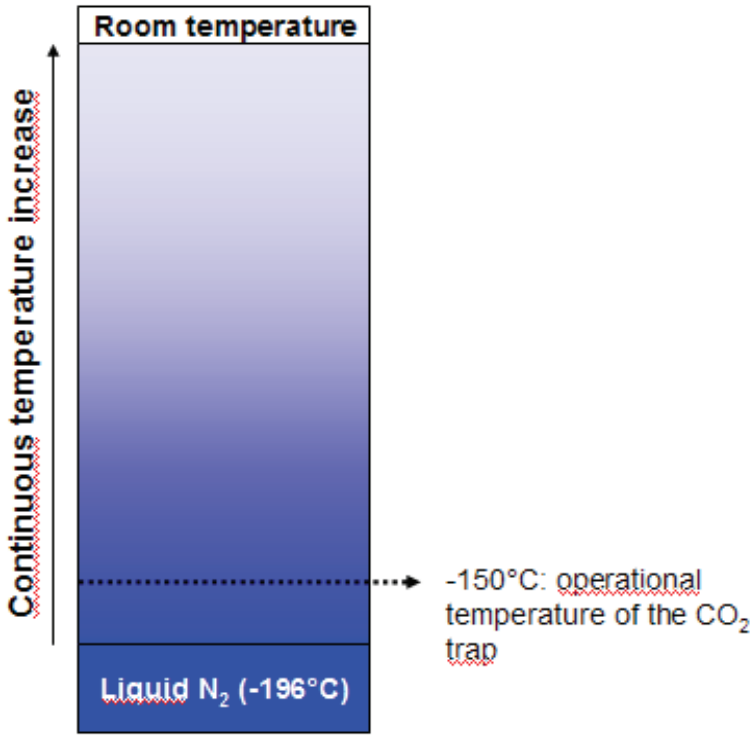

figure 5.6: scheme of the temperature inside a dewar partially filled with liquid nitrogen

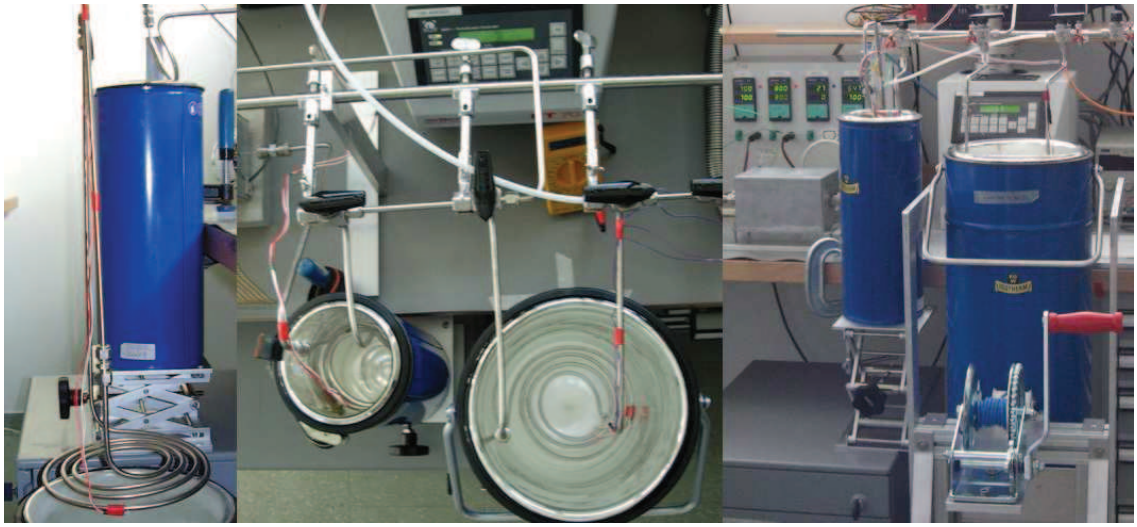

figure 5.7: left: CO_2 trap spiral; **centre:** water and CO_2 traps inserted in the dewars; **right:** dewars and controlling elevators

Before being installed in the sample preparation line, the CO_2 trap efficiency had been verified using Thermo Gravimetric-Infrared Analysis instrumentation (TGA-IR) by Perkin Elmer, which was accessible at the Department of Inorganic, Metallorganic and Analytical Chemistry of the University of Milan. A known carbon quantity was combusted and cryogenically trapped. In figure 5.8, the IR signal during CO_2 trapping and release phases is reported a for a vertical and a co-planar spiral configuration. It can be noticed that in the vertical spiral configuration the CO_2 was not trapped even when the lowest part of the spiral was at -150°C. On the contrary, in co-planar spiral configuration, no CO_2 signal was registered during the trapping phase, while a strong CO_2 peak was registered when the spiral was heated to ambient temperature. Therefore, co-planar spiral was used in the final set-up.

As the IR detector was calibrated, it was also checked that no CO_2 losses occurred during the whole procedure, using the CO_2 produced by a known quantity of sucrose. A 98% recovery efficiency was found in the co-planar spiral configuration.

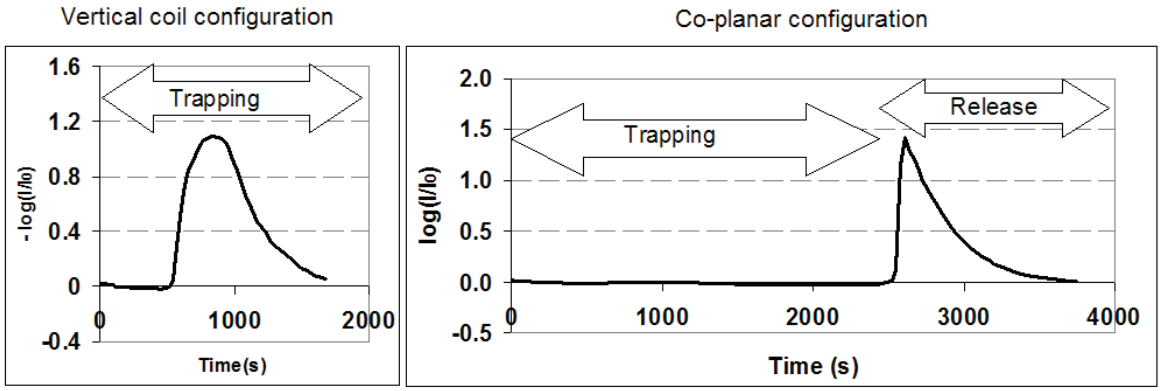

figure 5.8: left: IR signal in the vertical coil configuration during trapping phase (bottom at -150°C); **right:** the IR signal during trapping (-150°C) and release (coil outside dewar) phases in the co-planar coil configuration.

Once the CO_2 is trapped, it has to be transferred to the graphitisation line. To this aim, the trapping coil has to be isolated from the rest of the line and it has to be evacuated.

The CO_2 trap usually operates at -150°C. At this temperature, only primary vacuum (3-4 mbar) can be created in the spiral avoiding CO_2 sublimation (see table 5.1). To reach the $5 \cdot 10^{-4}$ mbar pressure needed to ensure that all impurities are removed

from the line, the spiral must be cooled to the LN_2 temperature to avoid CO_2 sublimation. However, at this temperature oxygen condensates; thus, before evacuating the spiral, the oxygen used as carrier gas has to be removed. Therefore, He flows in the spiral for 5 minutes after combustion, purging off all the oxygen. The coil can be now connected to the graphitisation line and primary vacuum is created, the spiral is cooled to LN_2 temperature, and high-vacuum is realised.
Then, the CO_2 can be moved to graphitisation line.

5.1.6 Graphitisation line

The last part of the line (called "graphitisation line") is devoted to the conversion of gaseous CO_2 into solid graphite and it was completely developed at the LABEC-INFN in Sesto Fiorentino [Calzolai, 2009]. Unlike the upstream parts of the line working with a gas flow, this part has to be kept under vacuum conditions (a few 10^{-4} mbar) before CO_2 insertion. Therefore, the graphitisation line is equipped with a compact dry vacuum system, based on a turbo-molecular pump backed by a diaphragm fore-pump (oil diffusion pumps were avoided because of the possible contamination deriving from malfunctioning).
Once moved to the graphitisation line, CO_2 is reduced to graphite according to the well-known Bosch reaction [Vogel et al., 1984; Lowe and Judd, 1987]:

$$CO_2 + 2H_2 \xrightarrow{Fe,600°C} C + 2H_2O$$

The core of this part of the line is the graphitisation reactor, which is constituted by a Swagelok Ultra-Torr ¼' Tee union, modified to lodge a pressure transducer. It is connected at one side to the upstream line and houses two quartz vials into the other two connections (see figure 5.9).

figure 5.9: the graphitisation reactor

As the reaction occurs at 600°C, one of the two vials is heated by insertion in an oven; the second vial is cooled to -30°C by a Peltier chiller and acts as a "cold-finger", where the water produced during the reaction is cryogenically trapped.
The H_2 for the reaction is supplied by a gas generator, producing 99.999% pure H_2 by hydrolysis of ultra-pure water. Iron powder (Alfa Aesar, 99.9+%, < 10 μm) is used as catalyst; it is pre-treated by heating for 30 minutes at 600°C in vacuum and subsequently at 350°C in H_2 environment for 30 minutes.
A low-vacuum capacitive pressure transducer placed on the upper part of the reactor allows the monitoring of the pressure trend during reaction: the reaction is completed when all the CO_2 has been converted into graphite, i.e. when the pressure settles to a constant value (note that the graphitisation is always carried out in excess of H_2). Finally, the iron powder coated by graphite is pressed into aluminium capsules (in the following called “cathodes”) to be inserted into the accelerator ion source for radiocarbon measurements (par. 4.4).

5.2 The final TC measurement protocol.

Before carrying out the first tests on the line, a measurement protocol was established for TC sample preparation to ensure that all the samples followed the same handling.
First of all, the catalyst for carrier gas purification and the oven with the traps for sulphate and halogens are switched on at 700°C and 800°C, respectively. He (180 cc/min) flows in the line during this phase. About 10 minutes are required for the catalyst oven to reach the temperature, thus ensuring pure gas enters the line. Then the sample is inserted in the combustion cell. He flows in the line for 20 minutes to completely purge the line before the sample combustion. After this period, the traps for water and NO_2 and for CO_2 are inserted in the dewars until the desired temperatures are reached (i.e. -55°C and -150°C, respectively). The importance of He flowing in the line in this phase is that, during traps positioning, it is possible that the spirals touch the LN_2 at the bottom of the dewar. In this case, oxygen would condense, while He remains in the gaseous state also at that temperature. Once traps are positioned, oxygen (100 cc/min) is injected in the line and the CuO catalyst for

combustion gases oxidation is switched on. When it reaches the correct temperature (700°C in about 10 minutes), the combustion of the sample can begin: the combustion oven is switched on (final temperature: 800°C) and combustion occurs for 20 minutes.

Then, oxygen has to be removed from the line (see par 5.1.5) and He (100 cc/min) is injected in the coil through the rapid line connecting the exit of the soda-lime trap to the entrance of the CO_2 trap spiral (see figure 5.1) for 5 minutes. The spiral is then isolated from the combustion line and it is connected to the graphitisation line creating a primary vacuum (a few mbar). The trap coil is then inserted in the LN_2 to avoid in-vacuum CO_2 sublimation while creating about $7 \cdot 10^{-4}$ mbar vacuum. Then the pump is turned off and the CO_2 is cryogenically transferred to the graphitisation reactor (where Fe pre-treatment has been performed in the meanwhile), and it is quantified. Only the CO_2 quantity established for a specific AMS measurement shift is selected, suitable amount of H_2 is added, and the graphitisation process can begin (it lasts about 150 minutes).

It is noteworthy that the procedure requires more than four hours to be completed. The preparation of these samples is very time-consuming and no more than two samples per day can be prepared.

5.3 Tests on the sample preparation line for TC measurements

To verify the reliability of the sample preparation procedure with the new line, several cathodes (i.e. graphite samples pressed inside capsules to be inserted into the AMS ion source), all having the same size (i.e. about 450 μgC), were produced and analysed by AMS. Samples were prepared following the matching-size method (i.e. samples and standards must have the same size): in fact, with this method, it is possible to compensate for machine induced isotopic fractionation [Pearson et al., 1998, Nadeau et al., 2004].

In total 20 cathodes were prepared as follows: 13 samples from NIST 4990C standard (OxAcII) to check the reproducibility of the results; 3 cathodes from “dead

graphite" samples (Alfa Aesar graphite) to investigate the background level in our measurements; 4 cathodes from the C7 reference material by IAEA (International Atomic Energy Agency) to measure the accuracy of the results.

Measurements lasted until collecting at least 40000 ^{14}C counts on every OxAcII cathode, to limit statistical uncertainties.

5.3.1 Reproducibility

The reproducibility was tested on the OxAcII standards. The average ^{14}R ratios (i.e. the $^{14}C/^{12}C$ ratios) in all the standard samples, calculated over all the measured batches, are shown in figure 5.10. The reproducibility is quantitatively evaluated as the ratio between the standard deviation of the mean (σ_{mean}) and the averaged isotopic ratio (R_{av}) over all the measured standards. As shown in table 5.2, the overall reproducibility of sample preparation and sample AMS measurement is better than 3‰ for both ^{13}R (i.e. the $^{13}C/^{12}C$ ratios) and ^{14}R.

Samples	$^{14}R_{av}$	σ_{14}^{mean}	$\sigma_{14}^{mean}/^{14}R_{av}$	$^{13}R_{av}$	σ_{13}^{mean}	$\sigma_{13}^{mean}/^{13}R_{av}$
OxAcII	1.5395E-12	0.0041E-12	2.7 ‰	0.011832	0.000023	2.0 ‰
Reference			< 5 ‰			< 3 ‰

table 5.2: statistics on $^{14}R_{av}$ and $^{13}R_{av}$ obtained by the average over all the standards. The reference values are taken by the laboratory protocols ^{14}C measurements for dating

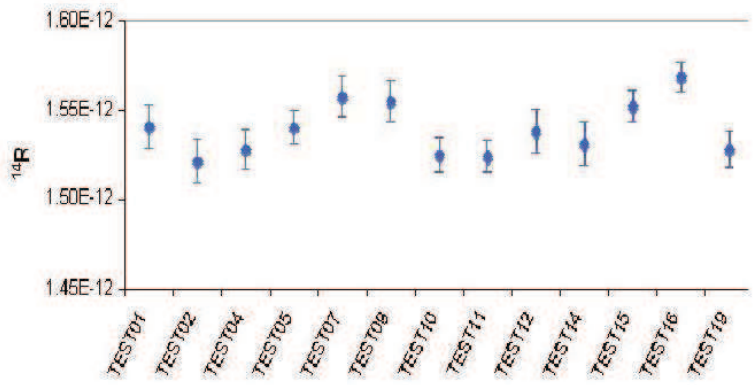

figure 5.10: ^{14}R ratio in the Oxalic Acid samples measured by AMS

5.3.2 Background

The background contribution is much less critical in aerosol source apportionment than in radiocarbon dating. However, it is important to keep this aspect under control; therefore, three cathodes from Alfa Aesar graphite were prepared and

analysed. The average background level is 0.43 ± 0.03 pMC (recall: pMC=100*f_m) and it does not represent a limitation for our measurements. Indeed, the minimum radiocarbon concentration expected in aerosol samples is at least one order of magnitude higher than the background value reported above. For example, a study on particulate matter collected in Göteborg reported radiocarbon concentrations in the range 5÷17 pMC for the EC fraction at an urban site, rising up to 35 pMC at a rural site, while radiocarbon concentration in the OC fraction were always higher than 50 pMC [Szidat et al., 2009].

5.3.3 Accuracy test

The accuracy of both sample preparation and AMS measurement was tested using some cathodes prepared from the IAEA C7 reference material, i.e. oxalic acid with pMC = 49.53 ± 0.12 [Le Clerq et al., 1998]. After background subtraction, the ^{14}R ratios (corrected for isotopic fractionation) were normalised to the isotopic ratio measured for the OxAcII standards. Results are summarised in figure 5.11, and the certified concentration is also reported for comparison. As can be seen, our results are fully consistent with the reference value.

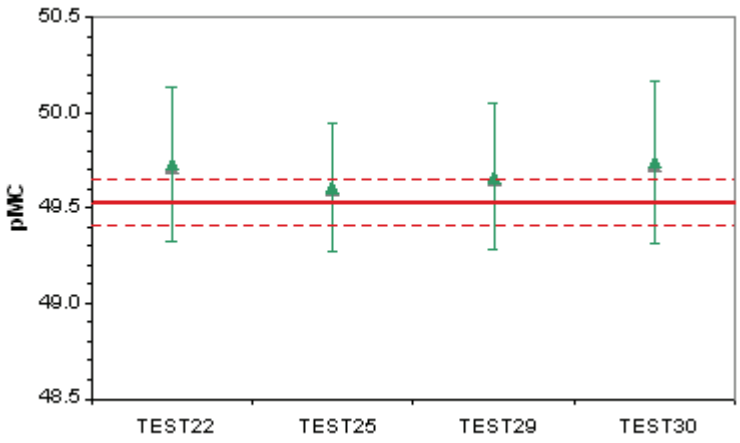

figure 5.11: Measured radiocarbon concentrations in the IAEA C7 samples; certified concentration and ±1 sigma uncertainty are shown with continuous and dashed lines, respectively.

5.3.4 Participation to an international inter-comparison

In September 2009, we were involved in an international inter-comparison on radiocarbon measurements on aerosol samples. At the time of the inter-comparison, we could perform only TC measurements, as the final procedures for OC/EC

separation were not available yet.

Two aerosol samples (JP2 and JP7) and a standard reference material RM8785 by NIST were available for the inter-comparison.

Only one graphitisation process was carried out starting from JP7 sample combustion. Problems during combustion and graphitisation occurred and AMS results gave low currents (i.e. not reliable results), thus it was rejected.

As for JP2, four graphitisation processes were carried out.

From RM8785, two graphitisation processes were carried out.

Measured data are represented in figure 5.12. Final data after elaboration (sent for the inter-comparison) are summarised in table 5.3.

Unfortunately, the results of the inter-comparison are not available yet.

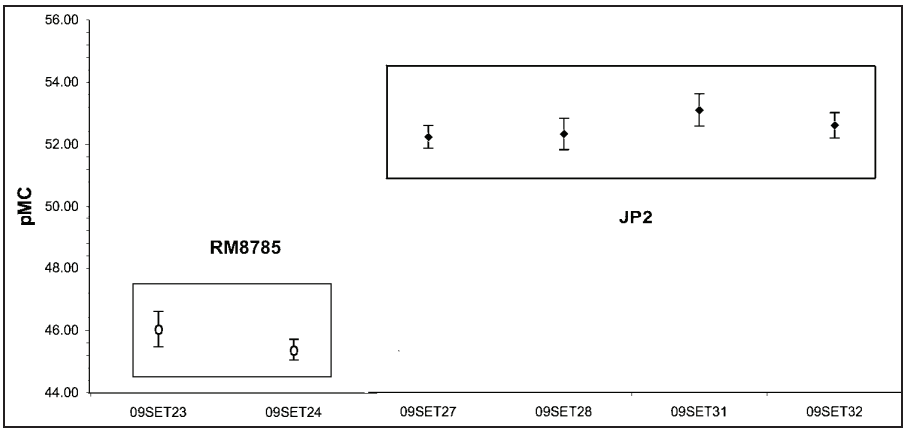

figure 5.12: measured pMC for the inter-comparison samples

Sample ID	pMC
RM8785	45.38 ± 0.33
JP2	52.32 ± 0.50

table 5.3: final data sent to the organising laboratory for the inter-comparison

5.4 Tests on OC and EC separation procedure

As previously mentioned (paragraph 4.3), the problem concerning OC and EC separation is still open. During this thesis, tests were carried out in our laboratory to select suitable protocols aimed at the separation of (at least) a representative part of the EC fraction from OC.

Attention was focused on the washing procedure for the filters and on the "best"

thermal protocol for OC/EC separation.

5.4.1 Set-up of the washing procedure

Different washing procedures were tested in our laboratory, to verify if there was a minimum water quantity necessary to completely eliminate the WSOC (Water Soluble Organic Compounds). All these tests were carried out using ultra-pure MilliQ water by Millipore (Resistivity: 18 MΩ•cm @ 25 °C, TOC < 5ppb). The filter washing was carried out punching PM10 samples collected on a 150 mm High-Volume (HV) quartz fibre filter into many circular parts (diameter 32 mm, see figure 5.13 left). Each punch was enclosed in two glass fibre filters that could be changed after each washing procedure to avoid contaminations, and placed on a porous membrane. The porous membrane was the lower base of a cylinder that can be filled with a known water quantity. The slow passage of the water through the filter and the porous membrane allowed WSOC removal (see figure 5.13 right).

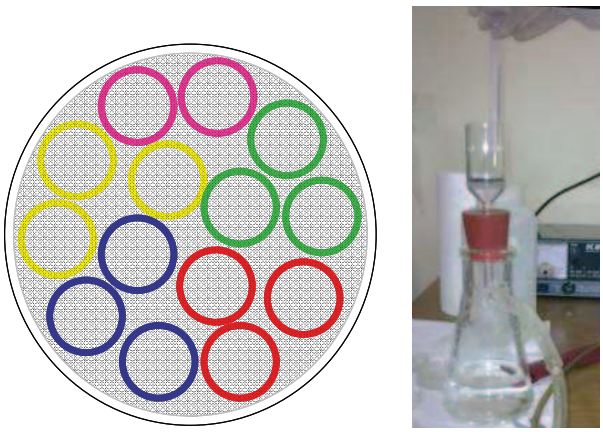

figure 5.13: (left): punches from HV filter; (right) washing set-up

First of all, the reproducibility of the washing procedure was verified. A sampled HV filter was cut in punches. Three punches were washed with each washing procedure, and 1cm^2 sub-punch per punch was analysed by TOT method. Reproducibility (standard deviation to average value ratio) is reported table 5.4.

Filter	Extraction volume	Reproduc. OC	Reproduc. EC	Reproduc. TC
FV15_1	2ml/cm^2	6%	7%	3%
FV15_2	4ml/cm^2	10%	5%	8%
FV15_3	7ml/cm^2	8%	6%	7%
FV15_4	10ml/cm^2	9%	6%	9%
FV15_5	13ml/cm^2	5%	6%	1%

table 5.4: reproducibility tests using different water quantities

Then, tests to choose the water quantity to use were carried out. Two filters with different carbon contents (27 and 57 μg/cm^2 TC, respectively) were divided in circular punches. Each punch of a filter was washed using different water quantities from 1 to 14 ml/cm^2. Average results for the two filters are shown in figure 5.14.

It can be noticed that strong reduction in PyC (Pyrolytic Carbon) formation is registered when washing is carried out. Moreover, TC quantification is nearly stable when a few ml/cm^2 of water are used for filter washing. Also EC quantification is very stable with small error bars when a few ml/cm^2 water are used. In the final procedure, 7 ml/cm^2 was chosen as the water quantity for washing filters.

The strong decrease registered in PyC when the filter is washed is a further evidence of the importance of washing filter for EC quantification and for EC/OC separation (see par. 4.3.2 and 4.3.3).

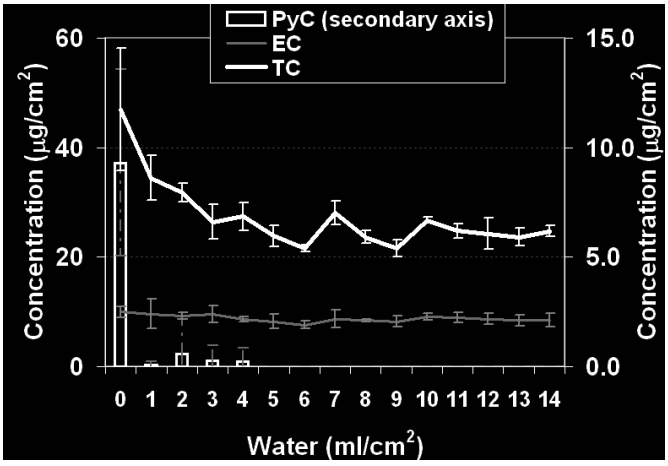

figure 5.14: test to evaluate the optimal water quantity for filter washing

5.4.2 Set-up of the EC separation procedure

The optimisation of the procedure for the EC isolation was a relevant and hard task to perform during this thesis.

The work was carried out as follows: parts of samples were washed and combusted in oxygen at different temperatures (325-400 °C) for variable times trying to optimise OC removal from the filter and limiting EC losses.

Then the residues on the samples were analysed using the TOT method (paragraph 4.3). For each combustion condition, three circular punches were combusted and at least one 1-cm^2 sub-punch per punch was analysed. The residual OC and EC measured on the combusted filters were compared to the values measured on the

corresponding washed non-combusted filter to evaluate possible OC remaining on the filter and EC losses due to the pre-combustion process.

In table 5.5 the average results of tests carried out using only a step in oxygen are shown. In yellow, reference results on washed non-combusted filters are reported. The other results are the residuals on filters after combustion at the reported measurement conditions compared to reference results in percent.

It is noteworthy that about 15% of OC is always found as residue, except in the combustion at 400°C, but in this case a significant EC loss is registered. Thus, it was clear that carrying out EC isolation working only in oxygen was not possible.

	Combustion temperature (℃)	Combustion time (min)	He	OC	EC	TC
FV6 (µg/cm^2)				14.32	4.88	19.20
FV6ABC	400	90	No	9%	27%	14%
FV6DEF	400	40	No	10%	39%	18%
FV6GHI	400	20	No	12%	66%	26%
FV18 (µg/cm^2)				16.34	14.07	30.40
FV18ABC	385	30	No	18%	73%	44%
FV18DEF	370	60	No	15%	64%	38%
FV18GHI	385	60	No	14%	58%	35%
FV18LMN	355	75	No	15%	68%	39%
FV18OP	340	75	No	15%	74%	42%
FV19 (µg/cm^2)				21.15	24.62	45.77
FV19ABC	340	95	No	14%	72%	45%
FV19DEF	355	95	No	12%	73%	45%
FV19GHI	325	120	No	14%	76%	48%

table 5.5: tests on EC isolation using only a step in oxygen

Therefore, a second step in He at high temperature was added. In fact, most of OC should have been combusted in the previous phase, thus the possibility of PyC formation from the residual OC is negligible. Tests were carried out to choose the most suitable combination of oxygen and He steps temperature and duration. During this set-up phase, the He step was not carried out in the combustion oven, but in the TOT instrument. Focus was mainly posed on the conditions that gave the best EC recovery in the tests carried out in oxygen (325°C, 120 min and 355°C, 75 min). The latter was chosen as two tests were carried out at 355°C: one for 75 min and one for 95 min. It is curious that in the second case (95 min) the recovery was higher than in the case of combustion for 75 minutes. This was probably due to differences in the composition of the samples analysed for the two different

protocols. Finally, it was chosen to test 355°C at the shorter time, to differentiate it from the other protocol (325°C, 120 min). Also a test at 375°C was carried out, as done in Szidat et al. (2009).

In table 5.6, TOT data referring to washed filters combustion without the He step are reported in white rows. In grey rows are the results after the He step (sometimes carried out also at different temperatures). For grey data, OC_{res} is the OC quantified by TOT on the filters after the oxygen and He steps. In the column "carbon available for ^{14}C measurements on EC", the ratio between the total carbon detected on the filter after the two pre-combustion steps and the EC measured on washed filters is presented. In fact, the residue on the filter after the two steps is definitely analysed as EC. He step at 750°C was chosen to perform the EC separation, as recovered carbon using this protocol is comparable to the EC measured on the filter after the oxygen step.

	T (°C)	t (min)	He step	OCres	EC res	Carbon available for ^{14}C measurements on EC
VG9ABCD_Nio	375	45	No	14%	75%	
VG9ABCD_HeEusRes	375	45	yes, 650°C	7%		90%
VG9ABCD_He750Res	375	45	yes, 750°C	4%		77%
VG9ABCD_HeNioRes	375	45	yes, 850°C	3%		57%
VG9EFGH_Nio	355	75	No	17%	67%	
VG9EFGH_HeEusRes	355	75	yes, 650°C	6%		76%
VG9EFGH_He750Res	355	75	yes, 750°C	2%		66%
VG9EFGH_HeNioRes	355	75	yes, 850°C	7%		63%
VG9ILMN_Nio	325	120	No	14%	80%	
VG9ILMN_HeEusRes	325	120	yes, 650°C	8%		87%
VG9ILMN_He750Res	325	120	yes, 750°C	4%		80%
VG9ILMN_HeNioRes	325	120	yes, 850°C	3%		73%
SC3A_LC	325	120		16%	88%	
SC3B_LC_He750Res	325	120	yes, 750°C	7%		74%
SC3C_LC	355	75		14%	69%	
SC3D_LC_He750_Res	355	75	yes, 750°C	6%		61%
SC4A_LC	325	120		22%	69%	
SC4B_LC_He750_Res	325	120	yes, 750°C	9%		69%
SC4D_LC	355	75		30%	77%	
SC4C_LC_He750_Res	355	75	yes, 750°C	11%		75%

table 5.6: tests for EC isolation using a combination of an oxygen step (T, t) and an He step.

Therefore, two main protocols were considered: 325°C, 120 min + He 750°C (i.e. the protocol with the best EC recovery) and 355°C, 75 min + He 750°C.

Once these protocols were identified, on-line tests were carried out to verify the reproducibility in combustion conditions and recovery when the He step is carried

out. After combustion in the main oven of the line, the residues on punches were analysed by TOT to verify the EC recovery (see figure 5.15).

It is noteworthy that oven temperature uniformity was tested at 400°C and this is further proved by the very good uniformity in EC recovery after the oxygen pre-combustion step only. However, when He step is added, a recovery efficiency reduction is registered in the outer part of the oven. This can ascribed to the construction features of the oven. Indeed, heating coil winds are closer each other at the outer part of the oven to overcome the thermostatic effect of the external atmosphere (about 20°C) and their configuration was optimised to have uniformity @ 400°C. However, as the time required to reach 750°C is definitely higher than the time needed to reach 400°C, it is possible an overheating of this part of the oven, that can justify a reduction in recovery efficiency.

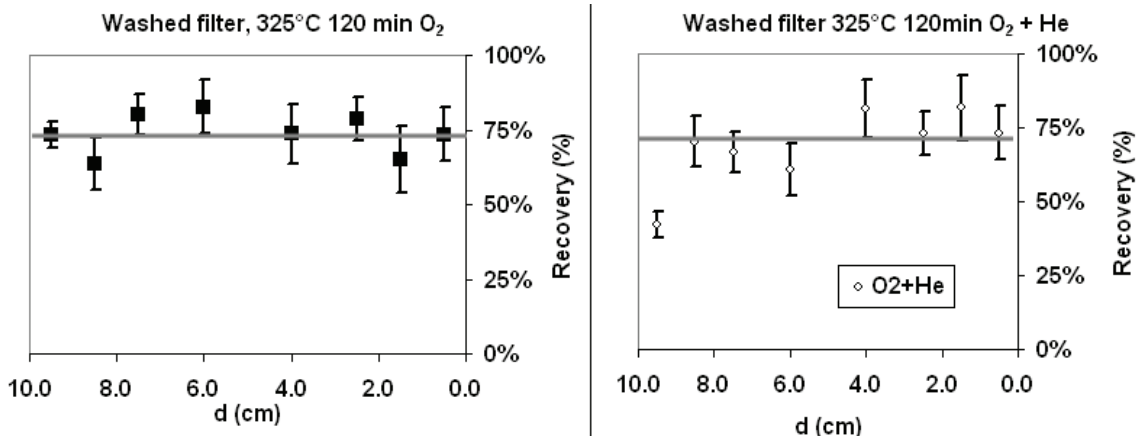

figure 5.15: comparison between the carbon recovery after pre-combustion @ 325°C-120min and after the same combustion +He step (750°C)

These tests confirmed the good recovery efficiency of the step @ 325°C for 120 min + He step @ 750°C, which was the protocol used to obtain the first data of f_m on OC and EC carbon fractions shown in this work.

Thus, the final procedure chosen for EC isolation consisted in different steps of sample preparation:

a) the sample is washed (with 7 ml/cm^2) of MilliQ water to remove WSOC, which are the main responsible of charring;
b) the sample is pre–combusted in 100% oxygen atmosphere @325°C for 120 minutes to eliminate as much as possible OC from the sample;

c) the pre-combusted sample is heated @750°C in He atmosphere to remove possible residual OC.

After these processes all the OC should have been removed from the filter. The remaining EC is combusted in oxygen @ 800°C for 20 minutes (following the TC protocol), the evolved CO_2 is separated from the carrier gas and sent to the graphitisation line. It is noteworthy that, due to pre-combustion steps (and consequent carrier gas changes), the procedure mentioned in paragraph 5.2 is further time-extended: two hours for oxygen pre-combustion, 20 minutes for purging-off line before He step, few minutes to reach 750°C, and 10 minutes after He step to cool the main oven below 325°C before re-injecting oxygen have to be added to the TC procedure. This makes impossible to produce more than one sample per day.

5.5 Comments on the sample preparation procedures.

As previously mentioned (paragraphs 5.2 and 5.4.2), the sample preparation procedure limits the possibility of producing more than 1-2 samples per day.

It is noteworthy that, if the available sample quantities allow performing two graphitisation procedures (i.e. the produced CO_2 is at least two times that established for the AMS measurement), it is useful to carry out both of them. Indeed, it is possible that problems occur during the graphitisation process, after sample preparation while pressing the graphitic samples into the aluminium capsules for cathodes production, or during the AMS analysis, thus causing complete sample loss. Therefore, the possibility to perform two graphitisation procedures of the same sample strongly reduces the possibility of missing data. Thus, no more than one sample per day is actually produced at the moment.

It is also worthy to note that even a single AMS measurement on real samples requires the production of normalisation standard samples, graphite (blank) samples, and checking standard samples (for a total of at least 10 samples). The prescribed standards to be prepared are usually increased of 1 every 7-8 real samples for a better quality assurance on the produced data. For each of these samples previous considerations about preparation time have to be considered.

55 samples (standards + first tests on the line + inter-comparison samples + summer TC data on real samples) in total were analysed during the TC set-up phase (par. 5.3), during 3 AMS shifts. They were all prepared during a Ph.D. thesis in Florence. [Calzolai, 2009]

Moreover, 79 samples (standards + TC + TC_{ww} + OC + EC) in total were prepared for EC/OC analyses during this Ph.D. thesis in joint collaboration with the LABEC staff.

5.6 Preliminary results

5.6.1 ^{14}C samples and AMS analysis.

In the next paragraphs (5.6.2, 5.6.3), ^{14}C data for TC in samples collected during summer 2008 and winter 2009-2010 and for the OC and EC fractions in the wintertime samples will be presented.

As regards TC summer data, they were obtained from 450 μgC samples analysed in the same AMS shift when tests on the preparation line were performed (paragraph 5.3). As previously mentioned, reliable AMS control data were obtained during that shift.

All the winter data were obtained from 220 μgC samples during a different AMS shift. In the following, AMS control data for the winter samples are presented. The halving of the analysed carbon quantity was necessary because of the reduced carbon quantity available for ^{14}C measurements on separated carbon fractions.

Seven OxAcII, six Alfa Aesar graphite, and four IAEA C7 samples were analysed for quality assurance during this measurement shift. These samples were produced at different steps of sample preparation, to be representative for possible modification occurring in our preparation line during the three months necessary for the whole preparation of the samples for the measurement shift. Among the analysed standard cathodes, results were obtained only for 3 OxAcII, 5 graphites, and 4 IAEA C7 samples due to some cathodes flaking off when irradiated by the Cs source.

More problems were detected during this shift if compared to what presented in

paragraph 5.3 during the TC set-up control. These problems might be ascribed to the lower size of the analysed samples (the smaller are the samples, the higher can be the contribution of possible contaminations and the greater can be problems during graphitisation, cathodes production, or AMS analysis), to a slight increase in the accelerator blank values recently reported at LABEC during other AMS shifts (1-2 pMC), and also by other causes which still have to be identified.

Oxalic Acid results used for pMC calculation are shown in figure 5.16. It is noteworthy that reproducibility for ^{14}R and ^{13}R ($\sigma_{14}^{mean}/^{14}R_{av}$ and $\sigma_{13}^{mean}/^{13}R_{av}$, see 5.3.1) was 12‰ and 5‰, respectively. These values are higher than the standard quality control values for radiocarbon dating analysis (<5‰ and <3‰, respectively, see par. 5.3.1), and it is also due to the limited number of standards that did not flake off in the source. However, we considered them acceptable for radiocarbon analysis on aerosol samples. In fact, final estimated uncertainties on source apportionment due to analytical uncertainties were few percents. We considered this analytical uncertainty acceptable, especially when considering that much higher (and variable) uncertainties can be associated to fractions separation, and to $f_{m,bb}$ and $(OC/EC)_{ER,bb}$ used for the OC apportionment in our model.

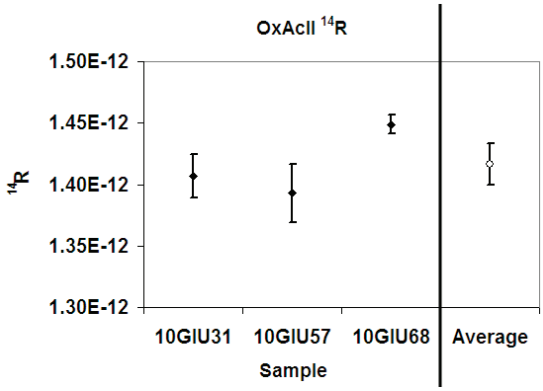

figure 5.16: measured ^{14}R for OxAcII samples used for normalisation

As for Alfa Aesar graphite results (blank, see figure 5.17), four samples resulted in few pMC contamination (3.58±0.30 pMC). As previously mentioned, 1-2 pMC was expected due to recent machine contribution. Moreover, at least a 2-fold increase in blank contamination if compared to data obtained with 450 µgC samples can be ascribed to the reduced carbon quantities analysed (i.e. about 1 pMC). Sample 10GIU28 resulted in 6.59±3.51. Its value is higher then the other blanks and

it is also affected by a greater uncertainty. However, a contamination of 10GIU28 sample could have occurred during graphitisation as a slight leakage in the graphitisation reactor (few mbar/h) was noticed only after the graphitisation was completed. However, our calculation predicted only tenths of pMC contamination due to this problem. This blank was excluded from the average blank evaluation for most samples. It was considered in the average only for four samples for which a slight leakage during graphitisation was detected.

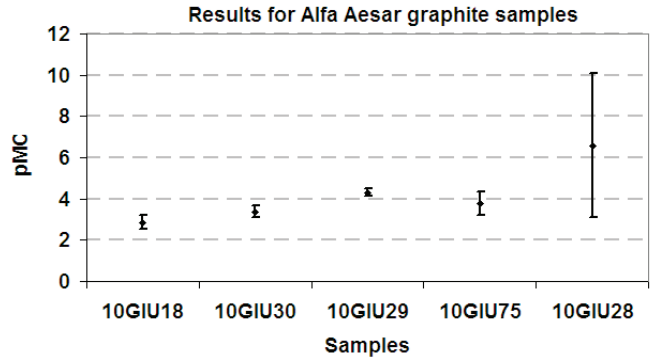

figure 5.17: Alfa Aesar graphite pMC results used for blank correction

IAEA C7 standards (figure 5.18) were used to check the reliability of the obtained results. IAEA C7 standard results were comparable to the certified values except for 10GIU39 sample. The uncertainty associated to 10GIU04 sample measurement (± 4.12 pMC) has to be ascribed to the rapid deterioration of the sample in the source (only 2 measurements were available).

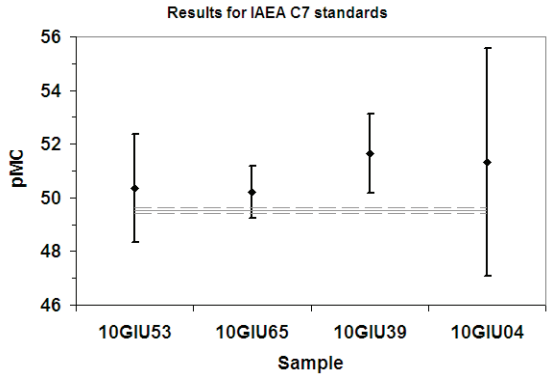

figure 5.18: C7 data, blank corrected using the average of all the measured graphite samples. Also the average certified value (± 1 σ) is represented in grey

It is noteworthy that for all the measured standard samples, the uncertainty associated to a single sample (error bar) measured in this run (220 µgC samples) is

often much higher than that measured with 450 μgC samples. This was ascribed to the specific features of the accelerator source, which had been designed for much bigger samples (> 600 μgC). The reduced size of our samples can lead to a non-uniformity of the layers sputtered during different batches and to a reduced count statistics, thus causing an increase of the uncertainties associated to a single sample measurement.

Moreover, the reduced carbon quantity graphitised made the cathodes more brittle, thus causing a higher number of sample losses if compared to standard analysis.

Summarising: data for quality assurance obtained during this measurement shift are affected by higher variability and uncertainty if compared to the data presented in paragraph 5.3. Moreover, higher blank values were measured and a higher number of cathodes was lost during the sputtering in the source. All these facts have to be ascribed to the lower carbon quantity analysed, to an increase in machine blank values, and to other reasons not completely understood yet. Thus, the measured winter samples will be generally affected by higher uncertainties if compared to the summer data analysed during the measurement shift presented in paragraph 5.3. However, this uncertainty was considered acceptable when compared to other parameters involved in the source apportionment and important indications were obtained by winter samples, especially concerning OC/EC separation strategies to be adopted in the future.

5.6.2 ^{14}C in TC measurements

^{14}C measurements on TC were carried out on both summer and winter samples collected at two urban background stations in Milan: Milan-Pascal, which is a monitoring site of the Environmental Protection Agency of Lombardy Region (ARPA Lombardia), and a site located at the Department of Physics of the University on Milan during summer and winter respectively. It is noteworthy that the two sites are placed at about 150 m distance, thus they can be considered completely comparable.

Three summer samples were analysed (450 μgC samples). The results obtained on the three samples were pMC = 67.3±0.6, 53.7±0.4, 52.2±0.7. These first results are comparable to the percent Modern Carbon found in other studies (range: 55-75

pMC) [Lewis et al., 2004; Szidat et al., 2004b].

These results do not significantly differ from the results obtained from five wintertime samples (220 μgC) analysed: for winter samples, pMC were in the range 49.2 – 64.8 (49.2±0.7; 50.5±0.8; 63.2±1.3; 63.4±1.2; 64.8±0.9). Also these data are in agreement to data reported in the literature for the winter period (range: 0.49-0.93 pMC) [Zencak et al., 2007; Huang et al., 2010].

5.6.3 ^{14}C in OC and EC measurements

Of great relevance are our first data on OC and EC. Indeed, few groups perform ^{14}C measurements on the EC fraction [Currie and Kessler, 2005; Zencak et al., 2007; Uchida et al., 2010]. It is noteworthy that different isolation methods are used in these works. An inter-comparison on ^{14}C measurements on EC was carried out on the Standard Reference Material 1649a by NIST, and discrepancies up to a factor 5 were detected by the different separation approaches used by the three involved groups [Currie et al., 2002]. Moreover, some research groups performed measurements on specific organic compounds or compound classes (PAHs) [Currie et al., 1997; Uchida et al., 2010].

Up to now only one research group published data on the whole OC and EC fractions [Szidat et al., 2004b; Szidat et al., 2006; Szidat et al., 2009].

In this work, during the performed testing phase, the direct measurement of f_m(EC) and the determination of f_m(OC) starting from WSOC and WINSOC fractions were investigated (see par. 4.3). Results for the five winter samples are given in table 5.7. Dark blue cells indicate carbon quantification carried out on not-washed filters; light blue cells refer to carbon quantification carried out on water washed filters. Yellow cells are directly measured pMC, while white cells represent physical quantities derived from the others using the formulas in paragraph 4.3.1 and 4.3.3.

It is noteworthy that wintertime pMC (EC) is about 20 on average (range: 11.9 – 25.9), while the OC components (i.e. WSOC and WINSOC) show a higher modern contribution: on average pMC (WINSOC) = 58.3 (range: 49.8 - 63.7) and pMC (WSOC) = 86.8 (range 82.7 – 88.9). The big uncertainty associated to pMC (WSOC) is also noteworthy (25%). This was ascribed to the quantification methodology which gives WSOC as the difference between TC and TC_{ww}. Indeed, statistically

combining the uncertainties on these two quantities, a 23% uncertainty is obtained for WSOC quantification on average. Of course this uncertainty also influences pMC (WSOC) evaluation.

	Sample	TC	TC_{ww}	EC	WINSOC	WSOC	pMC (TC)	pMC (TC_{ww})	pMC (EC)	pMC (WINSOC)	pMC (WSOC)
Data	SC6	35.9	26.3	11.1	15.2	9.6	50.5	N.A.	N.A.	N.A.	
	SC8	59.8	38.5	11.0	27.6	21.3	63.2	49.0	20.9	N.A.	88.9
	SC9	56.1	38.2	9.6	28.6	18.0	63.4	51.4	23.1	63.7	88.9
	SC10	69.9	36.5	7.4	29.1	33.4	64.8	N.A.	25.9	59.4	
	SC17	133.4	93.0	29.9	63.1	40.4	49.2	34.6	11.9	49.8	82.7
Uncertainties	SC6	2.1	1.6	0.8	1.0	2.7	0.8	N.A.	N.A.	N.A.	
	SC8	3.3	2.3	0.8	1.6	4.0	1.3	1.5	1.1	N.A.	20.5
	SC9	3.1	2.2	0.7	1.7	3.8	1.2	0.7	0.6	1.5	23.1
	SC10	3.8	2.2	0.6	1.7	4.4	0.9	N.A.	1.8	1.0	
	SC17	7.0	5.0	1.7	3.4	8.5	0.7	0.6	0.6	1.4	20.0

table 5.7: measured data and errors on the five samples analysed for carbon fractions. Carbon quantification (left) is in $\mu g/cm^2$.

On the two samples for which the data for all the measured fractions were available, pMC (OC) was evaluated using the two approaches explained in par. 4.3:

a) from TC and EC measurements: $f_m(OC)\cdot OC = f_m(TC)\cdot TC - f_m(EC)\cdot EC$;

b) from WSOC and WINSOC measurements:

$f_m(OC)\cdot OC = f_m(WSOC)\cdot WSOC + f_m(WINSOC)\cdot WINSOC$, where

$f_m(WSOC)\cdot WSOC = f_m(TC)\cdot TC - f_m(TC_{ww})\cdot TC_{ww}$.

Even if the uncertainty on pMC (WSOC) is significant, the results for the two filters for which the complete pMC data-set was available after AMS measurements are in agreement within 5% (see table 5.8). Thus, our approaches for OC/EC fractions separation can be considered reliable. It is also noteworthy that the uncertainties on pMC (OC) evaluated from the pMC (EC) are on average 11%, while when it is calculated by the separate analysis of OC sub-fractions this value rises up to 16%. Another indication on the best approach can be obtained when pMC (EC) is calculated starting from the pMC (OC) obtained by OC sub-fractions, and it is then compared to the directly measured value. It can be noticed (table 5.9) that significant discrepancies occur. It has also to be considered that errors associated to this measurement are higher than 100%, thus totally invalidating pMC calculation using this approach. The hypothesis of a systematic influence of the thermal protocol used for EC quantification by TOT was expressed. Tests were carried out estimating EC quantification by a different protocol (EUSAAR2 [Cavalli et al.,

2010], T_{max} for the He step: 650°C), but the corrections do not indicate systematic improvements of the obtained results.

		pMC(OC) (from EC)	pMC(OC) (from WSOC & WINSOC)	Δ pMC (OC) (%)
Data	SC9	71.6	73.4	-2%
	SC17	59.9	62.7	-4%
Uncertainties	SC9	7.8	11.8	
	SC17	6.3	10.5	

table 5.8: pMC (OC) derived from the two different approaches

	pMC (EC) directly measured	pMC (EC) from pMC (WSOC & WINSOC)	Δ pMC (EC) (%)
SC9	23.1	14	-38%
SC17	11.9	2	-80%

table 5.9: pMC (EC) directly measured and evaluated from pMC (OC) measured starting from OC sub-fractions

Therefore, the approach including only the determination of f_m(TC) and f_m(EC) has to be chosen for future measurements, even if information on the f_m of the OC sub-fractions will be lost.

Moreover, source apportionment was carried out using the formulas in paragraph 4.2.2 and an $(EC/OC)_{ER,bb}=0.16 \pm 0.05$ [Szidat et al., 2006]. Results are reported in table 5.10. Uncertainties on the obtained apportionment are calculated starting from analytical uncertainties on fractions and pMC measurements and from variability reported in the literature on $f_{m,bb}$ and $(EC/OC)_{ER,bb}$. A brief discussion on the limits of the applied model is presented in the following.

	EC_{bb}	EC_{fossil}	OC_{bb}	OC_{bio}	OC_{fossil}
SC8	18% ± 2%	82% ± 9%	25% ± 9%	41% ± 14%	34% ± 18%
SC9	20% ± 2%	80% ± 9%	26% ± 9%	40% ± 14%	35% ± 18%
SC10	22% ± 3%	78% ± 10%	17% ± 6%	48% ± 11%	36% ± 14%
SC17	10% ± 1%	90% ± 8%	19% ± 6%	36% ± 11%	45% ± 15%

table 5.10: carbon fractions source apportionment

It can be noticed that fossil fuel combustions strongly influence EC concentrations (about 80% on average). The apportionment for EC fraction is in agreement with literature data in urban area during wintertime (EC_{bb} = 25% ± 5%) [Szidat et al., 2006].

As for OC data, it is noteworthy that fossil contribution accounts for 34-45% only. Moreover, in the OC modern fraction (on average 62%), a strong contribution (about 40% of OC) is ascribed to a biogenic source by the applied model. Considering that during the winter season only a small contribution from biogenic activity is expected, this result has to be carefully analysed. It is noteworthy that the $(EC/OC)_{ER,bb}$ emission ratio is strongly dependent on the type of stove or fireplace used for wood combustion and on the type of wood burnt: literature studies over the last 10 years report average $(EC/OC)_{ER,bb}$ ratios for primary emissions from domestic heating in the range 0.086-0.213 [Szidat et al., 2006 and therein literature], but the range can be much wider depending on the wood type (e.g. 0.04-0.58 [Fine et al., 2001; Iinuma et al., 2007]). It is noteworthy that, if $(EC/OC)_{ER,bb} = 0.086$ is used, the biomass contribution in the OC fraction estimated by our model increases on average to 40%, while the "biogenic" contribution reduces to 21%. On the contrary, the possible variation of $f_{m,bb}$ as a function of the age of the burnt material (range 1.08-1.24, see par. 4.2.2) has negligible influence on the apportionment if compared to the variation of $(EC/OC)_{ER,bb}$.

It is also important to consider that $(EC/OC)_{ER,bb}$ ratios found in the literature (and applied in this study) account only for primary contribution, while no indication about secondary formation is available. Therefore, the real biomass burning contribution can be strongly underestimated by the applied model.

Another factor influencing the possible biogenic contribution overestimation is the addition of biodiesel (up to 7% fatty acid mixed esters in Europe [2009/30/EC]) to the diesel fuel. Bennett et al. (2008) showed that the addition of biofuel to the diesel fuel leads to the emission of ^{14}C proportionally to the inserted biofuel. Thus, a small modern OC fraction (no more than few percent) can be ascribed to biofuel this kind of emission. On the contrary, Lewis et al. (2006) did not found ^{14}C contribution in particulate emitted by small engines fuelled by gasoline and ethanol due to different partitioning of the two fuel emissions in particulate and gaseous form.

Finally, it has to be considered that, even if low emissions from biological activity are expected during wintertime, plant debris and fungal spores contribution cannot be completely excluded during this season [Puxbaum and Tenze-Kunit, 2003].

Conclusions

This work aimed at the set-up of innovative experimental methodologies for the atmospheric aerosol characterisation and source apportionment.

It is worth recalling that particle size and composition influence aerosol effects both at local (human health, air quality, visibility, cultural heritage degradation) and global scale (radiation balance). Thus, the study of size-segregated aerosol and the source identification are among the main topics of interest in up-to-date aerosol science.

In this work, attention was focused on the following points:

1) the set-up of an Energy Dispersive X-Ray Fluorescence (ED-XRF) for the analysis of size-segregated samples;
2) the application of Positive Matrix Factorization (PMF) analysis to a detailed dataset for source apportionment assessment, and the analysis of sources temporal trends and particle number concentration in different size bins from 0.25 to 32 μm aimed at obtaining indications on the size distribution of source emissions;
3) the design and set-up of a new sample preparation line for ^{14}C analysis in atmospheric aerosol samples. The line was realised fulfilling the requirements for organic and elemental carbon separation, in order to allow the discrimination between natural and anthropogenic source contributions to carbonaceous particles in atmosphere.

The set-up of the ED-XRF had to follow different steps due to the peculiar features of size-segregated aerosol samples (not-homogeneous deposit and small deposit quantities):

1) the identification of an homogeneous sensitivity area;
2) the determination of the sensitivity curve;
3) the sensitivity curve validation;
4) the inter-comparison with a different analytical technique (Particle-Induced X-Ray Emission: PIXE).

The validation of the sensitivity curve and the inter-comparison with PIXE showed

that reliable results can be obtained by our set-up. The set-up methodology has been recently presented at international and national conferences (see Appendix: C7, C8, D11, D13), and a paper was submitted to X-Ray Spectrometry (see Appendix: B2).
A winter sampling campaign was carried out to test the set-up and the first data of elemental size distribution in Milan area were obtained by our ED-XRF set-up. Data concerning this campaign were presented at a national conference (see Appendix, D13). However, further work is still needed for source apportionment of size-segregated samples in Milan area.
Moreover, the development of the ED-XRF set-up for size-segregated samples analysis (a similar set-up was realised at the University of Genoa for parallel analysis and joint measurement campaigns) allowed a comparison between measured data and size-segregated data modelled starting from a PM10, PM2.5, and PM1 database coupled to size-segregated number concentrations in Genoa area. The group presented the work in a recent paper ([Cuccia et al., 2010], see also Appendix A5), and at international and national conferences (see Appendix: C5, C10, D8, D10).

PMF was applied to a high-time resolved dataset. Elemental, ionic, and carbonaceous compositions had been determined in a previous work by ED-XRF, ion chromatography, and thermal-optical transmittance method, respectively. Moreover, levoglucosan had been measured by a methodology developed jointly with the Department of Inorganic, Metallorganic and Analytical Chemistry of the University of Milan, and presented in Piazzalunga et al. (2010) (Appendix: A6).
The dataset main features were reported in Vecchi et al. (2009a) and a peculiar episode was studied and presented in Vecchi et al. (2008) and at national and international conferences (see Appendix: A1, A3).
In this work, the identification and the contribution quantification of the sources influencing the Milan area were carried out by PMF analysis. Seasonal variability was evidenced and the importance of specific PM sources during peculiar episodes was evaluated. Moreover, indication on source contributions in different size bins was obtained following the methodology proposed in Mazzei et al. (2007). A paper

containing this information is now in preparation and 4-hours biomass burning apportionment was presented at an international conference (see Appendix, C2).

The design and set-up of the new preparation line for ^{14}C analysis was the most innovative, important, and demanding part of the work. The line was designed and set-up in close collaboration with the LABEC-INFN research group. Different prototypes were realised before achieving the final configuration. Some parts of the line (i.e. the combustion oven and the CO_2 trap) are based on original ideas; they were developed in this work and are now implemented in the line. Reliable results were obtained by our sample preparation line for TC data, and a paper presenting the line and the tests carried out for quality control on TC is under second revision on an international journal (see Appendix: B1). Moreover, the line final set-up and quality TC data control were presented at international and national conferences (Appendix: C3, C9, D9).

We also participated to an international inter-comparison exercise on ^{14}C analysis on aerosol samples, but its results are not available yet.

During the last months, tests were also carried out on separated carbon fractions on winter samples. These data are the first data in Italy and among the few ones in the world. However, work is still in progress to obtain smaller samples and to further verify thermal separation protocols, as well as to have data for the summer season. Moreover, further work is needed for the assessment of the secondary organic component deriving from biomass burning, which is probably not correctly accounted for by the applied model.

Finally, during my PhD thesis I also contributed to experimental or data analysis concerning other works carried out by the research group in the frame of the projects FIRST2007, PRIN2007, PUR2008 and of the INFN experiments NUTELLA and NUMEN. Papers and presentations to national and international conferences referring to these works are also presented in the Appendix (A2, A4, C1, C4, C5, C6, C11, C12, D1, D2, D3, D4, D5, D6, D7, D12, D14, D15).

Aknowledgements

The author is grateful to Roberta Vecchi, Gianluigi Valli, Francesco Riccobono, Laura La Gaccia (Phisics Department, Università degli Studi di Milano), Paola Fermo (Inorganic, Metallorganic and Analytical Chemistry Department, Università degli Studi di Milano), Andrea Piazzalunga (Environment and Territorial Sciences Department, Università degli Studi di Milano Bicocca), Franco Lucarelli (Phisics Department, Università di Firenze), Giulia Calzolai, Massimo Chiari, and Silvia Nava (INFN-Sezione Firenze) for their contribution to this work.

References

AA. VV. (2002). *Handbook of X-Ray Spectrometry: second edition,* Van Grieken and Markowicz editors

Andreae M. O. and Crutzen P. J., (1997). *Atmospheric Aerosols: Biogeochemical Sources and Role in Atmospheric Chemistry,* Science 276, 1052-1059

Azreg-Aïnou M. (2005). *Low-temperature Data for Carbon Dioxide*, Monatshefte für Chemie 136, 2017–2027

Berresheim H., **Wine P. H., Davis D. D.,** (1995). *Sulphur in the atmosphere,* in Singh H. B. editor, *Composition, Chemistry and Climate of the Atmosphere,* Van Nostrand Reinhold, 251-307

Bennett M., Volckens J., Stanglmaier R., McNichol A.P., Ellensond W.D., Lewis C..W., (2008). *Biodiesel effects on particulate radiocarbon (^{14}C) emissions from a diesel engine,* Aerosol Science 39, 667 – 678

Birch M.E., Cary R.A., (1996). Elemental Carbon–Based Method for Monitoring Occupational Exposures to Particulate Diesel Exhaust, Aerosol Science and Technology 25, 221–241

Bonazza A., Sabbioni C., Ghedini N., (2005). *Quantitative data on carbon fractions in interpretation of black crusts and soiling on European built heritage*, Atmospheric Environment 39, 2607-2618

Bond T.C., Streets D.G., Yarber K.F., Nelson S.M., Woo J–H, Klimont Z., (2004). *A technology–based global inventory of black and organic carbon emissions from combustion,* Journal of Geophysical Research 109, D14203, doi:10.1029/2003JD003697

Cachier H., Bremond M.P., Buat-Ménard P., (1989). *Determination of atmospheric soot carbon with a simple thermal method,* Tellus B 41B, 379-390

Calzolai G., Chiari M., Garcìa-Orellana I., Lucarelli F., Migliori A., Nava S., Taccetti F., (2006). *PIXE and XRF analysis of particulate matter samples: an inter-laboratory comparison,* Nuclear Instruments and Methods B 249, 928-931

Calzolai G., (2009). *AMS radiocarbon measurements for carbonaceous aerosol source apportionment at LABEC***,** Ph.D.Thesis, Florence, 31 December 2009

Cavalli F., Viana M., Yttri K.E., Genberg J., and Putaud J.-P., (2010). *Toward*

a standardised thermal-optical protocol for measuring atmospheric organic and elemental carbon: the EUSAAR protocol, Atmospheric Measurement Techniques 3, 79-89

CEN, (1998). *Air quality. Determination of the PM10 fraction of suspended particulate matter. Reference method and field test procedure to demonstrate reference equivalence of measurement methods.* BS EN 12341:1999

CEN, (2005). *Ambient Air Quality – Reference gravimetric measurement method for the determination of the PM2.5 mass fraction of suspended particulate matter in ambient air.* DIN EN 14907:2005

CEN, (2008). *DIRECTIVE 2008/50/EC OF THE EUROPEAN PARLIAMENT AND OF THE COUNCIL of 21 May 2008 on ambient air quality and cleaner air for Europe,* Official Journal of the European Union, L 152/1

Chow J.C., Watson J.G., Pritchett L.C., Pierson W.R., Frazier C.A., Purcell R.G., (1994)**.** *The DRI Thermal Optical Reflectance carbon analysis System – Description, evaluation and applications in the United-States Air-Quality studies,* Atmospheric Environment – Part A General Topics 27, 1185-1201

Chow J.C., Watson J.G., Crow D., Lowental D.H., Merrifield T., (2001). *Comparison of IMPROVE and NIOSH Carbon Measurements*, Aerosol Science and Technology 34, 23–34

Chow J.C., Watson J.G., (2002). *PM2.5 carbonate concentration at regionally representative Interagency Monitoring of Protected Visual Environment sites*, Journal of Geophysical Research 107, D218344, doi:10.1029/2001JD000574

Chow J.C., Watson J.G., Lowenthal D.H., Magliano K.L., (2005). *Loss of PM2.5 nitrate from filter samples in Central California,* Journal of Air and Waste Managemant Association 55, 1158–1168

Chow J.C., Yu J.Z., Watson J.G., Hang Ho S.S., Bohannan T.L., Hays M.D., Fung K.K., (2007). *The application of thermal methods for determining chemical composition of carbonaceous aerosols: A review*, Journal of Environmental Science and Health Part A 42, 1521–1541

Cuccia E., Bernardoni V., Massabò D., Prati P., Valli G., Vecchi R. (2010). *An alternative way to determine the size distribution of airborne particulate matter,*

Atmospheric Environment 44, 3304-3313

Currie L.A., Eglinton T.I., Benner B.A., Pearson A., (1997). *Radiocarbon "dating" of individual chemical compounds in atmospheric aerosol: First results comparing direct isotopic and multivariate statistical apportionment of specific polycyclic aromatic hydrocarbons*, Nuclear Instruments and Methods in Physics Research B 123, 475-486

Currie L.A., Benner B.A., Kessler J.D., Klinedinst D.B., Klouda G.A., Marolf J.V., Slater J.F., Wise S.A., Cachier H., Cary R., Chow J.C., Watson J., Druffel E.R.M., Masiello C.A., Eglinton T.I., Pearson A., Reddy C.M., Gustafsson O., Quinn J.G., Hartmann P.C., Hedges J.I., Prentice K.M., Kirchstetter T.W., Novakov T., Puxbaum H., Schmid H. (2002). *A Critical Evaluation of Interlaboratory Data on Total, Elemental, and Isotopic Carbon in the Carbonaceous Particle Reference Material, NIST SRM 1649a,* Journal of Research of the National Institute of Standards and Technology 107, 279-298

Currie L. A. and Kessler J. D. (2005). *On the isolation of elemental carbon (EC) for micro-molar ^{14}C accelerator mass spectrometry: development of a hybrid reference material for ^{14}C-EC accuracy assurance, and a critical evaluation of the thermal optical kinetic (TOK) EC isolation procedure.* Atmospheric Chemistry and Physics 5, 2833-2845

Dockery D. W., Pope C. A., Xu X., Spengler J. D., Ware J. H., Fay M. E., Ferris B. G., and Speizer F. E. (1993). *An Association between Air Pollution and Mortality in Six U.S. Cities*, The New England Journal of Medicine 329, 1753-1759

EPA (1999a). *Determination of Metals in Ambient Particulate Matter using X-Ray Fluorescence Spectroscopy* in Compendium of Methods for the Determination of Inorganic Compounds in Ambient Air, EPA/625/R-96/010a

EPA (1999b)**.** *Regional Haze Regulations; Final Rule*, Federal Register, Vol. 64, No. 126 35714–35774

EPA (2004). *Air Quality Criteria for Particulate Matter (Final Report, Oct 2004)* U.S. Environmental Protection Agency, Washington, DC, EPA 600/P-99/002aF-bF

Fedi M. E., Cartocci A., Manetti M., Taccetti F., Mandò P.A., (2007). *The ^{14}C AMS facility at LABEC, Florence*, Nuclear Instruments & Methods in Physics Research B 259, 18-22

Fine P.M., Cass G.R., Simoneit B.R., (2001). *Chemical Characterization of Fine Particle Emissions from Fireplace Combustion of Woods Grown in the Northeastern United States.* Environmental Science and Technology 35, 2665-2675

Ghedini N., Gobbi G., Sabbioni C., Zappia G., (2000). *Determination of elemental and organic carbon on damaged stone monuments*, Atmospheric Environment 34, 4383-4391

Ghio A. J., Silbajoris S., Carson J. L., Samet J. M., (2002). *Biologic Effects of Oil Fly Ash,* Environmental Health Perspectives 110, 89-94

Grohse P.M.. (1999). *Trace element analysis of airborne particles by Atomic Absorption Spectroscopy, Inductively Coupled Plasma-Atomic Emission Spectroscopy, and Inductively Coupled Plasma-Mass Spectrometry.* In: Elemental Analysis of Airborne Particles, edited by S. Landsberger and M. Creatchman. Gordon and Breach Science Publishers

Harrison R.M., (2004). *Key pollutants-airborne particles,* Science of the Total Environment 334-335, 3-8

Haywood J. and Boucher O., (2000). *Estimates of the direct and indirect radiative forcing due to atmospheric aerosols: a review,* Reviews of Geophysics 38, 513–543

Hillamo R., Kauppinen E. I. (1991). *On the Performance of the Berner Low Pressure Impactor*, Aerosol Science and Technology 14, 33-47

Hinds W.C., (1999). *Aerosol technology.* John Wiley and Sons, Inc

Huang J., Kang S., Shen C., Cong Z., Liu K., Wang W., Liu L., (2010). *Seasonal variations and sources of ambient fossil and biogenic-derived carbonaceous aerosols based on ^{14}C measurements in Lhasa, Tibet.* Atmospheric Research 96, 553–559

Iinuma Y., Brüggemann E., Gnauk T., Müller K., Andreae M. O., Helas G., Parmar R., Herrmann H., (2007). *Source characterization of biomass burning*

particles: The combustion of selected European conifers, African hardwood, savanna grass, and German and Indonesian peat, Journal of Geophysical Research, 112, D08209, doi:10.1029/2006JD007120

IPCC, (2007)**.** *Climate Change 2007: the physical Science Basis. Contribution of Working Group I to the Fourth Assessment Report of the Intergovernamental Panel on Climate Change*, Salomons et al. (eds), Cambridge University Press

Ito A. and Penner J.E., (2005). *Historical emissions of carbonaceous aerosols from biomass and fossil fuel burning for the period 1870–2000*. Global Biogeochemical Cycles 19, doi:10.1029/2004GB002374

Jacob D.J. (2000). *Heterogeneous chemistry and tropospheric ozone*, Atmospheric Environment 34, 2131-2159

Jacobson M.C., Hansson H.–C., Noone K.J., Charlson R.J., (2000). *Organic atmospheric aerosols : review and state of the science,* Reviews of Geophysics 38, 267–294

Jaenike R., (1980)**.** *Natural aerosols***,** in *Aerosols: Anthropogenic and natural, sources and transport*, Proceedings of the Conference, New York, N.Y., January 9-12, 1979. (A81-13656 03-45) New York, New York Academy of Sciences, 1980, 317-329. Deutsche Forschungsgemeinschaft

Jaenicke R. (1986)**,** *Physical characterization of aerosols,* In Lee S. D., Schneider T., Grant L.D., Verkerk P.J., Eds., *Aerosols*, Lewis Publ., Chelsea, Mi, 97-106

Johansson S.A.E., Campbell J.L., (1988). *P.I.X.E. A novel technique for elemental analysis.* John Wiley & Sons, New York

Keck L. and Wittmaack K., (2005). *Effect of filter type and temperature on volatilisation losses from ammonium salts in aerosol matter,* Atmospheric Environment 39, 4093–4100

Kim E., Hopke P.K., Edgerton E.S., (2004). *Improving source identification of Atlanta aerosol using temperature resolved carbon fractions in positive matrix factorization,* Atmospheric Environment 38, 3349–3362

Kim E. and Hopke P.K., (2006). *Characterization of fine particle sources in the Great Smoky Mountains area.* Science of the Total Environment 368, 781–794

Kirchstetter T.W., Corrigan C.E., Novakov T. (2001). *Laboratory and field*

investigation of the adsorption of gaseous organic compounds onto quartz filters, Atmospheric Environment 35, 1663-1671

Kleeman M.J., Shauer J., Cass A., (1999). *Size and Composition Distribution of Fine Particulate Matter Emitted from Wood Burning, Meat Charbroiling, and cigarettes,* Environmental Science and Technology 33, 3516-3523

Le Clerq M., Van Der Plicht J., Gröning M., (1998). *New ^{14}C reference materials with activities of 15 and 50 pMC.* Radiocarbon 40, 295

Lee E., Chan C.K., Paatero P., (1999). *Application of positive matrix factorization in source apportionment of particulate pollutants in Hong Kong***,** Atmospheric Environment 33, 3201-3212

Lewis C.W., Klouda G.A., Ellenson W.D., (2004). *Radiocarbon measurement of the biogenic contribution to summertime PM-2.5 ambient aerosol in Nashville, TN*, Atmospheric Environment 38, 6053-6061

Lewis C.W., Volckens J., Braddock J.N., Crews W.S., Lonneman W.A., McNichol A.P. (2008). *Absence of 14C in PM2.5 Emissions from Gasohol Combustion in Small Engines,* Aerosol Science and Technology 40, 657–663

Lohmann U. and Feichter J., (2005). *Global indirect aerosol effects: a review*, Atmospheric Chemistry and Physics 5 715–737

Lough G., Shauer J. J., Soopark J., Shafer M., Deminter J., Weinstein J., (2005), *Emissions of Metals Associated with Motor Vehicle Roadways*, Environmental Science and Technology 39, 826-836†

Lowe D.C. and Judd W.J., (1987). *Graphite target preparation for radiocarbon dating by accelerator mass spectrometry.* Nuclear Instruments & Methods B28, 113-116

Maenhaut W., Hillamo R., Mäkelä T., Jaffrezo J.-L., Bergin M. H., Davidson C. I. (1996). *A new cascade impactor for aerosol sampling with subsequent PIXE analysis,* Nuclear Instruments and Methods in Physics Research B 109/110 482-287

Marcazzan G.M., Valli G., Vecchi R., (2002). *Factor influencing mass concentration and chemical composition of fine aerosols during a PM high pollution episode*, The Science of the Total Environment 298, 65-79

Marcazzan G.M., Ceriani M., Valli G., Vecchi R., (2003). *Source apportionment of PM10 and PM2.5 in Milan (Italy) using receptor modelling,* The Science of the Total Environment 317, 137-147

Marple V.A., Rubow K.L., Behm S.M. (1991). *A microorifice uniform deposit impactor (MOUDI): Description, calibration, and use,* Aerosol Science and Technology 14, 434-446

Mauderly J.L., Chow J.C., (2008). *Health Effects of Organic Aerosols*, Inhalation Toxicology 20, 257-288

Maxwell J.A., Teesdale W.J., Campbell J.L., (1995). *The Guelph PIXE software package II,* Nuclear Instruments & Methods in Physics Research B 95, 407

Mazzei F., Lucarelli F., Nava S., Prati P., Valli G., Vecchi R., (2007). *A new methodological approach: The combined use of two-stage streaker samplers and optical particle counters for the characterization of airborne particulate matter,* Atmospheric Environment 41, 5525–5535

Mohn J., Szidat S., Fellner J., Rechberger H., Quartier R., Buchmann B., Emmenegger L., (2008). *Determination of biogenic and fossil CO2 emitted by waste incineration based on $^{14}CO_2$ and mass balances,* Bioresource Technology 99, 6471

Monks P.S., Granier C., Fuzzi S., Stohl A., Williams M.L., Akimoto H., Amanni M., Baklanov A., Baltensperger U., Bey I., Blake N., Blake R.S., Carslawn K., Cooper O.R., Dentener F., Fowler D., Fragkou E., Frost G.J., Generoso S., Ginoux P., Grewet V., Guenther A., Hansson H.C., Hennew S., Hjorth J., Hofzumahaus A., Huntrieser H., Isaksen I.S.A., Jenkin M.E., Kaiser J., Kanakidou M., Klimont Z., Kulmala M., Laj P., Lawrence M.G., Lee J.D., Liousse C., Maione M., McFiggans G., Metzger A., Mieville A., Moussiopoulos N., Orlando J.J., O'Dowd C.D., Palmer P.I., Parrish D.D., Petzold A., Platt U., Pöschl U., Prévôt A.S.H., Reeves C.E., Reimann S., Rudich Y., Sellegri K., Steinbrecher R., Simpson D., ten Brink H., Theloke J., van der Werf G.R., Vautard R., Vestreng V., Vlachokostas Ch., von Glasow R. (2009). *Atmospheric composition change – global and regional air*

quality, Atmospheric Environment 43 5268–5350

Nadeau M.-J., Litherland A. E., Rieck A., Grootes P. M., (2004). *Isotopic fractionation in recombinator based ^{14}C AMS measurements: how can we live with it?,* Nuclear Instruments & Methods B 223-224, 346

Nava S., Becherini F., Bernardi A., Bonazza A., Chiari M., García-Orellana I., Lucarelli F., Ludwig N., Migliori A., Sabbioni C., Udisti R., Valli G., Vecchi R. (2010). *An integrated approach to assess air pollution threats to cultural heritage in a semi-confined environment: The case study of Michelozzo's Courtyard in Florence (Italy),* Science of the Total Environment 408, 403–1413

Novakov T., (1997). *Airborne measurements of carbonaceous aerosols on the east coast of United States*, Journal of Geophysical Research 102, D25, 30023-30030 doi:10.1029/97JD02793

O'Dowd C. D., de Leeuw G. (2007). *Marine aerosol production: a review of current knowledge*, Philosophical transaction of the Royal Society A 365, 1753-1774

Paatero P. and Tapper U. (1994). *Positive Matrix Factorization: a non-negative factor model with optimal utilization of error estimates of data values*, Environmetrics 5, 111–126

Paatero P. (1997). *Least squares formulation of robust, non-negative factor analysis,* Chemometrics and Intelligence Laboratory System 37, 23-35

Paatero P., Hopke P.K., Song X.H., Ramadan Z., (2002). *Understanding and controlling rotations in factor analytic models,* Chemometrics and Intelligence Laboratory System 60, 253-264

Paatero P. and Hopke P.K., (2003)**.** *Discarding or downweighting high-noise variables in factor analytic models.* Analytica Chimica Acta 90, 277-289

Pearson A., McNichol A. P., Schneider R. J., Von Reden K. F., Zheng Y., (1998). *Microscale AMS ^{14}C measurement at NOSAMS,* Radiocarbon 40, 61

Piazzalunga A., Fermo P., Bernardoni V., Vecchi R., Valli G., De Gregorio M.A., (2010). *A simplified method for levoglucosan quantification in wintertime atmospheric particulate matter by high performance anion-exchange chromatography coupled with pulsed amperometric detection,* International

Journal of Environmental Analytical Chemistry 90, 934-947

Pierce J. R. and Adams P. J., (2009). *Uncertainty in global CCN concentrations from uncertain aerosol nucleation and primary emission rates,* Atmospheric Chemistry and Physics 9, 1339–1356

Polissar A.V., Hopke P.K., Paatero P., Malm W.C., Sisler J.F. (1998). *Atmospheric aerosol over Alaska - 2. Elemental composition and sources.* Journal of Geophysical Research 103, D15, 19045-19057 doi:10.1029/98JD01212

Pope III C.A., Burnett R.T., Thun M.J., Calle E.E., Krewski D., Ito K., Thurston G.D., (2002). *Lung Cancer, Cardiopulmonary Mortality, and Long-term Exposure to Fine Particulate Air Pollution,* JAMA, Journal of the American Medical Association 287, 1132-1141

Popovicheva O., Subramanian R., Baumgardner D., Kok G., Cary R., Vlasenko E., Khokhlova T., Shonija N., and Kireeva E. (2010). *Towards the development of standard reference materials for soot measurements – Part 1: Tailored graphitized soot*, Atmospheric Measurement Techniques Discussion, 3, 1743-1773, doi:10.5194/amtd-3-1743-2010

Puxbaum H., Tenze-Kunit M., (2003). *Size distribution and seasonal variation of atmospheric cellulose,* Atmospheric Environment 37, 3693–3699

Querol X., Alastuey A., Rodriguez S., Plana F., Mantilla E., Ruiz C.M., (2001) *Monitoring of PM10 and PM2.5 around primary particulate anthropogenic emission sources*, Atmospheric Environment 35, 845-858

Ramanathan V., Crutzen P. J., Kiehl J. T., Rosenfeld D., (2001). *Aerosols, Climate, and the Hydrological Cycle,* Science 294, 2119-2125

Rodriguez-Navarro C., Sebastian E., (1996). *Role of particulate matter from vehicle exhaust on porous building stones (limestone) sulfation,* Science of the Total Environment 187, 79-91

Salma I., Maenhaut W., (2006). *Changes in elemental composition and mass of atmospheric aerosol pollution between 1996 and 2002 in a Central European city,* Environmental pollution 143, 479-488

Schmid H., Laskus L., Abraham H.J., Baltensperger U., Lavanchy V., Bizjak

M., Burba P., Cachier H., Crow D., Chow J., Gnauk T., Even A., ten Brink H.M., Giesen K.–P., Hitzenberger R., Hueglin C., Maenhaut W., Pio C., Carvalho A., Putaud J.–P., Toom–Sauntry D., Puxbaum H., (2001). *Results of the "carbon conference" international aerosol carbon round robin test stage I,* Atmospheric Environment 35, 2111–2121

Seagrave JC., McDonald J. D.,1 Bedrick E., Edgerton E. S., Gigliotti A. P., Jansen J. J., Ke L., Naeher L. P., Seilkop S. K., Zheng M., Mauderly J. L., (2006)**.** *Lung Toxicity of Ambient Particulate Matter from Southeastern U.S. Sites with Different Contributing Sources: Relationships between Composition and Effects,* Environmental Health Perspectives 114, 1387-1393

Seinfeld J.H. and Pandis S.N., (1998). *Atmospheric Chemistry and Physics*. John Wiley and Sons, Inc

Sternbeck J., Sjödin A., Andréasson K., (2002). *Metal emissions from road traffic and the influence of resuspension—results from two tunnel studies,* Atmospheric Environment 36, 4735–4744

Stier P., Seinfeld J.H., Kinne S., Boucher O., (2007). *Aerosol absorption and radiative forcing,* Atmospheric Chemistry and Physics 7, 5237–5261

Storelvmo T., Kristj´ansson J. E., Myhre G., Johnsrud M., and Stordal F., (2006). *Combined observational and modelling based study of the aerosol indirect effect,* Atmospheric Chemistry and Physics 6, 3583-3601

Szidat S., Jenk T.M., Gäggeler H.W., Synal H.-A., Hajdas I., Bonani G., Saurer M. (2004a). *THEODORE, a two-step heating system for the EC/OC determination of radiocarbon (14C) in the environment,* Nuclear Instruments and Methods in Physics Research B 223–224, 829–836

Szidat S., Jenk T.M., Gäggler H.W., Synal H.-A., Fisseha R., Baltensperger U., Kalberer M., Samburova V., Wacker L., Saurer M., Schwilowski M., Hajdas I., (2004b). *Source apportionment of aerosols by ^{14}C measurements in different carbonaceous particle fractions.* Radiocarbon 46, 475-484

Szidat S., Jenk T.M., Synal H.-A., Kalberer M., Wacker L., Hajdas I., Kasper-Giebl A., Baltensperger U., (2006). *Contributions of fossil fuel, biomass-burning, and biogenic emissions to carbonaceous aerosols in Zurich as traced by*

^{14}C, Journal of Geophysical Research 111, D07206, doi:10.1029/2005JD006590

Szidat S., Ruff M., Perron N., Wacker L., Synal H.-A., Hallquist M., Shannigrahi A. S., Yttri K. E., Dye C., and Simpson D., (2009). *Fossil and non-fossil sources of organic carbon (OC) and elemental carbon (EC) in Göteborg, Sweden,* Atmospheric Chemistry and Physics 9, 1521-1535

Textor C., Schulz M., Guibert S., Kinne S., Balkanski Y., Bauer S., Berntsen T., Berglen T., Boucher O., Chin M., Dentener F., Diehl T., Easter R., Feichter H., Fillmore D., Ghan S., Ginoux P., Gong S., Grini A., Hendricks J., Horowitz L., Huang P., Isaksen I., Iversen T., Kloster S., Koch D., Kirkevåg A., Kristjansson J. E., Krol M., Lauer A., Lamarque J. F., Liu X., Montanaro V., Myhre G., Penner J., Pitari G., Reddy S., Seland Ø., Stier P., Takemura T., Tie X., (2006). *Analysis and quantification of the diversities of aerosol life cycles within AeroCom,* Atmospheric Chemistry and Physics 6, 1777–1813

Uchida M., Kumata H., Koike Y., Tsuzuki M., Uchida T., Fujiwara K., Shibata Y. (2010). *Radiocarbon-based source apportionment of black carbon (BC) in PM10 aerosols from residential area of suburban Tokyo,* Nuclear Instruments and Methods in Physics Research B 268, 1120–1124

Vecchi R., Bernardoni V., Cricchio D, D'Alessandro A., Fermo P., Lucarelli F., Nava S., Piazzalunga A., Valli G. (2008). *The impact of fireworks on airborne particles,* Atmospheric Environment 42, 1121–1132

Vecchi R., Bernardoni V., Fermo P., Lucarelli F., Mazzei F., Nava S., Prati P., Piazzalunga A., Valli G. (2009a)**.** *4–hours resolution data to study PM10 in a "hot spot" area in Europe,* Environmental Monitoring and Assessment 154, 283-300

Vecchi R., Valli G., Fermo P., D'Alessandro A., Piazzalunga A., Bernardoni V. (2009b). *Organic and inorganic sampling artefacts assessment,* Atmospheric Environvent 43, 1713-1720

Viana M., Kuhlbusch T.A.J., Querol X., Alastuey A., Harrison R.M., Hopke P.K., Winiwarter W., Vallius M., Szidat S., Prévôt A.S.H., Hueglin C., Bloemen H., Wåhlin P., Vecchi R., Miranda A.I., Kasper-Giebl A.,

Maenhaut W., Hitzenberger R., (2008). *Source apportionment of particulate matter in Europe: A review of methods and results.* Aerosol Science 39, 827–849

Viksna A., Lindgren E.S., Standzeniekes P., Jacobsson J., (2004). *EDXRF and TXRF analysis of elemental size distribution and environmental mobility of airborne particles in the city of Riga, Latvia*, X-Ray Spectrometry 33, 414-420

Vincent J.H., (1989)**.** *Aerosol Sampling Science and Practice*, John Wiley & Sons Ltd

Vogel J.S., Southon J.R., Nelson D.E., Brown T. A., (1984). *Performance of catalytically condensed carbon for use in accelerator mass spectrometry*. Nuclear Instruments and Methods in Physics Research B5, 289–293

Volkamer R., Jimenez J. L., San Martini F., Dzepina K., Zhang Q., Salcedo D., Molina L. T., Worsnop D. R., Molina M. J. (2006). *Secondary organic aerosol formation from anthropogenic air pollution: Rapid and higher than expected,* Geophysical Research Letters 33, L17811-L17815

Watson J.G. (2002). *Visibility: Science and Regulation*, Journal of Air & Waste Management Association 52, 628–713

Watson J.G., Chow J.C., Chen L.–W.A. (2005). *Summary of Organic and Elemental carbon/Black Carbon Analysis Methods and Intercomparisons*. Aerosol and Air Quality Research 5, 65–102

Weckwert G., (2001). *Verification of traffic emitted aerosol components in the ambient air of Cologne (Germany),* Atmospheric Environment 35, 5525–5536

Whitby K.T., (1978). *The physical characteristics of sulphur aerosol,* Atmospheric Environment 12, 135-159

Wolfenbarger J.K. and Seinfeld J.H. (1990). *Inversion of aerosol size distribution data*, Journal of Aerosol Science 21, 227–247.

Yu J.Z., Xu J.H., Yang H. (2002). *Charring Characteristics of Atmospheric Organic Particulate Matter in Thermal Analysis*, Environmental Science and Technology 36, 754-761

Zencak Z., Elmquist M., Gustafsson O. (2007). *Quantification and radiocarbon source apportionment of black carbon in atmospheric aerosols using the CTO-375 method,* Atmospheric Environment, 7895–7906

Appendix: List of publications.

A. Papers published on international journals

A.1. Roberta Vecchi, Vera Bernardoni, Diana Cricchio, Alessandra D'Alessandro, Paola Fermo, Franco Lucarelli, Silvia Nava, Andrea Piazzalunga and Gianluigi Valli (2008): "*The impact of fireworks on airborne particles: results of a case study*", Atmospheric Environment, 42, 1121-1132, doi: 10.1016/j.atmosenv.2007.10.047 , ISSN: 1352-2310

A.2. Roberta Vecchi, Gianluigi Valli, Paola Fermo, Alessandra D'Alessandro, Andrea Piazzalunga, Vera Bernardoni (2009) "*Organic and inorganic sampling artefacts assessment*", Atmospheric Environment, 43, 1713-1720, doi: doi:10.1016/j.atmosenv.2008.12.016, ISSN: 1352-2310

A.3. Roberta Vecchi, Vera Bernardoni, Paola Fermo, Franco Lucarelli, Federico Mazzei, Silvia Nava, Paolo Prati, Andrea Piazzalunga, Gianluigi Valli (2009): "*4-hours resolution data to study PM10 in a "hot spot" area in Europe*", Environmental Monitoring and Assessement, 154, 283–300, doi: 10.1007/s10661-008-0396-1, ISSN: 0167-6369 (Print) 1573-2959 (Online))

V. Ariola, V. Bernardoni, G. Calzolai, M. Chiari, E. Cuccia, F. Lucarelli, F. Mazzei, S. Nava, P. Prati, G. Valli, R. Vecchi (2008). "*Nuclear techniques and the particulate matter pollution in big harbours".* Il nuovo cimento della Società Italiana di Fisica, 31C-4, 527-536 doi: 10.1393/ncc/i2008-10306-5**,** ISSN: 1124-1896

E. Cuccia, V. Bernardoni, D. Massabò, P. Prati, G.Valli, R. Vecchi, "*An alternative way to determine the size distribution of airborne particulate matter".* Atmospheric Environment 44, 3304-3313, doi:10.1016/j.atmosenv.2010.05.045, ISSN: 1124-1896

A. Piazzalunga, P. Fermo, V. Bernardoni, R. Vecchi, G. Valli M. A. De Gregorio (2010). *"A simplified method for levoglucosan quantification in wintertime atmospheric particulate matter by high performance anion-exchange chromatography coupled with pulsed amperometric detection"*, International Journal of Environmental Analytical Chemistry 12, 934-947, DOI: 10.1080/03067310903023619, ISSN 1029–0397

B. Papers submitted to international journals

B.1. G. Calzolai, V. Bernardoni, M. Chiari, M. Fedi, F. Lucarelli, S. Nava, F. Riccobono, F.

Taccetti, G. Valli, R. Vecchi (**2010**): "*The new sample preparation line for radiocarbon measurements on atmospheric aerosol at LABEC"*, Nuclear Instruments and Methods B, **UNDER SECOND REVISION.**

B.2. Vera Bernardoni, Eleonora Cuccia, Giulia Calzolai, Massimo Chiari, Franco Lucarelli, Dario Massabò, Silvia Nava, Paolo Prati, Gianluigi Valli, Roberta Vecchi (**2010**): "*ED-XRF set-up for size-segregated aerosol samples analysis",* X-Ray Spectrometry, **SUBMITTED**

C. Presentation to international conferences with abstracts publication (name in bold when speaker).

C.1. R. Vecchi, A. D'Alessandro, V. Bernardoni, P. Fermo, A. Piazzalunga and G. Valli (2008): "*Organic and inorganic sampling artefacts assessment in Milan (Italy)"*, **Abstract T10A023O**, European Aerosol Conference 2008, Salonicco, 25-29 August 2008 (orale)

C.2. R. Vecchi, G. Valli, V. Bernardoni, A. Piazzalunga, and P. Fermo (2009): "*Apportioning the wood burning source in an urban area by Positive Matrix Factorization using 4-hour resolved PM10 data",* **Abstract T057A01**, European Aerosol Conference 2009, Karlsruhe, 07-11 September 2009 (poster)

C.3. V. Bernardoni, G. Calzolai, M. Chiari, M. Fedi, F. Lucarelli, S. Nava, F. Riccobono, G. Valli, R. Vecchi (2009): "*Radiocarbon measurements on aerosol samples at LABEC (Florence, Italy)*" **Abstract T059A08**, European Aerosol Conference 2009, Karlsruhe, 07-11 September 2009 (poster)

C.4. A. Piazzalunga, P. Fermo, R. Vecchi, G. Valli, S. Comero, V. Bernardoni, O. Cazzuli, A.Giudici, G.Lanzani (2009): "*OC, EC, and SOA contribution to PM in Lombardy (Italy): results of three winter campaigns (2005-2007)*", **Abstract T059A09**, European Aerosol Conference 2009, Karlsruhe, 07-11 September 2009 (poster)

C.5. E. Cuccia, F. Mazzei, V. Bernardoni, P. Prati, G. Valli, R. Vecchi (2009): "*Source apportionment of particle number and PM10 concentration*", **Abstract T091A04**, European Aerosol Conference 2009, Karlsruhe, 07-11 September 2009 (poster)

C.6. R. Vecchi, G. Valli, **V. Bernardoni**, A. Franchin (2009): "*Ten-year measurements of Radon's decay products to study the role of atmospheric dispersion on PM levels*", **Abstract T121A01**, European Aerosol Conference 2009, Karlsruhe, 07-11 September 2009 (presentazione orale)

C.7. E. Cuccia, V. Bernardoni, G. Calzolai, M. Chiari, L. La Gaccia, F. Lucarelli, D.

Massabò, S. Nava, P. Prati, G. Valli and R. Vecchi (2010): "*Analysis of aerosol samples collected by multi-stage cascade impactors by ED-XRF"*, **Abstract OS11-7**, European Conference on X-Ray Spectrometry 2010, Figueira da Foz, 20-25 June 2010

C.8. E. Cuccia; V. Bernardoni; G. Calzolai; M. Chiari; L. La Gaccia; F. Lucarelli; D. Massabò; S. Nava; P. Prati; G. Valli; R. Vecchi (2010): *"Analysis of atmospheric aerosol collected by multi-stage cascade impactors by Energy Dispersive X-Ray Spectrometry",* **Abstract P1E40**, International Aerosol Conference 2010, Helsinki, 29 August-3 September 2010 (poster presentation)

C.9. V. Bernardoni; G. Calzolai; M. Chiari; M. Fedi; F. Lucarelli; S. Nava; F. Riccobono; F. Taccetti; G. Valli; R. Vecchi (2010): *"The sample preparation line for radiocarbon measurements on atmospheric aerosol at LABEC",* **Abstract P2K107**, International Aerosol Conference 2010, Helsinki, 29 August-3 September 2010 (poster presentation)

C.10. P. Prati; V. Bernardoni; E. Cuccia; D. Massabò; G. Valli; R. Vecchi; (2010): *"Measuring the size distribution of airborne particulate matter concentration without multi-stage cascade impactors"*, **Abstract 9E1**, International Aerosol Conference 2010, Helsinki, 29 August-3 September 2010 (oral presentation)

C.11. A. Piazzalunga; C. Abate; V. Bernardoni; F. Bianchi; P. Fermo; C. Paganelli; G. Valli; R. Vecchi (2010): *"BC/EC assessment on real samples by optical/thermal methods with and without WSOC removal and using different protocols",* **Abstract 11D4,** International Aerosol Conference 2010, Helsinki, 29 August-3 September 2010 (oral presentation)

C.12. R. Vecchi; V. Bernardoni; S. Broccoletti; P. Canepa; E. Cuccia; D. Massabò; C. Paganelli; A. Piazzalunga; P. Prati; G. Valli (2010): "*Black Carbon and Elemental Carbon measurements in Milan (Po Valley, Italy) by different optical and thermal-optical methods",* **Abstract 11E2**, International Aerosol Conference 2010, Helsinki, 29 August-3 September 2010 (oral presentation)

D. Presentations to national conferences (name in bold when speaker)

D.1. Piazzalunga A., Fermo P., Bernardoni V., Vecchi R., Valli G. (2008): "*Wood combustion contribution to PM: results from different winter campaigns in Milan*",

XI Congresso Nazionale di Chimica dell'Ambiente e dei Beni Culturali-Dalla conoscenza alle strategie di intervento, Muggia (TS), 16-20 June 2008 (Oral presentation)

D.2. Bernardoni V., Cuccia E., Calzolai G., Chiari M., Lucarelli F., Mazzei F., Nava S., Prati P., Valli G., Vecchi R. (2008): *"Tecniche nucleari per lo studio dell'inquinamento prodotto dai grandi porti"*, XCIV Congresso nazionale della Società Italiana di Fisica, Genova, 22-27 September 2008 (Oral presentation)

D.3. A. Piazzalunga, P. Fermo, V. Bernardoni, S. Comero, G. Valli, R. Vecchi (2008): "*Valutazione del contributo della combustione di legna al particolato atmosferico*", **Abstract OB1-11**, PM2008-3° Convegno Nazionale sul Particolato Atmosferico, Bari, 6-8 October 2008 (Oral presentation)

D.4. **V. Bernardoni**, R. Vecchi, A. D'Alessandro, P. Fermo, A. Piazzalunga, G. Valli (2008): "*Valutazione degli artefatti di campionamento organici e inorganici a Milano*", **Abstract OB7-64**, PM2008-3° Convegno Nazionale sul Particolato Atmosferico, Bari, 6-8 October 2008 (Oral presentation)

D.5. A. Piazzalunga , C. Abate, V. Bernardoni, F. Riccobono, P. Fermo, G. Valli, R. Vecchi (2008): "*Quantificazione dei WSOC mediante Thermal Optical Transmittance e valutazione dell'errore sulla EC*", **Abstract OB8-77**, PM2008-3° Convegno Nazionale sul Particolato Atmosferico, Bari, 6-8 October 2008 (poster)

D.6. R. Vecchi, V. Bernardoni, P. Fermo, A. Piazzalunga, G. Valli (2008): "*Il PM10 a Milano: risultati di una campagna di misura invernale*", **Abstract PA5-068**, PM2008-3° Convegno Nazionale sul Particolato Atmosferico, Bari, 6-8 October 2008 (poster)

D.7. P. Fermo, F. Tuccillo, R. Vecchi, V. Bernardoni, G. Valli , A. Piazzalunga (2008): "*Caratterizzazione di Humic-Like Substances all'interno del particolato*", **Abstract PB8-112**, PM2008-3° Convegno Nazionale sul Particolato Atmosferico, Bari, 6-8 October 2008 (poster)

D.8. D. Massabò, E. Cuccia, P. Prati, V. Bernardoni, G.Valli, R. Vecchi (2009): *"Una metodologia per l'apporzionamento del numero di particelle aereodisperse e del PM10",* **Abstract P6.19,** Environment including Global Change, Palermo, 5-9 October 2009 (Oral presentation)

D.9. G. Calzolai, V. Bernardoni, M. Chiari, M. Fedi, F. Lucarelli, S. Nava, F. Riccobono, F. Taccetti, G. Valli, R. Vecchi (2010): *"Misure di radiocarbonio su aerosol atmosferici per l'identificazione delle sorgenti: preparazione dei campioni e primi*

test al LABEC di Firenze", **Abstract O-33,** PM2010-4° Convegno Nazionale sul Particolato Atmosferico, Venezia, 18-20 May 2010 (Oral presentation)

D.10. E. Cuccia, V. Bernardoni, D. Massabó, P. Prati, G. Valli, R. Vecchi (2010): "*Un modo alternativo per misurare la distribuzione dimensionale dei componenti del particolato atmosferico",* **Abstract O-70,** PM2010-4° Convegno Nazionale sul Particolato Atmosferico, Venezia, 18-20 May 2010 (Oral presentation)

D.11. P. Prati, V. Bernardoni, M. Chiari, E. Cuccia, F. Lucarelli, D. Massabò S. Nava, G. Valli, R. Vecchi (2010). *"Analisi composizionali in fluorescenza X su campioni raccolti con impattori inerziali multistadio",* **Abstract P-24,** PM2010-4° Convegno Nazionale sul Particolato Atmosferico, Venezia, 18-20 May 2010 (Oral presentation)

D.12. A. Piazzalunga, C. Abate, V. Bernardoni, F. Bianchi, P. Fermo, G. Valli, R. Vecchi (2010). "*Valutazione del rapporto* $(OC/EC)_{primario}$ *in Regione Lombardia"* **Abstract O-11,** PM2010-4° Convegno Nazionale sul Particolato Atmosferico, Venezia, 18-20 May 2010 (Oral presentation)

D.13. R. Vecchi, G. Valli, **V. Bernardoni**, L. La Gaccia, C. Paganelli (2010). "*Aerosol atmosferico urbano separato dimensionalmente: risultati di una campagna di misura invernale"*, **Abstract O-26,** PM2010-4° Convegno Nazionale sul Particolato Atmosferico, Venezia, 18-20 May 2010 (Oral presentation)

D.14. R. Vecchi, V. Bernardoni, S. Broccoletti, E. Cuccia, D. Massabò, C. Paganelli, P. Prati, G. Valli (2010). "*Studio delle proprietà ottiche dell'aerosol atmosferico e determinazione del carbonio elementare con metodo ottici",* **Abstract O-22,** PM2010-4° Convegno Nazionale sul Particolato Atmosferico, Venezia, 18-20 May 2010 (Oral presentation)

D.15. R. Vecchi, V. Bernardoni, C. Paganelli, G. Valli (2010). "*Sviluppo di un fotometro polare per la determinazione del black carbon in campioni di aerosol atmosferico",* **Abstract pag. 118**, XCVI Congresso nazionale della Società Italiana di Fisica, Bologna, 20-24 September 2010 (Oral presentation)

Ringraziamenti

In primo luogo grazie ad Alessandro, mio marito, per quello che abbiamo avuto e perso insieme, per tutto ciò che ha fatto e che soprattutto sta facendo per me anche se il momento non è facile neanche per lui.

Grazie a mamma, papà e Nanò: grazie di essere Mamma, Papà e Sorella. Sempre.

Grazie a Roberta e Gianluigi: tutto questo lavoro è merito vostro. Ma soprattutto grazie perché non siete solo "i miei capi", ma siete la Roby e Gianlu: e scusate se è poco… E grazie al Teo per la sua (irruente e costante) presenza quotidiana.

E grazie ai nonni, a zii e cugino, agli amici di sempre e a chiunque altro mi sia vicino, specialmente ora.